“The epigenetic landscape of the heart in ischemia-reperfusion injury“

Dissertation

zur Erlangung des Grades

Doktor der Naturwissenschaften

Am Fachbereich Biologie

Der Johannes-Gutenberg Universität Mainz

Ina Caroline Kirmes

Geboren am 19. Oktober 1986 in Bad Soden

Mainz, 13. Juni 2016

Table of contents

Zusammenfassung 1
Summary 2
1. Introduction 3
1.1 The heart 3
1.2 The blood 5
1.3 Ischemic heart disease 5
1.4 Cardiac ischemia-reperfusion injury 7
1.5 From physioxia to hypoxia 10
1.6 Ischemic conditioning 12
1.7 Epigenetics 13
1.7.1 The histone code 14
1.7.2 DNA methylation 17
1.7.3 non-coding RNAs 18
1.8 Nuclear architecture 20
1.9 Epigenetics in hypoxia and ischemia-reperfusion injury 22
1.10 Objectives 23
2. Materials and Methods 25
2.1 Materials 25
2.2 Methods 28
2.2.1 Mouse model of ischemia-reperfusion injury 28
2.2.2 Cell culture 29
2.2.3 Oxygen and Nutrient Deprivation (OND) 30
2.2.4 Next Generation Sequencing of cardiac tissue 31
2.2.5 Next Generation Sequencing of HL-1 cells 33
2.2.6 NGS data analysis 33
2.2.7 Western Blot analysis 34
2.2.8 Flow cytometry analysis 35
2.2.9 Confocal microscopy 37
2.2.10 Single Molecule Localization Microscopy 37
2.2.11 Calculation of chromatin-free regions 39
2.2.12 Transmission electron microscopy 40
2.2.13 DNaseI sensitivity assay 41
2.2.14 Fluorescence Recovery After Photobleaching (FRAP) 42
2.2.15 Chromatin immunoprecipitation followed by sequencing 43
2.2.16 Labeling of nascent RNA with BrU 45
2.2.17 ATP energy depletion assay 46
2.2.18 Treatments 46
3. Results 47
3.1 Transcriptome analysis of cardiac ischemia-reperfusion and OND 47
3.1.1 Cardiac IR induces a transcriptional burst 47

3.1.2 OND in HL-1 cells induces gene down-regulation 51
3.1.3 Transcription in HL-1 cells is generally impaired under OND 55
3.1.4 Egr1, Egr2, Fos and FosB are induced upon OND and during ischemia 56
3.1.5 Recovery/reperfusion induces impaired chromatin organisation 58
3.2 Western Blot analysis of histone modifications 59
3.2.1 Histones become deacetylated in OND 59
3.2.2 Histone methylation is constant upon OND 63
3.2.3 Histones become re-acetylated within the first minutes of recovery 65
3.2.4 Histone modifications are not altered in ischemia and reperfusion 65
3.3 Confocal microscopy analysis 66
3.3.1 The signal of histone H3 and acetylated H3 decreases in OND 66
3.3.2 Histone methylation is not altered significantly upon OND 69
3.3.3 H3S28p increases upon OND and recovery 71
3.3.4 Chromatin compacts under OND conditions 72
3.3.5 The combination of oxygen and nutrient deprivation induces the OND phenotype 73
3.4 SMLM analysis of DNA structure and histone acetylation 74
3.4.1 OND induces ring-like structures and DNA-sparse voids 74
3.4.2 The signal of core histone H3 decreases under OND conditions 75
3.4.3 The distribution of Lamin B is not altered upon OND 75
3.4.4 Recovery from OND induces a more open chromatin conformation 76
3.4.5 Electron microscopy analysis of the DNA structure under OND 77
3.5 Flow cytometry analysis of histone modifications 78
3.5.1 Activating histone modifications decrease upon OND 78
3.5.2 Acetylation of histones recovers within 15 minutes 80
3.6 Analysis of chromatin compaction under OND conditions 80
3.6.1 Chromatin digestion time increases upon OND 80
3.6.2 The mobility of linker histone H1.1 decreases upon OND 81
3.7.1 OND depletes intercellular ATP levels 83
3.7.2 OND induces relocation of the polyamine pool into the nucleus 84
3.8 Deacetylated genes are associated with cardiac diseases 84
3.9 Prevention of chromatin compaction by inhibition of HDACs and ODC 88
4. Discussion 91
5. Outlook 98
6. References 100
7. Appendix 108
7.1 List of figures 108
7.2 List of tables 109
7.3 Abbreviation index 110

Zusammenfassung

Ischämische Herzerkrankungen sind die häufigste Todesursache weltweit. Herzmuskelzellen können ischämische Zustände wahrnehmen und ihre Transkription, Translation und ihren Metabolismus an die hypoxischen, nährstoffarmen Bedingungen anpassen. In der vorliegenden Studie wurden die Auswirkungen einer künstlich induzierten Ischämie auf die Nanostruktur des Chromatins von Herzmuskelzellen untersucht. Eine kurzzeitige Sauer- und Nährstoffunterversorgung der murinen Herzmuskelzelllinie HL-1 induziert eine bis dato unbeschriebene Architektur des Chromatins, bestehend aus ringförmigen DNA-Atollen, die zwischen großen, DNA-freien Regionen liegen. Neben der starken Verdichtung des Chromatins wird Histon H3 deacetyliert und die Transkription kommt zum Erliegen. Ein hoher Anteil genomischer Regionen, die von der Deacetylierung betroffen sind, liegen in der Nähe von Genen, deren veränderte Expression im Kontext mit Herzerkrankungen beschrieben wurden. Sowohl Die Verdichtung des Chromatins als auch die Deacetylierung von H3 sind reversibel sobald die Sauer- und Nährstoffversorgung wieder hergestellt wird. Das Chromatin nimmt nach der Wiederversorgung eine offenere Konfiguration an und Histongene werden herabreguliert.

Kompaktes Chromatin verhindert Transkription, während die offene Struktur des Chromatins nach dem Ende der Mangelversorgung einen vorübergehenden Anstieg der Genexpression verursacht. Mechanistisch wird die Verdichtung des Chromatins durch den Abfall in Adenosintriphosphat und die Freisetzung von Polyaminen verursacht, die sich per Ladungsausgleich vom Zytoplasma in den Zellkern verlagern.

Die Hemmung von Histondeacetylasen und Enzymen der Polyaminsynthese vor der induzierten Ischämie bewirkt eine weniger kompakte Struktur des Chromatins während der Mangelversorgung und kann daher als Behandlungsmethode von akut ischämischen Zuständen in Erwägung gezogen werden.

Die Ergebnisse der vorliegenden Arbeit sind ein Beispiel für die dynamische Kapazität des Chromatins auf Veränderungen des Milieus zu reagieren. Diese Studie verbindet den zellulären Energiehaushalt mit der Struktur des Chromatins und gibt Einblick in die nukleare Architektur von Zellen.

Summary

Ischemic heart diseases are the leading cause of death worldwide. Cardiomyocytes detect and adapt to hypoxic and nutritional stress through immediate transcriptional, translational and metabolic responses. The environmental effects of ischemia on chromatin nanostructure were analysed by characterising and integrating chromatin structure with differential gene expression analysis. Short-term oxygen and nutrient deprivation (OND) of the cardiomyocyte cell-line HL-1 induces a previously undescribed chromatin architecture, consisting of large, chromatin sparse voids interspersed between ring-like structures. Along with chromatin compaction, histones become deacetylated and transcription is repressed. Among the regions which are affected by altered acetylation are genes previously reported to be differentially expressed in cardiac diseases.

OND induced chromatin compaction and histone deacetylation are reversible, and upon restitution of normoxia and nutrients, chromatin adopts a more open structure than in untreated cells, with in particular the expression of histone genes becoming repressed. The compacted state of chromatin reduces transcription, while the open chromatin structure, induced upon recovery, provokes a transitory increase in transcription. Mechanistically, chromatin compaction is associated with depletion of ATP and redistribution of the polyamine pool into the nucleus by mass action. Inhibition of histone deacetylation or polyamine synthesis prior to OND promotes a more relaxed chromatin structure, implicating that HDAC inhibitors could have considerable therapeutic benefit in the treatment of ischemic heart diseases.

These studies exemplify the dynamic capacity of chromatin architecture to physically respond to environmental conditions, directly link cellular energy status to chromatin compaction and provide insight into the effect ischemia has on the nuclear architecture of cells.

1. Introduction

Ischemic heart disease has a high impact on human morbidity and mortality worldwide. Every sixth man and every seventh woman in Europe dies from myocardial infarction. Conventional treatment strategies are insufficient to provide a remedy. About 12% of patients die within the first 6 months after infarction and the 5-year-survival of patients, diagnosed with chronic post-infarction heart failure, is only about 50% (Steg et al., 2012). These appalling facts clearly justify continuous efforts to obtain a more encompassing knowledge about the underlying molecular events of ischemic heart disease and to consider new treatment strategies.

1.1 The heart

The heart is a powerful muscle, which supplies all parts of the body with oxygenated blood. During a human's lifetime the heart beats more than 3 billion times (http://www.gwheartandvascular.org/education/cardiovascular-diseases/basic-anatomy-of-the-heart/). The heart is surrounded by the pericardium, a liquid filled sac attaching the organ to the diaphragm, which separates the abdominal cavity from the chest cavity. The heart consists of four chambers: the right atrium receives deoxygenated blood from the circulation through the superior and inferior vena cava and the right ventricle pumps the blood through the pulmonary artery into the lungs for the uptake of oxygen and the removal of carbon dioxide. The left atrium receives the freshly oxygenated blood from the pulmonary vein and the strong left ventricle pumps it through the aorta into the arteries and capillaries of the body. The left and the right ventricle are separated by the septum. Valves between the atria and the ventricles and at the trunks of the aorta and the pulmonary arteries inhibit the reflux of blood (Figure 1). The coronary arteries provide the oxygenated blood needed for cardiac performance. A proper function of these vessels is essential, since they are the only blood supply to the myocardium.

The heart is a heterogeneous tissue comprised of four cell populations with different physiological, biochemical and mechanical properties (Figure 1). Cardiomyocytes are short, interconnected muscle cells, branching into a syncytium, which gives the organ an extraordinary circumferential strength. Action potentials are conducted through pores in the intercalating discs, which connect the individual myocytes. Cardiomyocytes are

packed with mitochondria, which extract oxygen provided by the coronary blood flow to generate energy in the form of adenosine triphosphate (ATP). Cardiomyocytes which do not express actin or myosin cannot contract but instead form the electrical conduction system of the heart. The sinoatrial node (SAN) is the pacemaker of the heart, the atrioventricular node (AVN) electrically connects atria and ventricles, and the Purkinje fibers conduct the action potential throughout the ventricles.

The vessel walls consist of vascular smooth muscle cells, whose main function is to maintain the muscle tonus, thereby regulating the blood pressure. Endothelial cells form the inner lining of the heart, the endocardium, and the inner surface of the vessel walls. This monolayer is in direct contact with the cardiomyocytes and can signal to them via secreted factors. More than 50% of the cells within the heart are fibroblasts, which form the interstitium of the myocardium. Fibroblasts synthesize and deposit extracellular matrix, mainly type I collagen, which tethers muscle cells and blood vessels, forming a scaffold for additional strength (Xin et al., 2013). Fibroblasts play a crucial role in cardiac remodeling under pathological conditions, in particular in an overactive fibrotic phenotype arising after myocardial infarction. It can be anticipated that every cell type of the heart responds individually to stress and injury and therefore contributes to different extents to cardiac diseases.

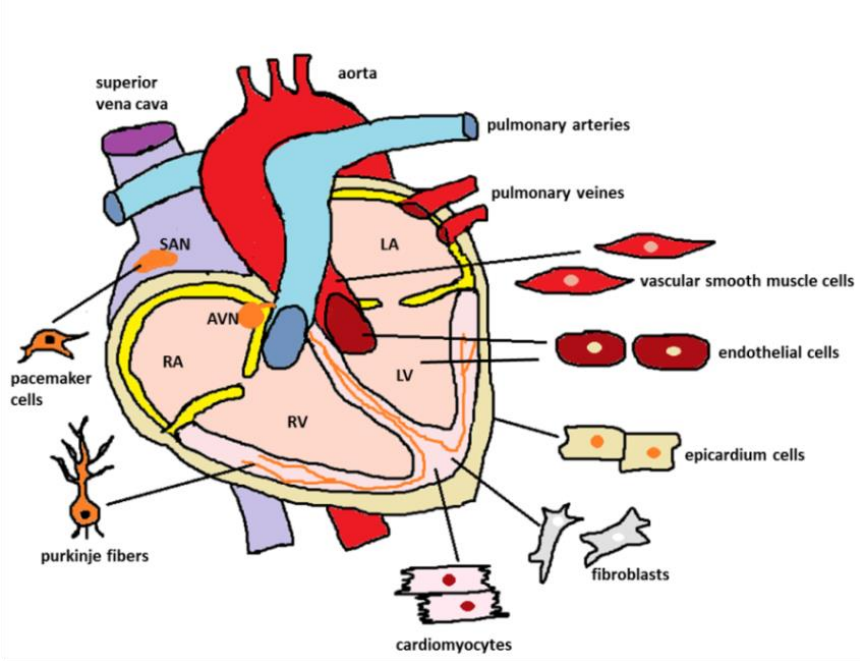

Figure 1. Cross-section of the mammalian heart.
The four chambers of the heart with their respective valves in yellow and their main vessels. Different cell types are shown according to their occurrence in the tissue. The electrical conduction system is orange, myocardium in rose, epicardium in beige. AVN: atrioventricular node, LA: left atrium, LV: left ventricle, RA: right atrium, RV: right ventricle, SAN: sinoatrial node. Image modified from Xin et al., 2013.

1.2 The blood

The fundamental purpose of the blood is to deliver o and nutrients to cells and to remove carbon dioxide (CO_2) and metabolic waste, such as urea and lactic acid. The principle nutrients are glucose, amino and fatty acids, but the blood also transports hormones and ions, mainly sodium and chloride. The blood consists of blood cells and of plasma, which is composed of water and proteins, like albumin and antibodies. Erythrocytes are red blood cells, which have hemoglobin to bind oxygen. Mature erythrocytes have neither a nucleus nor organelles, but they increase the blood's oxygen carrier capacity about 70 fold. After a short life of 120 days, erythrocytes become degraded in the spleen and in the Kupffer cells of the liver. Leucocytes are immune cells in the blood, which can be further classified into monocytes, lymphocytes, eosinophils, basophils, and neutrophils. Thrombocytes, or platelets, induce coagulation of the blood in case of vessel injury (Zucker-Franklin, 1990). In adults, hematopoiesis takes place in the bone marrow within the bodies of the vertebrae, the sternum and ribcage, in pelvic bones, as well as in the upper arm and upper leg bones. Restricted blood supply to an area of tissue is called ischemia, which can induce cell death due to energy depletion.

1.3 Ischemic heart disease

Ischemic heart disease refers to the imbalance between oxygen supply and oxygen demand of the myocardium. The restriction of oxygen leads to energy depletion, the generation of reactive oxygen species (ROS), and the accumulation of metabolic waste. Ischemic heart disease is the major cause of death worldwide, followed by ischemic brain disease, known as stroke (Figure 2).

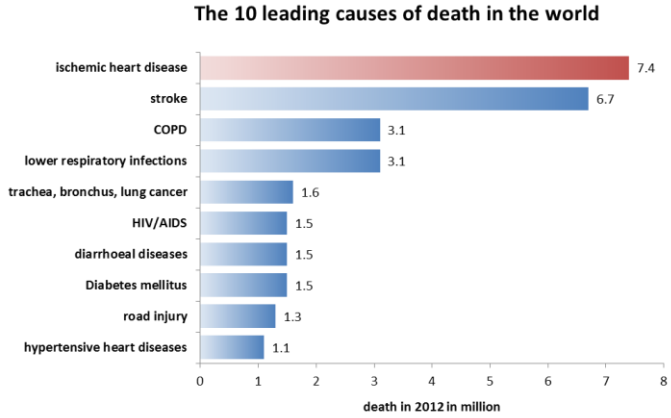

Figure 2. The 10 leading causes of death in the world.
Ischemic heart diseases were the major cause of death, counting for 7.4 million dead people in 2012. Statistic by the World Health Organization (WHO), http://www.who.int/mediacentre/factsheets/fs310/en/

In highly metabolic tissues, like the heart and the brain, irreversible ischemic injury happens within minutes. Without intervention, persistent ischemia causes cell death and massive organ damage. Among ischemic heart disease, coronary heart disease (CHD) is the most common type. CHD is caused by the narrowing or complete occlusion of the coronary arteries by atherosclerotic plaques or by coronary vasospasms. Atherosclerotic plaques, or atheroma, can arise between the endothelial cell layer and the smooth muscle cell layer of vessels. These plaques can contain macrophages, lipids, fatty acids, calcium, and fibrous connective tissue. If a plaque ruptures through the artery wall and accumulates platelets on its surface, a thrombus forms, which narrows the arterial lumen, blocks blood flow and causes myocardial infarction (Figure 3). Cardiomyocytes at the ischemic site of infarction die and a subsequent activation of compensatory fibroblast proliferation induces fibrosis and ventricular remodeling. Since fibroblasts can only replace the mass of the dead cardiomyocytes but not their contractility, the heart cannot pump sufficient blood to meet the demands placed upon the cardiovascular system – a pathology known as heart failure (Weber, 1989). Symptoms of clinical heart failure are dyspnoea, sinus tachycardia, a third heart sound, left ventricle dilatation and a reduced ejection fraction.

Cardiomyocytes which survive an ischemic event are able to activate adaptive programmes that resemble the neonatal metabolic phenotype with reduced contractility and a preferential use of glycolysis for obtaining energy. This phenomenon is known as myocardial hibernation or stunning, and can be reversed upon normal physiological conditions (Depre et al., 2007).

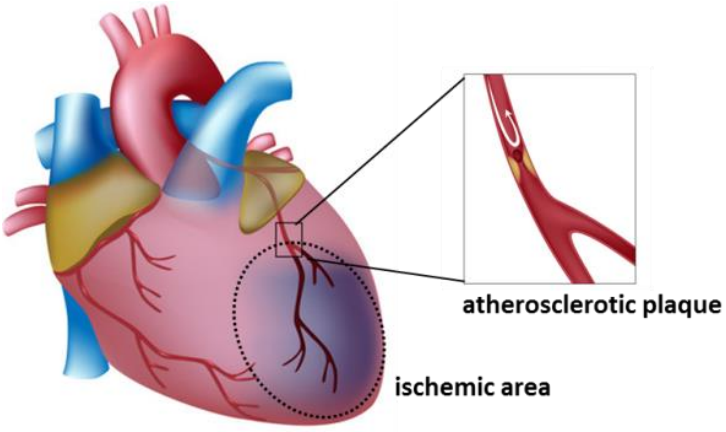

Figure 3. Myocardial infarction.
Occlusion of the left descending coronary artery by an atherosclerotic plaque induces ischemia. Inadequate blood supply of the myocardium leads to necrosis and apoptosis of cells in the infracted area. Image modified from http://yourhealtheducator.com/myocardial-infarction-mi-heart-attack/.

1.4 Cardiac ischemia-reperfusion injury

Early intervention of ischemia is essential to reduce the death of cardiomyocytes, according to the maxim “time is muscle”. The time after the initial call of the emergency care unit until intervention should be less than 60 minutes (Steg et al., 2012). Irreversible cardiomyocyte damage already occurs within the first 20 minutes of ischemia and reperfusion of the myocardium within the first two hours after acute myocardial infarction has the best survival prognosis (Davie et al, 1996).

The treatment of myocardial ischemia aims to improve the blood flow to the myocardium and to reduce its O_2 demand. The therapy is based on medications and/or surgery. Anti-coagulants like heparin or acetylsalicylic acid make the blood thinner and prevent thrombus formation, nitrates, provided as nitroglycerin, dilate the vessels and increase the blood flow. Beta blockers and calcium channel blockers reduce the workload of the heart and relax the vessels as well as the myocardium. Depending on the severity, patients may receive a percutaneous coronary intervention, such as angioplasty or atherectomy with subsequent stenting, or a coronary artery bypass graft in case of multiple vessel obstructions (Pepine et al., 1998).

The term *ischemia-reperfusion injury* (IRI) describes the resulting myocardial damage, which occurs as a consequence of re-initiated blood flow. IRI may account for up to 50% of the final infarct size (Piper et al, 1998). Consequences of reperfusion can be arrhythmias, myocardial stunning, microvascular obstruction and lethal reperfusion injury and the death of cardiomyocytes by necrotic, apoptotic and autophagic mechanisms. Necrosis, rather than apoptosis, occurs when cellular ATP levels are below the threshold required to initiate the apoptotic machinery. Necrotic cells swell until they burst, which induces an inflammatory response.

Upon ischemia-reperfusion (IR), infiltrated neutrophils release cytokines and chemokines, along with other pro-inflammatory stimuli, which induce a sterile inflammation, which accelerates of myocardial death, and vessel re-occlusion. The inflammatory response of reperfused tissue can be so intense, that injury is manifested in distant organs, an event known as remote organ injury (Carden et al., 2000).

It is not clear yet, whether the inflammatory response, that accompanies acute myocardial ischemia, contributes to lethal myocardial reperfusion injury, or if this is a reaction to the acute myocardial injury (Vinten-Johansen et al, 2004). Notably, the induced cell death after IR can continue for up to three days (Zhao et al., 2000).

IR further induces endothelial and mitochondrial dysfunction, oxidative stress, intracellular calcium (Ca^{2+}) overload, changes in pH, and perturbation of the cellular metabolism (Hausenloyet al., 2013).

Endothelial dysfunction is an induced permeability of vessels, which allows fluid diffusion across tissues. Endothelial cells release ROS and decrease their nitric oxide production inducing vasoconstriction. Infiltrating activated leukocytes accumulate on the surface of endothelial cells, further narrowing the vessel lumen and further reducing blood flow again. These activated leucocytes induce the destruction of potentially viable myocytes.

Oxidative and nitrosative stress is caused by the burst of ROS and reactive nitrogen species at the onset of reperfusion. ROS at low concentrations are signaling molecules, however, at high dosages these highly reactive molecules destroy membranes by lipid peroxidation, oxidase protein structures and induce damage to DNA. ROS can interact with RNS to produce reactive nitrogen oxide species, such as the strong pro-oxidant peroxynitrite. The majority of ROS in the ischemic heart are generated by the enzymes xanthine oxidase and nicotinamide adenine dinucleotide phosphate oxidase (NADPH oxidase), located in the mitochondrial electron transport chain (Zweier et al., 2006).

Under ischemia, the NAD-reducing dehydrogenase xanthine oxidase transforms into an oxygen-reducing oxidase. Hypoxanthine accumulates and in consequence, upon reperfusion, a burst of superoxide (O_2^-) and hydrogen peroxide (H_2O_2) occurs, which can further react to generate the hydroxyl radicals ($^{\cdot}OH$) (Granger, 1988). Low amounts of O_2^- are also generated under normal physiological conditions in the mitochondrial respiratory chain, known as “electron leak”. The reduction-oxidation (redox) chain is located in the inner membrane of the mitochondria and generates a proton gradient across the membrane to accomplish oxidative phosphorylation of adenosine diphosphate (ADP) to adenosine triphosphate (ATP), the energy currency of the cell. Physiological levels of O_2^- under normoxic conditions are enzymatically converted to H_2O_2, which is further reduced to water (H_2O) (Andreyev et al., 2005).

Mitochondria are the power stations of the cell. Energy consuming muscle cells have a high mitochondrial density, which makes them extremely sensitive towards IRI. The mitochondrial permeability transition pore (MPTP) is a non-specific channel within the inner membrane, which opens within the first minutes reperfusion due to a shift in pH, excessive production of ROS, and an overload of calcium (Baines et al., 2009). The opening of MPTP induces the permeability for molecules with a size less than 1.5 kilo

kDa, which depolarizes the inner membrane and subsequently impairs oxidative phosphorylation, leading to the depletion of ATP. Moreover, the osmotic gradient allows water to enter mitochondria, which induces swelling, rupture, and the release of the pro-apoptotic factor cytochrome c. Opening of the MPTP might be a key mediator or even the end-effector of lethal reperfusion injury and the inhibition of MPTP opening by the drug cyclosporine A is speculated as a potential treatment of IRI (Gomez et al., 2009).

Calcium is an important ion in cardiac homeostasis, since it is crucial for the contraction of cardiomyocytes. During ischemia, the energy supply for the myocardium is provided by anaerobic glycolysis, which accumulates protons (H^+) and leads to a subsequent decrease of the pH. An H^+ overload stimulates the sodium (Na^+) - H^+ exchanger and in exchange for Na^+ ions, Ca^{2+} ions are transported into the cell (Dhalla, 2000). This exchange is further stimulated by reperfusion, because oxidative stress adversely influences the Ca^{2+} uniporters in the sarcoplasmic reticulum (SR) and the sarcolemma. Cellular Ca^{2+} overload triggers MPTP opening, as well as electrical and mechanical abnormalities within the cardiomyocytes (Bersohn et al., 1997).

It is unknown which event in IRI triggers and which events are then subsequent. The pathogenesis of IRI is multifactorial, arising from a combination of vascular leakage, sterile inflammation, generation of ROS, MTPT opening and calcium overload. These events influence and exacerbate each other (Figure 4).

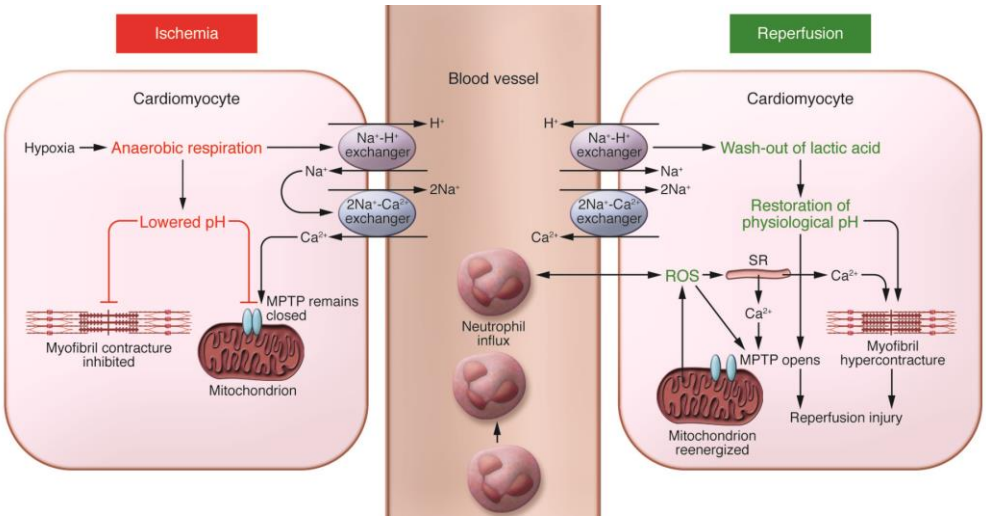

Figure 4. Molecular key events of acute myocardial IRI.
Under ischemia the cell switches to anaerobic metabolism, which induces a decrease of the pH. Proton accumulation creates a Na^+ overload in the cell via the H^+-Na^+ exchanger, which in turn activates the Na^+-Ca^{2+} exchanger to import Ca^{2+}. The resulting acidic conditions induce MPTP opening and hypercontraction of the myocyte. During reperfusion, the electron transport chain is reactivated and generates ROS, which further trigger MPTP opening, attract neutrophils, induce dysfunction of the sarcoplasmic reticulum, membrane oxidation, and DNA damage. Image modified from Hausenloy and Yellon, 2013.

1.5 From physioxia to hypoxia

Oxygen (O_2) is retrieved from the air, which is composed of 78% nitrogen (N_2), roughly 1% argon, 0.04% CO_2 and 21% O_2 at sea level. This oxygen content is referred to as normoxia and corresponds to a partial pressure of 160 mmHg or 21 kPa. The diffusion from the airways of the lung into the blood stream and further to the organs passively follows a concentration gradient. Each tissue has a characteristic pO_2, called physioxia, which depends on its vascularization, its oxygen supply and demand (Carreau et al., 2011).

When the pO_2 value drops below the level of physioxia, as in cardiac ischemia or stroke, cells are experiencing hypoxia. Cellular hypoxia plays also an important role in cancer, when the inner mass of a solid tumor is not sufficiently provided with oxygen. Tumor hypoxia induces angiogenesis, a hallmark of tumor growth and metastasis and is associated with increased aggressiveness and therapy resistance. Noteworthy, hypoxic tumor cells have a distinct epigenetic profile (Ramachandran et al., 2015).

Hypoxia can be experienced during extensive workout but also at high altitude, where the pO_2 is lower than 160 mmHg, which in turn leads to a lower oxygen saturation of the blood; this can cause discomfort, known as altitude sickness.

Interestingly, intermittent periods of mild hypoxia at high altitude are used to improve athletic performance, because the hypoxic stimulus increases the erythrocyte production, which subsequently raises the oxygen binding capacity of the blood (Gore et al., 2007). Moderate experimental hypoxia ranges from 1 – 5% (7.5 – 37.5 mmHg), levels below 1 % are considered to be strongly hypoxic and the absence of oxygen is called anoxia. The physioxia of distinct tissues needs to be taken into account, when designing experimental strategies for *in vitro* ischemia (Table 1).

Table 1. Partial oxygen pressures of air and different tissues in the human body.
Highlighted in red is the value of muscle tissue used as guide value for this study. Table modified from Carreau et al., 2011.

	pO_2	
	mmHg	%
Air	160	21.1
Inspired air (in the tracheus)	150	19.7
Air in the alveoli	110	14.5
Arterial blood	100	13.2
Venous blood	40	5.3
Cell	9.9–19	1.3–2.5
Mitochondria	<9.9	<1.3
Brain	33.8 ± 2.6	4.4 ± 0.3
Lung	42.8	5.6
Skin (sub-papillary plexus)	35.2 ± 8	4.6 ± 1.1
Skin (dermal papillae)	24 ± 6.4	3.2 ± 0.8
Skin (superficial region)	8 ± 3.2	1.1 ± 0.4
Intestinal tissue	57.6 ± 2.3	7.6 ± 0.3
Liver	40.6 ± 5.4	5.4 ± 0.7
Kidney	72 ± 20	9.5 ± 2.6
Muscle	29.2 ± 1.8	3.8 ± 0.2
Bone marrow	48.9 ± 4.5	6.4 ± 0.6

In order to deal with hypoxia, tissues need to adjust their transcriptional programme for survival by promoting red blood cell production, inducing angiogenesis, modulating vascular tone, enhancing glycolysis and cellular glucose uptake, as well as limiting down energy consuming processes.

The hypoxic stress response in mammalian cells is mainly driven by the hypoxia inducible factors HIF-1 and HIF-2. These transcription factors are induced by hypoxia within minutes. HIF-1 is activated as an acute response on hypoxia, whereas HIF-2 increases with time and becomes more important in later phases of hypoxia. Prolonged moderate hypoxia of 5% O_2 stabilizes HIF-2, but not HIF-1, suggesting that HIF-2 might be responsible for the transcription of genes involved in physioxia (Löfstedt et al., 2007).

HIF-1 is composed of the constitutively expressed nuclear HIF-1β subunit (aryl hydrocarbon receptor nuclear translocator, ARNT) and an oxygen dependent cytosolic HIF-1α subunit. The activity of HIF-1α is regulated by protein degradation; in the presence of oxygen, prolyl hydroxylases (PHDs) target HIF-1α for ubiquitination by von Hippel Lindau (VHL) protein and subsequent proteosomal degradation. Additionally, the factor inhibiting HIF-1 (FIH) further prevents the assembly of HIFα with its transcriptional co-activators p300 and CREB binding protein.

Under low oxygen conditions, HIF-1α is no longer targeted for degradation, translocates to the nucleus, dimerises with HIF-1β to form a competent transcription factor which

induces target gene transcription (Semenza et al., 2009). HIF-1 binds to hypoxia responsive elements (HREs) in promoters of hypoxia-inducible genes. More than 70 HIF-1α target genes have been identified, which are associated with the restoration of oxygen hemostasis through induction of vascular growth, vasodilatation, increased oxygen transport, survival with minimal energy production by promoting enzymes for glycolysis, and cell death (Rocha et al., 2007). Energy consuming processes, mRNA translation and initiation of DNA replication, become arrested (Liu et al., 2006, Hammond et al, 2004). However, RNA transcription and translation do not stop completely, as HIF-1 prioritises a set of genes that are expressed under hypoxia.

HIF-1α and -2α were observed to be induced primarily at the border of the infarct in cardiomyocytes, endothelial and fibroblasts cells after experimental cardiac ischemia induced by coronary artery ligation. An increase in HIF-2α protein was also detected in areas remote from the infarct (Jurgensen et al., 2004).

Cells which survive and recover from IRI, or hypoxia, are likely to have a persistent altered gene expression profile, which can either prevent tissues from full recovery, or improve cellular performance in future ischemic events, a phenomenon called ischemic conditioning.

1.6 Ischemic conditioning

In 1986, Murry *et al.* found that cardiac tissue is able to withstand short periods of ischemia without detectable injury and that this induces an ischemic tolerance towards the consequences of a subsequent prolonged ischemic insult. This procedure was named ischemic pre-conditioning (IPC). Four cycles of five minutes of intermitted occlusion of the left-descending artery in dog hearts significantly protected the myocardium during a subsequent artery ligation of 40 minutes, reducing the resulting infarct about 75% (Murry et al., 1986). This IPC stimulus induces an early protection window within the first 2 – 4 hours and a late protection window after 12 – 24 hours. These two protection windows are most likely regulated by different molecular mechanisms (Bousselmi et al., 2014).

How IPC protects the heart from myocardial stunning and necrosis is not fully understood yet. It is known that adenosine, bradykinin, opioids, and endorphins are released into the blood stream upon IPC, and that repeated reperfusion washes off catabolites, like lactate and H^+ from the myocardium. Nevertheless, these facts alone do not explain the strong, enduring protective effect of IPC.

A blood transfusion of an IPC stimulated rabbit into a naïve rabbit induced protection against IRI, arguing for a "blood-borne" factor as a mediator of IPC (Dickson et al., 1999). Since cardiac IPC is a highly invasive procedure and is not applicable to an acute coronary syndrome, post-conditioning was investigated for interventional cardiology. A protocol of two 30-second-cycles of clamping and de-clamping of the ascending aorta before the cessation of the cardiopulmonary bypass revealed a protective effect (Luo et al., 2008). Noteworthy, conditioning effects were abolished in a knock-out mouse model of HIF-1α, indicating the involvement of the hypoxic response in IPC (Cai et al., 2013). The involvement of HIF-1α in modulating the protective effect of IPC also explains that hypoxic conditioning at high altitude can induce resistance towards IR-induced myocardial necrosis, ventricular arrhythmia, and apoptosis (Verges et al., 2015).

In 1993, remote ischemic preconditioning (RIPC) was shown to have similar effects as IPC. This method is non-invasive, since short periods of ischemia and reperfusion are induced by applying a cuff around the upper or lower limb (Przyklenk et al., 1993).

The key features of ischemic conditioning seem to be a adapted repression and activation of specific genes, thus establishing the "tolerosome", a genetic memory-effect, which protects organs from future ischemic damage. This tolerosome, adaptive activity changes in hundreds of genes, is most likely established by epigenetic mechanisms, which can transduce environmental stimuli in genetic memory. Once deciphered, these mechanisms could be manipulated therapeutically.

1.7 Epigenetics

Conventional treatment strategies for myocardial infarction primarily focus on myocardial tissue reperfusion by the restoration of the coronary flow, revascularization and prevention of re-obstruction. Predominantly, the symptoms of IRI are treated, rather than the causes of subsequent inner-cardiac changes, which finally induce heart failure. Epigenetic changes are likely to provide the basis of persistently changed gene expression and subsequent cardiac remodeling after IR.

Cells can quickly and persistently adapt their transcriptional programmes in response to external stimuli, like environmental changes as the availability of oxygen and nutrients. Apart from mutations, every cell of an individual has the same DNA sequence. However, the body consists of 250 different cell types, which all differentiated from one zygote. The basis of this diversity and adaptive potential of the genome is epigenetic regulation,

which enables a tuned read-out of the underlying DNA sequence. The epigenetic landscape of a cell is established by the accessibility of genes by DNA methylation and the modification of histone tails and the regulation of transcriptional output by RNA interference.

1.7.1 The histone code

In eukaryotes, 147 base pairs of DNA are wrapped around a protein octamer consisting of two histone H2A-H2B heterodimers and one histone H3-H4 tetramer (Luger et al., 1997). This complex forms the basic unit of chromatin, the nucleosome (Figure 5). Multiple nucleosome arrays are often compared with beads on string and these arrays can be further coiled into a 30-nm fiber, stabilized by the mobile linker histone H1. This organisation enables two meters of DNA organized into a nucleus with an approximate diameter of 5 – 10µm.

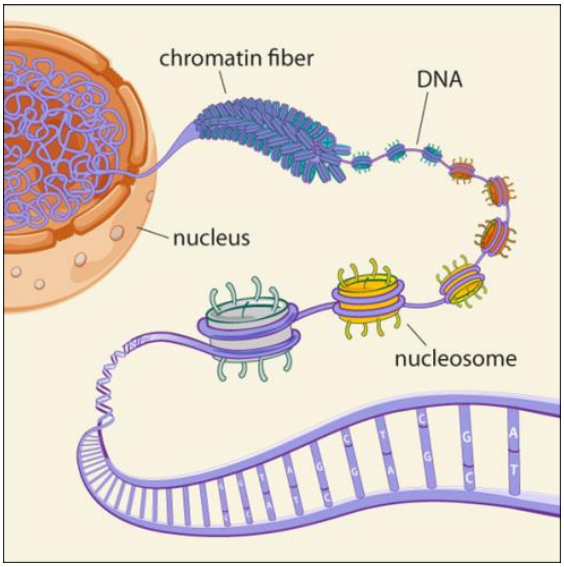

Figure 5. Chromatin organisation.
The chromatin fiber consists of nucleosomes arranged like beads on a string. Protruding tails are targets of chemical modifications, which have further impact on DNA accessibility or binding of transcription factors. Image modified from Broad Communications https://www.broadinstitute.org/news/1504.

The accessibility of nucleosome DNA can also be altered by modifications to the histone proteins. Moreover, modified histone proteins act as a "landing platform" for regulatory proteins that interact with chromatin. All four histone variants have protruding N-terminal tails, which are targets of chemical modification. More than 60 different residues have been identified so far, which can be acetylated, mono,-di,-tri-methylated, phosphorylated, ubiquitinilated, sumoylated, ADP ribosylated, and deiminated (Figure 6).

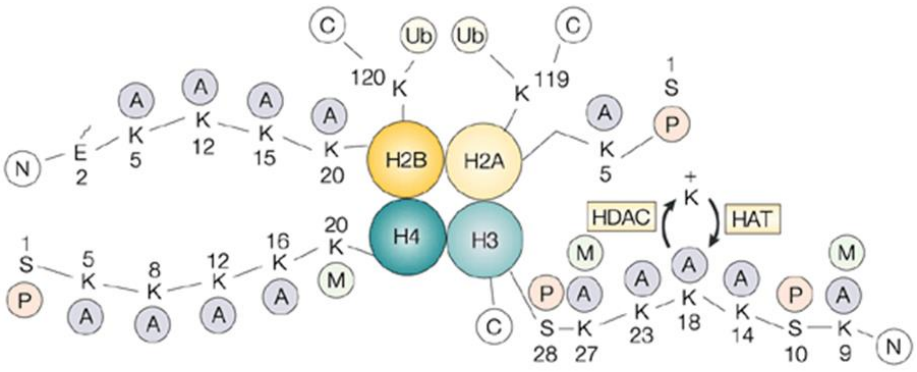

Figure 6. Post-translational modifications of histone tails.
Amino acid residues within the tails of the core histones can be chemically modified. Depending on the combination of modifications, the DNA sequence associated with the particular nucleosome can be accessible for transcription.

Acetylation, phosphorylation, and ubiquitination are associated with gene activation, whereas histone ubiquitination, sumoylation, deimination, and proline isomerization have been implicated in gene repression (reviewed in Kouzarides, 2007). Methylation can be either activating and repressing, depending on the modified residue. Amino acid residues can be reversibly modified with more than one modification, and the resulting histone code determines the transcriptional potential of the DNA by sequence availability and the recruitment of specific readers of these modifications.

Acetylation of positively charged lysine residues within the histone tails neutralizes their charge and presumably weakens the interaction between DNA and nucleosomes, thereby facilitating access to DNA. Histone acetylation is enriched at promoters and the 5' end of the coding regions. Acetylation is performed by histone acetyl transferases (HATs), which transfer an acetyl group from acetyl coenzyme-A (acetyl-CoA) to the amino group of the lysine (K) residue. HATs are grouped by their location in the cell: type A is nuclear and mediates transcription, whereas type B is cytoplasmic and acetylates newly synthesised histones. Further, type A HATs are categorised in different families (GNAT, MYST, p300/CBP), according to their sequence homology, structural features and

functional roles (Kuo et al., 1998). Additionally, HATs also acetylate non-histone proteins, like transcriptional activators, basal transcription factors, structural proteins and polyamines (Wong et al., 1991).

Histone deacetylation is implemented by histone deacetylases (HDACs). The removal of the acetyl group tightens the binding between the DNA and the histone, which hinders transcription. HDACs are grouped in four classes: Class I (HDAC 1 – 3, 8, nuclear) and class II (HDAC 4 – 7, 9, 10) are dependent on zinc, class II members are able to shuttle between the nucleus and the cytoplasm. Zinc-dependent HDACs can be inhibited by hydroxamic acids like Trichostatin A (TSA) and suberoylanilide hydroxamic acid (SAHA), and by the carboxylic acid sodium butyrate. Hydroxamate-based HDACIs have been approved as oncology therapeutics by the US Food and Drug Administration (FDA), as they were found to induce apoptosis and cell cycle arrest (Marks and Dokmanovic, 2005). Class III HDACs, the sirtuins (1 – 7), are dependent on the cofactor nicotinamide adenine dinucleotide (NAD+). HDAC 11 is the only member of class IV and shares similarities between class I and II. Like HATs, HDACs can also modify proteins, apart from histones, like transcription factors and co-regulators.

Histone methylation changes the basic and hydrophobic properties, which can induce or reduce the binding affinity for other proteins. Histone methyl transferases (HMTs) are specific to histone proteins, which can methylate lysines and arginines. Lysine methylation can have different transcriptional outcomes; it can be either repressive, like for histone 3 (H3) lysine 9 (K9), H3K27, and H4K20, or promote transcription, as for H3K4, H3K36, and H3K79. HMTs are categorized in SET domain-containing HMTs, which transfer the methyl group of S-adenosyl methionine (SAM) onto lysine residues within the histone tails, and non-SET domain-containing HMTs, which methylate the globular core of the histone (Ng et al., 2002).

Lysine demethylases (LSDs) catalyze the removal of methyl groups. So far, two demethylase families are characterised: the LSD1 domain containing family, which are flavin adenine dinucleotide (FAD)-dependent amine oxidases and the Jumonji C (JmjC) domain family, which are dependent on iron, oxogluterate, and oxygen (Pedersen et al., 2010). Also arginines within histone tails can be methylated and demethylated; for the estrogen regulated pS2 promoter arginine methylation/demethylation was shown to be cyclic, switching it from the off to the on state (Metivier et al., 2003).

Beside direct steric effects, histone modifications can recruit proteins, which further interpret or modify the histone code. It is known, that certain modifications can provoke

others, so that the context of the modifications is influencing their effect. For example, H3K27me recruits a polycomb group (PcG) protein with ubiquitin ligase activity for H2A, and H3K9me is bound by the heterochromatin-protein 1 (HP1), which has deacetylase and methyltransferase activity.

Highly condensed DNA, decorated predominantly with marks repressive for transcription, is called heterochromatin. Open, transcriptionally active chromatin is referred to as euchromatin. For transcription to occur, the start side of a gene needs to be accessible for the RNA polymerase II (Pol II) and the transcriptional machinery, therefore it is necessary to loosen and remove the nucleosomes from the initiating stretch of DNA. This is achieved by nucleosome remodeling, mediated by the Switch (SWI)/Sucrose Non-Fermentable (SNF) complex or INO80, which move nucleosome(s) away from DNA by disrupting interactions between the DNA and the histones, using energy from ATP hydrolysis (reviewed in Flaus et al., 2003).

Post-translational histone modifications (PTMs) are dynamic and can change within minutes enabling fast genomic regulation upon environmental stimuli, like energy status or oxygen availability. It is likely that the chromatin landscape during ischemia is shaped by changes in PMTs, which could be potential drug targets, due to their reversibility.

1.7.2 DNA methylation

DNA methylation is an epigenetic modification causing gene repression, as found for genomic imprinting (Li et al., 1993), X-chromosome inactivation (Panning et al., 1996) and retro-element silencing (Walsh et al.,1998). The DNA base cytosine can be methylated at the 5’-position in regions of the genome, which are rich of cytosine-phosphate diester-guanine islands (CpG sites) (Figure 7). Unmethylated CpG sites mostly occur in clusters at the 5' end of regulatory regions of many genes.

Methylation of cytosine residues is performed by DNA methyl transferases (DNMT) using SAM as the methyl donor; DNMT1 is responsible for methylation maintenance, whereas DNMT3a and 3b are responsible for *de novo* methylation after DNA replication. Repression of gene transcription by DNA methylation can be induced directly via physical impairment of transcription factor binding, or indirectly by the binding of methyl-CpG-binding domain proteins (MBDs), which recruit further inhibitors of transcription like histone deacetylases (Nan et al., 1998).

Another modification of the 5' position of cytosine is hydroxymethylcytosine (5hmC), which is present at high levels in human and mouse neurological tissue (Kriaucionis et al., 2009). The formation of 5-hmc is catalyzed by the Ten-eleven translocation (TET) enzymes and speculated to be an intermediate state of oxidative DNA demethylation pathways, but it could also be a further level of epigenetic regulation (Dahl et al., 2011). Besides 5mC and 5hm, also 5-formylcytosine (5fC) and 5-carboxycytosine (5caC) residues exist but their impact on the genome is not fully understood yet.

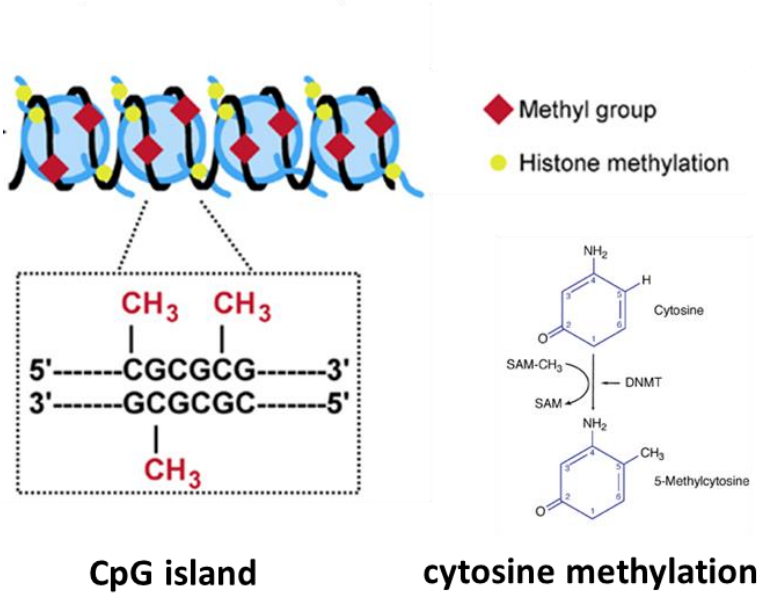

Figure 7. DNA methylation.
Cytosine residues can be methylated within CpG islands by DNA methyl transferases. This methylation can be accompanied by histone methylation and induces heterochromatin formation and gene repression. Image modified from http://dx.doi.org/10.3389/fpsyt.2013.00080.

1.7.3 non-coding RNAs

Non-coding RNAs (ncRNAs) include short ncRNAs, which are less than 30 nucleotides long, like micro (mi), small interfering (si), and PIWI-interacting (pi) RNAs, and long non-coding (lnc) RNAs, consisting of more than 100 nucleotides. Unlike mRNAs, these RNAs are not coding for proteins but can regulate gene expression as epigenetic regulators defining DNA methylation patterns and recruiting chromatin remodelers (Gomes et al., 2013).

miRNAs are transcribed by Pol II from pseudogenes, introns, and repeats. miRNAs induce the cleavage, destabilization or impaired translation of its partly complementary mRNA sequence and promote a post-transcriptional regulation of genomic output (Bartel, 2009). miRNA transcripts are capped at the 5' end, polyadenylated and spliced.

The resulting pre-miRNA hairpin structures are cleaved by the microprocessor complex within the nucleus and transported into the cytoplasm, where they are cleaved by the RNAse Dicer, creating a miRNA duplex of 22 nucleotides (Gregory et al., 2004, Lee et al., 2003). One strand of the mature miRNA is further incorporated in the RNA-induced silencing complex (RISC), binds to the complementary mRNA sequence and impairs the translation into a protein or induces its degradation (Figure 8). It is believed that about 60% of protein coding genes are regulated by miRNAs and that their transcription is regulated by DNA methylation and histone modifications.

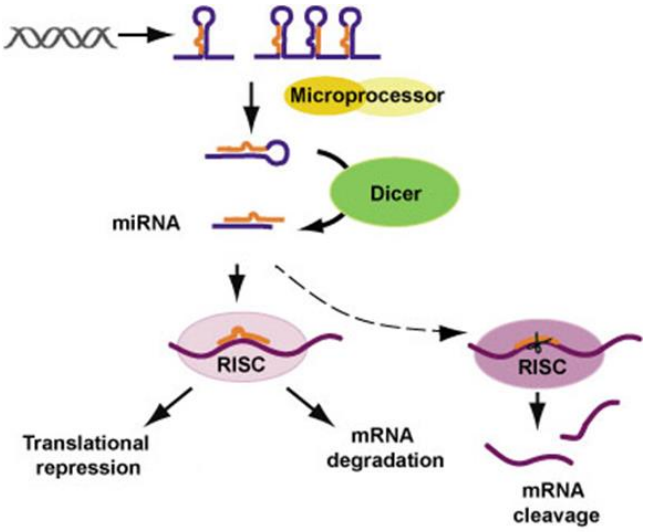

Figure 8. miRNA biogenesis and posttranscriptional gene silencing.
miRNA transcripts are processed sequentially by the RNAses Microprocessor and Dicer. The mature miRNA strand is further incorporated into the RISC complex, which recognizes the target mRNAs and down-regulates their expression via degradation or impaired translation. Image: https://mcb.berkeley.edu/faculty/CDB/hel.html.

siRNAs are similar to miRNAs but completely complementary to their target sequences and they generally induce target degradation via the Dicer-RISC pathway. siRNAs can be of exogenous origin but they can also originate from endogenous lncRNAs (Gomes et al., 2013).

piRNAs are involved in heterochromatin formation and maintenance of the genome integrity by suppressing transposon activity in the germline and in somatic cells. piRNAs are mainly transcribed from pericentromeric or subtelomeric domains, but also from transposable elements and 3' untranslated regions (UTRs) of protein-coding genes.

lncRNAs are transcribed from intergenic and promoter regions but their sequences can also overlap antisense to annotated protein-coding genes. lncRNAs are processed like

mRNAs, show cell-specific expression patterns, and can recruit histone and chromatin modifiers, as well as transcription factors. A well-studied example is the lncRNA X-inactive specific transcript (Xist), which recruits the Polycomb repressive complex 2 (PRC2) to the X chromosome leading to its inactivation (Zhao et al., 2009).

1.8 Nuclear architecture

Nuclear architecture is a dynamic product of epigenetic modifications and contributes to genomic regulation. Chromosomes are not distributed randomly within the nucleus, but occupy distinct territories, called chromosome territories (CT) (Cremer et al., 2010). The position of a chromosome influences the transcription of the genes located within. Further, the transcriptional activity of specific genes has been correlated with their positioning relative to the periphery of the nucleus (Peric-Hupkes et al., 2010). Moreover, the three-dimensional folding of the chromosomes provokes contact between distant functional elements via looping, such as promoters and enhancers.

The basic elements of CTs are chromatin domains (CDs) with a DNA content of a few hundred kilobases to several megabases (Cremer et al., 2001). The DNA-free space between the chromosome territories is referred to as the interchromatin compartment (IC) and is constituted of a network of channels and lacunas, which dynamically contract or expand according to the state of chromatin condensation. The IC channels initiate from the nuclear pore complexes and expand through the periphery of the nucleus as well as into the interior of CTs. The size and shape of the IC depend on the cell type. The IC in rat liver endothelial cells represents about 40 % of the total nuclear volume, whereas it is about 60 % in rat hepatocytes (Rouquette et al., 2009).

Further, the nuclear architecture changes during development: It was shown by Popken *et al* in 2014 that a major lacuna formed in the nuclear interior of 8-cell stage bovine preimplantation embryos and that the chromosome territories (CTs) were shifted to the nuclear periphery. This developmental stage is characterised by activation of the genome. Upon further development, this organisation was reversed, the major lacuna disappeared, and CTs were redistributed throughout the nuclear interior (Popken et al., 2014).

Chromatin loops can expand into the IC to achieve access to molecules, like nuclear bodies, splicing speckles, and other proteins involved in the processing of the genomic output. Active, de-condensed chromatin forming loops on the surface of compacted, inactive chromatin is called perichromatin (PR). These two different chromatin

compartments are referred to as chromatin domain clusters (CDCs). The PR region harbours transcription factories consisting of active genes, RNA-Pol II clusters, nascent RNA and DNA. The maintenance of the PR is dynamically regulated by histone acetylation and other active histone marks, like H3K4me3, whereas the interior of CDCs are buried under repressive histone marks, like H3K9me3 and H3K27me3 (Görisch et al., 2005) (Figure 9).

Although this overall model of functional nuclear architecture is speculative, recent findings in the field of super resolution microscopy and chromatin conformation capture assays followed by deep sequencing (HiC) support these concepts (for review see Thomas Cremer et al., 2015). It was further shown, that chromatin architecture can respond quickly to environmental stimuli: Hyperosmotic conditions, as well as ATP depletion, induce chromatin condensation (Albiez et al., 2006, Visvanathan et al., 2013). As ischemia decreases intracellular ATP levels and provokes major changes in transcriptional output, it can be anticipated that ischemia can further lead to significant changes in nuclear architecture.

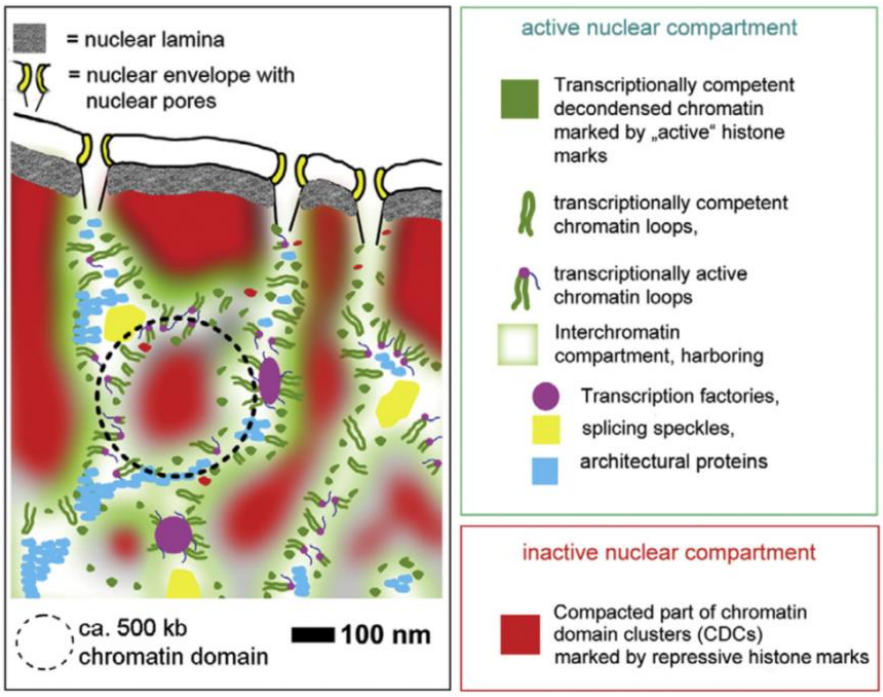

Figure 9. Chromatin compartments.
The active perichromatin (green) covers the inactive chromatin (red) and is in contact with the interchromatin compartment (white), where transcription takes place. Image modified from T. Cremer et al., 2015.

1.9 Epigenetics in hypoxia and ischemia-reperfusion injury

Hypoxia and ischemia provoke dramatic alterations in gene expression, which are likely to be the result of changes to the chromatin landscape. It is known that HIF-1α can recruit chromatin modifiers, like SWI/SNF, to target genes, is able to associate with HATs, like p300/CBP and steroid receptor co factor-1 (SRC-1), and can form complexes with HDAC4, 5 and 7 (Melvin and Rocha, 2012). HIF-dependent activation or repression of a gene is determined by epigenetic events. It was found that HDAC activity is necessary for 70 % of all HIF target genes and that genes coding for HDAC 1, 2, 4 and 11 are upregulated in hypoxia (Kasper et al., 2005, et al., 2006). Increased histone acetylation was reported for specific gene loci, like the promoters of vascular endothelial growth factor (VEGF), erythropoietin (EPO), early growth response protein 1 (EGR1) and others, which are found to be highly transcribed under hypoxia (Perez-Perri et al., 2011).

Hypoxia induces a set of histone modifications at gene promoters. Since individual gene promoters are non-suitable drug targets, global changes are of particular interest. Thus far, only few studies have reported on global alterations in histone modifications: A general decrease in histone acetylation under hypoxia was reported for H3K9, H3K16, and H4 (Johnson et al., 2008) (Dmitriev et al., 2015, Qin Li, 2009). However, it can be assumed that under hypoxia, when cellular metabolism switches to anaerobic glycolysis and pyruvate is converted to lactate instead of acetyl-CoA, protein acetylation becomes generally impaired.

JmjC domain containing histone demethylases (JHDM), which are dependent on oxygen and resemble FIH, are poised to respond to hypoxia. It was shown that 17 out of 22 characterised JHDMs are transcriptionally induced under hypoxia and at least four of them are targets of HIF-1α (Yang et al., 2009). Their transcriptional upregulation is assumed to be a compensative mechanism for their impaired enzymatic activity under low oxygen concentrations (Xia et al., 2009). However, a global increase in di- and tri-methylation of K9 and H3K4me was reported under hypoxic conditions (Johnson et al., 2007).

Global DNA hypomethylation was reported within the hypoxic tumor environment (Hattori et al., 2015) (Shahrzad, Bertrand, Minhas, 2007). A specific group of miRNAs, the hypoxamirs, are only transcribed under hypoxic conditions. It was found that HIF can induce some of the hypoxamirs, while it represses the transcription of other miRNAs (Nallamshetty et al., 2013). Correspondingly, several miRNAs were identified as

potential biomarkers for myocardial infarction and can be detected in the blood stream of MI patients (reviewed in Udali et al., 2013)

Not only hypoxia, but also cardiac ischemia-reperfusion introduces subsequent epigenetic changes, which influence the resulting tissue damage. In correlation with gene expression, alterations in histone modifications and DNA methylation were reported for specific promoter regions, like for nitric oxide synthase (NOS) and VEGF (reviewed in Webster et al., 2013). HDAC activity seems to be highly involved in myocardial infarction. In a murine model of IR, a global loss of pan-acetylation of H3 and H4 was reported. Administration of group I and II HDAC inhibitors, TSA or Scriptaid, minimized the resulting infarct by half, prevented the induction of HIF-1α, and reduced cell death and vascular permeability. Treatment with inhibitors 12 hours post-reperfusion revealed no effect, arguing for an earlier epigenetic treatment window (Granger et al., 2008). Pre-administration of inhibitors of histone demethylases, like deferoxamine mesylate salt (DFOM), and dimethyloxaloylglycine (DMOG) were shown to reduce the infarct size in stroke in mice, independent of their effect on HIF-1α stability (Zeynalov et al., 2009). These studies were the first to prove a general epigenetic component in the pathogenesis of cardiac IRI and stroke, and might pave the way for novel therapeutic approaches. It is speculated, that the tolerosome upon ischemic conditioning is mediated by epigenetic mechanisms, which have the power to transduce sub-lethal stresses in durable gene expression patters, triggering an adaptive programme (Gidday et al., 2015).

1.10 Objectives

There is a gap in knowledge about how chromatin globally reacts upon IR. The identification of a global, common reaction of different cell types on IR and hypoxia would reveal a powerful therapeutic target, not only for MI, but also for other diseases with an ischemic component, like stroke, organ transplantation, and cancer.

Previous studies have shown that chromatin is able to respond to external stimuli, like changing osmotic conditions (Albiez et al., 2006), and the introduction of positively charged molecules and ions (Visvanathan et al., 2013). These dramatic changes in nuclear architecture must have consequences on the transcriptional output. Further, histone modifications were shown to change under hypoxic, as well as ischemic conditions.

Inhibition of histone deacetylation in an IR mouse model improved survival after infarction and decreased the infarct size (Granger et al., 2008).

Chromatin is not only a sensor of changing conditions; it can react, adapt, and establish a memory. The objective of this work is an integrative analysis of chromatin nanostructures and histone modifications, as well as their influence on transcriptional output under cardiac IR and hypoxia/reoxygenation of the cardiomyocyte cell line HL-1.

Upon identification and characterisation, these changes can be manipulated rationally and analysed for their beneficial outcome in therapies.

2. Materials and Methods

2.1 Materials

Table 2. Reagents.

Name	Rereference	Company
2-Deoxy-D-glucose	D8375	Sigma-Aldrich
Acrylamide	1610154	Bio Rad
Ammonium persulfate	A3678	Sigma-Aldrich
β-mercaptoethanol	4227.3	Carl Roth
Bovine serum albumin	A3675	Sigma-Aldrich
Bromouridine	850187	Sigma-Aldrich
Catalase	C1345	Sigma-Aldrich
Claycomb Medium	51800C	Sigma-Aldrich
Coomassie Plus	23236	Life Technologies
Diethylpyrocarbonate	D5758	Sigma-Aldrich
Difluoromethylornithine hydrochloride hydrate	D193	Sigma-Aldrich
DMP-30	00553	Polysciences Inc.
Dodecylsuccinic anhydride (DDSA)	00563	Polysciences Inc.
Dulbecco's Phosphate Buffered Saline (DPBS)	BE17-512F/12	Lonza
Dulbecco's Modified Eagle Medium (DMEM)	BE12-614F	Lonza
ECL Chemiluminescent Substrate Reagent Kit	WP20005	Invitrogen
Ethanol reagent grade	1009831000	Merck
Fetal bovine serum	F2442	Sigma-Aldrich
Fibronectin	F-1141	Sigma-Aldrich
Fixogum	290117000	Marabu
Gelatin from bovine skin	G9391	Sigma-Aldrich
Glucose	G0350500	Sigma-Aldrich
Glucose Oxidase	G2133	Sigma-Aldrich
Glutaraldehyde	G5882	Sigma-Aldrich
Glycerol	G5516	Sigma-Aldrich
Glycine	G8898	Sigma-Aldrich
HEPES	H3375	Sigma-Aldrich
L-Ascorbic acid sodium salt	A7506	Sigma Aldrich
L-Glutamine	17-605E	Lonza
Lithium chloride	L4408	Sigma-Aldrich
Methanol	8388.5	Carl Roth
Nadic methyl anhydride	00886	Polysciences Inc.
Norepinephrine [(+-)-Arterenol]	A0937	Sigma-Aldrich

Name	Rereference	Company
Osmium tetroxid	201030-100MG-D	Sigma-Aldrich
Paraformaldehyde (PFA)	16005	Sigma-Aldrich
phenylmethanesulfonyl fluoride	P7626	Sigma-Aldrich
Picodent Twinsil	1300 1000	Picodent
PolyBed 812	08791	Polysciences Inc.
Ponceau	P3504	Sigma-Aldrich
Protein G beads	LSKMAGG02	Milipore
Protease Inhibitor Cocktail	04693159001	Roche
RPMI medium	32404-014	Gibco
Sodium butyrate (SB)	B5887	Sigma-Aldrich
Sodium cacodylate trihydrate	C0250	Sigma-Aldrich
sodium dodecyl sulfate	L3771	Sigma-Aldrich
Soybean trypsin inhibitor	T6522	Sigma-Aldrich
Sucrose	84097	Sigma-Aldrich
Tetramethylethylenediamine	T9281	Sigma-Aldrich
Trichostatin A	T8552	Sigma-Aldrich
Triton-X 100	T8787	Sigma-Aldrich
Trizol	15596-018	Ambion
Tween-20	P1379	Sigma-Aldrich

Table 3. Antibodies.

Name	Reference	Company
anti-Histone H3 (tri-methyl K4)	04-745	Millipore
anti-Histone H3 (acetyl K9)	9649	Cell Signaling Technology
anti-Histone H3 (tri-methyl K9)	39161	Active Motif
anti-Histone H3 (acetyl K14)	5275s	Cell-Signaling
anti-Histone H3 (acetyl K14)	ab82501	Abcam
anti-Histone H3 (acetyl K27)	ab4729	Abcam
anti-Histone H3 (tri-methyl K27)	39155	Active Motif
anti-Histone H3 (phospho S28)	ab5169	Abcam
anti-Histone H3	ab1791	Abcam
anti-Lamin B1	ab16048	Abcam
anti-spermidine/spermine	ab26975	Abcam
anti-rabbit Alexa 488	A-11034	Invitrogen
anti-rabbit Alexa 647	A-21245	Invitrogen
Anti-rabbit HRP	sc-2030	Santa Cruz Biotechnology

Table 4. Enzymes.

Name	Reference	Company
Alkaline phosphatase	EF0651	Fermentas
DNAseI	M0303S	New England Biolabs
Micrococcal Nuclease	Mo247S	Bio Labs
Nucelase P1	N8630-1VL	Sigma-Aldrich
Proteinase K	311315	Invitrogen
RNase Cocktail	AM2286	Ambion
Snake venom phosphodiesterase	P3243-1VL	Sigma-Aldrich
5% Trypsin-EDTA(1X)	25200-056	Life technologies, UK

Table 5. Kits.

Name	Reference	Company
ATP Determination Kit	A22066	Molecular Probes
High Sensitivity DNA Kit	5067-4626	Agilent
NEBNext ChIP-Seq Library Prep Master Mix Set	E6240S	New England Biolabs
RNA 6000 Nano Kit	5067-1511	Agilent
TruSeq RNA Library Preparation Kit v2	S-122-2001	Illumina
Qubit® dsDNA HS Assay Kit	Q32851	Molecular Probes

Table 6. DNA dyes

Name	Reference	Company
DRAQ5	ab108410	Abcam
Hoechst 33342	B2261	Sigma-Aldrich
Vibrant DyeCycle Violet	V35003	Life technologies
YOYO-1	Y3601	Life technologies

Table 7. Instruments.

Name	Type	Company
Bioanalyzer	2100	Agilent
Confocal microscope	TCS SP5 II	Leica, Germany
DNASequencer	HiSeq	Illumina
Electrocardiogram		Hugo Sachs Elektronik
Electrical homogenizer	T25 Ultra-Turrax	IKA
Flow cytometer	Fortessa LSR	BD Biosciences
hypoxia chamber	Whitley H35	Don Whitley Scientific LTD
NanoDrop	2000	Thermo
Rodent respirator	Typ 845	Hugo Sachs Elektronik
Super resolution microscope (Lemmer et al., 2008)	SPDM	Cremer group, IMB

Table 8. Software.

Name	Type	Company
Genomatix Genome Analyzer	v3.40820	Genomatix Software GmbH
FastSPDM	"R" programme	Gruell et al., 2011
ImageJ	Java programme	Wayne Rasband
LAS AF	Lite	Leica
Mendeley	1.14	Mendeley Ltd.
Microsoft Excel	2010	Microsoft
Microsoft Word	2010	Microsoft
Microsoft PowerPoint	2010	Microsoft

2.2 Methods

2.2.1 Mouse model of ischemia-reperfusion injury

Male mice of the laboratory inbred strain C57BL/6 were used for all animal experiments. The mice had an average weight of 20 g and were two to three months old. Animals were anaesthetised with an intraperitoneal injection of a mixture of 5 mg/kg Midazolam, 0.5 mg/kg Medetomidin and 0.05 mg/kg Fentanyl. The eyes were protected from drying out by the application of Bepanthen eye cream. The depth of narcosis was determined by the middle toe reflex. The thorax was unhaired with depilatory cream and mice were fixed on a heating plate at 37 °C and intubated and ventilated with a rodent respirator. The skin of the chest was disinfected with Cutasept and a medioclaviculary cut of 1 cm length was set at the left side of the body. After cutting through the *musculus pectoralis major* and *musculus pectoralis minor*, the upper and lower rip of the surgery window were spread with a 6-0 Prolene thread. The intercostal muscles were cut and the pericard was removed. The left arteria descendens (LAD), which is located mediolateral from the left atrium, was permanently ligated with an 8-0 Prolene thread. If the ligation was successful, the myocardium turned white and excitation disturbances were visible on the electro cardiogram (ECG). Subsequently, the muscles and the rib cage were sutured and narcosis was antagonized with a subcutaneous injection of 0.05 mg/kg Atipamezol and 0.01 mg/kg Flumazenil (Figure 10). Analgesic treatment was provided by subcutaneous injection of 0.075 mg/kg Buprenorphin. Animals which received a placebo surgery (SHAM) experienced the same treatment as the infarct animals, except the LAD ligation.
This particular treatment protocol of ischemia-reperfusion was designed with a ligation time of 60 minutes, adopted from the duration of the onset of acute myocardial infarction

until the treatment in hospital (Steg et al., 2012). After 60 minutes of ischemia, the ribcage was re-opened, the thread was removed and the myocardium was reperfused. The tissues were sutured, mice were supplied with analgesics and allowed to recover for two, four and 24 hours before removing their hearts for analysis. Hearts analysed without reperfusion were harvested directly after 60 minutes of ischemia. For harvesting the hearts, mice were sacrificed under narcosis by overstretching the neck. The ischemia-reperfusion surgeries were performed together with Stefanie Finger, PhD student at the Centrum for Thrombosis and Hemostasis (CTH), University Medical Center Mainz.

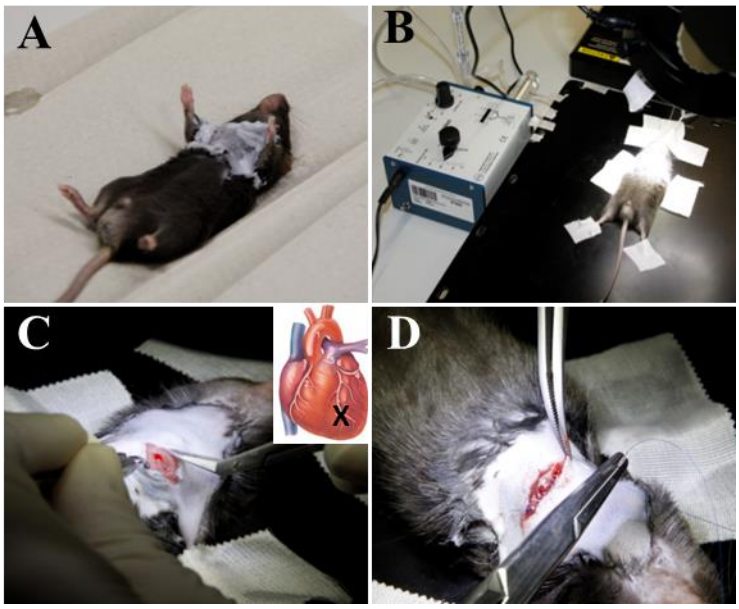

Figure 10. Surgery for the induction of myocardial infarction.
A. Unhairing of the anesthetized mouse. **B.** Fixation of the mouse, intubation and connection to a rodent respirator. **C.** Medioclaviculary cut at the left side of the body. **D.** Suture of the rib cage after surgery.

2.2.2 Cell culture

HL-1 cells are a cardiac muscle cell line derived from a murine atrial cardiomyocyte tumour lineage, which retains the morphology and gene expression profile of adult cardiomyocytes, as well as the ability to contract (Claycomb et al., 1998). HL-1 cells were seeded in either 3.5 cm, 10 cm or 20 cm diameter tissue culture dishes coated with 200 µl, 1 ml or 2 ml of 0.02 % gelatine and 0.005 mg fibronectin and cultured in 2 ml, 10 ml or 20 ml of Claycomb medium supplemented with 2 mM glutamine, 0.1 mM norepinephrine, and 10 % fetal bovine serum (FBS) in an incubator at 37 °C, 5 % CO_2 and 95 % humidity. The cells were passaged at full confluence every three days as

indicated in Claycomb *et al.*, 1998. Experiments were performed at 80 – 100% confluence. This cell line was a kind gift of Professor Claycomb from the LSU School of Medicine in New Orleans.

HeLa cells are a stable human epithelial cell line obtained from a cervix carcinoma. HeLa cells were seeded in uncoated culture dishes as indicated above and maintained in Dulbecco's Modified Eagle Medium (DMEM) supplemented with 2 mM glutamine and 10 % FBS. The cells were passaged before reaching 80 % confluence. Experiments were performed at 40 – 70% confluence. 3T3 cells are a standard fibroblast mouse cell line, which was established from primary mouse embryonic fibroblasts cultured with the "3T3 protocol" (3-day transfer, inoculum 3 x 10^5 cells). These cells were maintained as indicated for HeLa cells.

The mouse cardiac endothelial cell line (MCEC) was prepared from microvascular neonatal mouse cardiac endothelial cells by the transfection with lentiviral vectors carrying SV40 antigen and human telomerase. MCEC display normal endothelial characteristics, markers and intercellular junctions (CELLutions Biosystems Inc., 2013). The cells were seeded as indicated for HeLa cells and maintained in DMEM high glucose without pyruvate, supplemented with sodium bicarbonate,10 mM 2-(4-(2-Hydroxyethyl)-1-piperazinyl)-ethansulfonic acid (HEPES) and 5 % FBS. MCEC were passaged and experiments were performed before the cells reached 80 % confluency.

Passaging of all cell lines was performed in the same way; the cells were washed with 2 ml, 10 ml, 20 ml of phosphate buffered saline (PBS) and detached with 200 µl, 1 ml or 2 ml of 0.25 % trypsin. The cells were collected in culture medium, centrifuged at 300 g for 5 min, resuspended, counted, and seeded in the respective medium and desired dish size.

2.2.3 Oxygen and Nutrient Deprivation (OND)

OND was used as an *in vitro* model of ischemia. Acute, moderate hypoxia was simulated by a one hour incubation of the cells in a hypoxia chamber (H35 Don Whitley Scientific), providing an atmosphere of 1 % O_2, 5 % CO_2, 94 % N_2 and 60 – 75 % humidity (Figure 11). A lack of nutrients was emulated by adding 2 ml, 10 ml or 20 ml of balanced salt solution without amino acids, pyruvate or glucose. The buffer also contained deoxyglucose which is an inhibitor of glycolysis. The formula of the ischemic stress buffer (115 mM NaCl, 1.2 mM $MgCl_2$, 12 mM KCl, 2 mM $CaCl_2$, 25 mM HEPES,

5 mM deoxyglucose) was modified from Vivar et al., 2012. One hour prior to OND, the buffer was put inside the hypoxia chamber to equilibrate to 1 % O_2 content. Samples analysed without reoxygenation, were OND treated and fixed or lysed under hypoxic atmosphere inside the chamber. Reoxygenation of the samples was performed by removing the ischemic buffer, washing the cells with PBS, adding medium, and returning to normoxic culture conditions for 5, 15, 60 and 240 minutes.

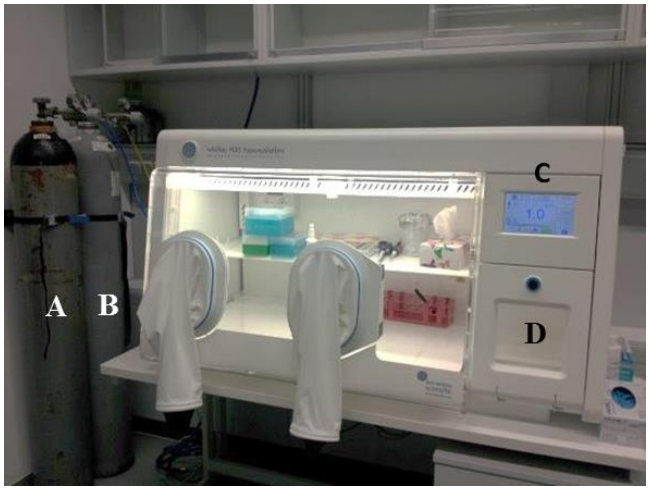

Figure 11. Hypoxia chamber.
A. Nitrogen replaces the oxygen inside the chamber, **B.** 5 % of CO_2 gas are added to the nitrogen atmosphere, **C.** control panel for O_2, CO_2, N_2, temperature and humidity, **D.** Lock for introducing material into the chamber.

2.2.4 Next Generation Sequencing of cardiac tissue

Next generation sequencing (NGS) is a technique for the analysis of the transcriptome of a population of cells, or even a single cell.

The samples for transcriptome analysis comprised triplicates of non-reperfused infarcts and infarcts, which had been reperfused for 2, 4, or 24 hours. Cardiac tissue of the infarcted area were cut from the heart, washed in ice cold PBS and were immediately snap frozen in liquid nitrogen. The infarcts were determined by their position in the heart and the colour of the tissue; the weight of the pieces was between 20 – 80mg.

The RNA was extracted following the Trizol extraction protocol. Centrifugation was performed at 12000 x g at 4 °C and incubations were performed at room temperature. Briefly, the tissues were homogenised in 1 ml of Trizol reagent with an electrical homogeniser and incubated for 5 min. Subsequently, 200 µl of chloroform were added, the samples were vortexed for 15 seconds and incubated for three minutes. After

centrifugation for 15 min, the aqueous supernatant was collected and 0.5 ml of isopropanol was added. After 10 min of incubation, the samples were centrifuged for 10 min and the resulting pellet washed with 1 ml of 75 % ice cold ethanol, centrifuged for 5 min at 7500 x g, air dried, and resuspended in 30 µl of Diethyldicarbonat (DEPC) treated, RNAse-free water. The RNA content was determined with NanoDrop and the RNA integrity number (RIN) was calculated using a Bioanalyzer 2100. The RIN is calculated from the ratio of the ribosomal bands; a RIN of 10 indicates the highest quality to be achieved. Only samples with a RIN higher than 8 were used for subsequent library preparation.

Sequencing libraries were prepared according to the TruSeq sample protocol with the TruSeq RNA Library Preparation Kit v2 (Illumina). Five micrograms of total RNA were used as input for the library preparation. The first step of the protocol selects for mRNAs, by binding their poly-A tails to poly-T beads; unbound RNAs were washed off. Reverse transcriptase was used to produce a cDNA template in a polymerase chain reaction (PCR). In the subsequent second strand PCR, the RNA template is removed and the cDNA becomes double stranded. The end repair reaction converts the overhangs of the cDNA into blunt ends. The adenylation of the 3' ends prevents self-ligation during the adapter ligation. The 6 – 8 bp long adapters, also called barcodes or indexes, are short sequences, comprising A, T, C, and G nucleotides, which were attached to every sample for future identification and hybridization to the flow cell. The barcoded cDNA libraries become enriched in a final PCR reaction with 25 cycles.

The resulting sequencing libraries were evaluated with the Bioanalyzer for their respective size and concentration. Because every sample had its own identifier, the samples could be pooled in equimolar ratios and submitted for sequencing on an Illumina HiSeq instrument. The amount of samples per flow cell is limited by the desired sequencing depth. The samples were sequenced from one end as 50 bp single reads. Before sequencing, the libraries were denatured, distributed over the flow cell, hybridized to the surface and undergo "bridge amplification", in order to create clonal clusters of single stranded DNA molecules. The Illumina technique is based on sequencing by synthesis: A fluorescently labeled reversible terminator-bound dNTP is added, incorporated by a DNA polymerase and the fluorescent pattern of several clusters is detected by a camera and computationally reconstructed into sequences (Figure 12). Then the terminators are cleaved and washed off to allow the incorporation of the next base

along the growing DNA strand (http://www.illumina.com/technology/next-generation-sequencing/sequencing-technology.html).

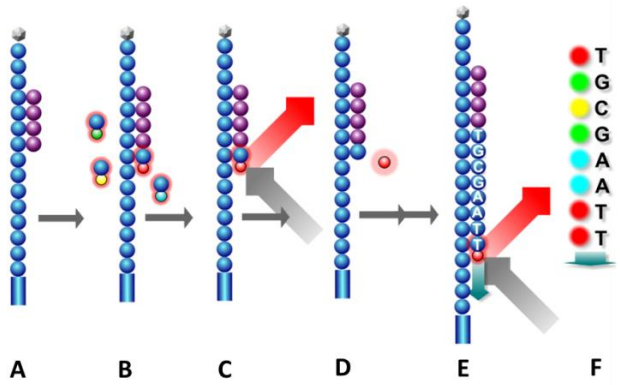

Figure 12. Sequencing by synthesis.
A. The denatured sequencing library is hybridized to a flow cell. **B.** A fluorescently labeled reversible terminator-bound dNTP is incorporated by a polymerase. **C.** The incorporated fluorescently labeled dNTP is exaggerated by a laser and the emission is detected. **D.** The terminator is cleaved from the dNTP. **E.** The next fluorescently labeled reversible terminator-bound dNTP becomes incorporated. **F.** The fluorescent signals are translated into the bases, reading-out the sequence of the library. Figure adopted from Abizar Lakdawalla, http://www.crick.ac.uk/research/science-technology-platforms/advanced-sequencing/.

2.2.5 Next Generation Sequencing of HL-1 cells

In order to compare *in vivo* ischemia with *in vitro* ischemia, RNA samples obtained from HL-1 cells after OND and recovery were subjected to NGS. Triplicates of HL-1 cells were treated with OND only, or treated with OND followed by a recovery of 1 hour or 4 hours. Controls were left untreated. The RNA was extracted with Trizol, sequencing libraries were prepared according to the TruSeq sample protocol and sequenced as indicated in 2.2.4.

2.2.6 NGS data analysis

The raw data was analysed in regard of read quality, sequence bias, and duplication rate and mapped to the mouse genome version mm9 with STAR (version 2.4, max. two mismatches per read). Additional quality controls of the mapped reads were performed to check for gene body coverage, specific RNA types and batch effects, to ensure most accurate results. This work was performed by the Core Facility Bioinformatics at IMB.
The mapped Bam files were further subjected to comparative differential gene expression analysis using edgeR (Expression analysis for RNAseq, Genomatix). Gene lists were sorted for up- and down-regulation, thresholded for p-values lower than 0.005 and a fold

change higher than 2. Gene Ontology (GO) terms for "biological processes" (GeneRanker, Genomatix) were thresholded for p-values lower than 9E-05.

2.2.7 Western Blot analysis

Western Blot analysis is a technique to identify and quantitate proteins of interest, expressed in a population of cells. For the analysis of posttranslational modifications, histones were acid extracted from cell nuclei following the abcam histone extraction protocol (www.abcam.com/ps/pdf/protocols/histone%20extraction%20protocol.pdf). Histones are basic proteins, which are highly soluble in acidic solutions. This protocol conserves histone modifications, if appropriate inhibitors are added to the extraction buffer.

Briefly, cells were grown in 10 cm dishes and subjected to OND with and without recovery, or kept under control conditions. The dishes were washed with 10 ml of PBS supplemented with 5 mM sodium butyrate (SB) to maintain acetylation levels during sample preparation. The cells were scraped in 800 µl of Triton Extraction buffer (TEB; 0.5 % Triton X-100, 2 mM phenylmethylsulfonyl fluoride (PMSF), protease inhibitor, 5mM SB in PBS) and lysed for 10 min on ice. After centrifugation at 2000 rpm for 10 min at 4 °C, the resulting nuclei pellet was dissolved in 0.2 N hydrochloric acid (HCL) and histones were extracted overnight rotating at 4 °C. Subsequently, the samples were centrifuged at 2000 rpm for 10 min at 4 °C and the supernatant, containing the histones, was analysed for protein content by Bradford assay.

For the extraction of histones from tissues, the samples were cut with a scalpel, forced through a cell strainer in 1 ml of PBS supplemented with SB, centrifuged and processed as described for cultured cells.

Five micrograms of extracted proteins were analysed on a 15 % sodium dodecyl sulfate polyacrylamide gel electrophoresis (SDS-PAGE). The samples were supplemented with Laemmli buffer (2X: 4 % SDS, 20 % glycerol, 10 % β-mercaptoethanol, 0.004 % bromophenol blue, 0.125 M Tris) boiled for 5 min, loaded in the pockets of a 6 % acrylamide stacking gel (2.6 ml of water, 1 ml of 30 % acrylamide, 1.25 ml of 0.5 M Tris, pH 6.8, 50 µl of 10 % SDS, 50µl of 10 % APS, 5 µl tetramethylethylenediamine (TEMED)) and were allowed to migrate at 120 V through a 15 % separating gel (1.8 ml of water, 4 ml of 30 % acrylamide, 2 ml of 1.5 M Tris, pH 8.8, 80 µl of 10 % SDS, 80 µl of 10 % APS, 8 µl TEMED) in running buffer (25 mM Tris, 190 mM glycine, 0.1 %

SDS) until the buffer front reached the bottom. The gels containing the size-separated proteins were blotted on a methanol-activated PVDF membrane with a pore size of 0.45 µm in a tank filled with transfer buffer (25 mM Tris, 190 mM glycine, 0.1 % SDS, 10 % methanol, pH 8.3) for one hour, at 100 V at 4 °C.

Ponceau staining (0.2 % Ponceau S, 5 % glacial acid) was performed as a transfer control and subsequently removed by washes with Tris buffered saline supplemented with 0.1 % Tween20 (TBST, 20 mM Tris pH 7.5, 150 mM NaCl, 0.1 % Tween20). The membrane was blocked in 5 % bovine serum albumin (BSA) in TBST for one hour at room temperature. The membranes were incubated overnight at 4 °C in 5 ml blocking buffer containing 1 µg of the respective primary antibody. The blots were washed three times with 10 ml of TBST and incubated for 45 min in 5 ml blocking buffer with 1 µg secondary antibody conjugated to horse radish peroxidase.

After three washes with TBST, the membranes were incubated with 1 ml ECL reagent (500 µl luminol mixed with 500 µl enhancer), containing the substrate for horse radish peroxidase to visualize protein bands by chemiluminescence under a ChemiDoc station (BioRad). Exposure times were adjusted to the respective band intensity. Subsequently, the blots were acid-stripped two times for 10 min in 10 ml of stripping buffer (0.15 g glycine, 0.01 g SDS, 0.1 ml Tween20, pH 2.2 with HCl) at room, washed twice with TBST, blocked, and re-probed as loading control with 0.5 µg total H3 antibody in a in 5 ml blocking buffer.

2.2.8 Flow cytometry analysis

Flow cytometry is a laser-based technique which enables analysis of the properties of thousands of single cells within a short time. Cell size, granularity, viability, cell cycle profiles, fluorescent protein expression or staining of internal or surface structures can be detected and quantified. Cells displaying the desired properties can be sorted with Fluorescence-Activated Cell Sorting (FACS) machines. In order to quantify particular histone modifications, samples of the different OND treatments were subjected to flow cytometrical analysis.

Cells were trypsinized, spun at300 x g for 5 min and fixed with methanol, or with 2 % paraformaldehyde (PFA) for 5 min on ice (1 ml/6 x 10^6cells). To remove the fixative, cells were spun and resuspended in permeabilisation buffer (PBS with 0.3 % Triton X-100, 1ml/6 x 10^6cells) and incubated for 10 min on ice. Subsequently, cells were washed

twice with 1ml PBS containing 2 % FBS and 0.1 % Tween20 (washing buffer), resuspended in 500 µl washing buffer, counted and 2 x 10^6cells were aliquoted per staining in a total volume of 300 µl of washing buffer. All antibodies were used at a 3 µg/ml dilution and incubated for one hour on ice with regular mixing every 10 min. After three washes with 1 ml of washing buffer, the secondary fluorescent antibody was applied at a 1 µg/ ml dilution for 45 min on ice with regular mixing.

After three washes, the cells were resuspended 300 µl PBS and analysed with a LSR-FortessaSORP (BD Biosciences) equipped with five air-cooled spatially separated lasers (375 nm, 405 nm, 561 nm, 488 nm and 640 nm), run with BD FACSDiva software. The cells were gated on single cells and these were further gated for 488-positive cells, as estimated from unstained cells and secondary antibody only controls (Figure 13).

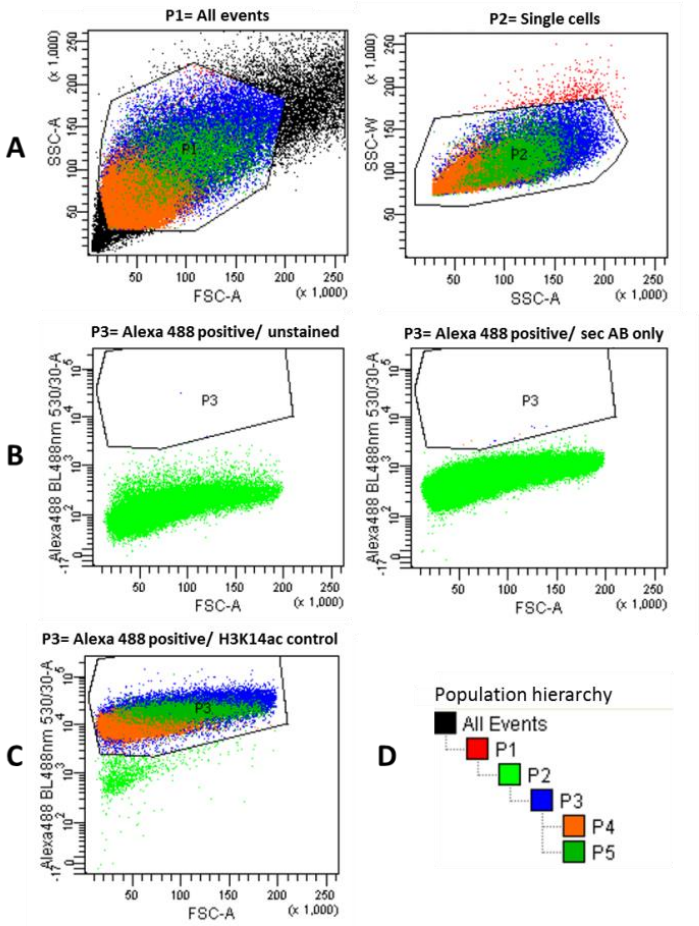

Figure 13. Gating strategy.
A. Left: 10000 events recorded by the flow cytometer. **A.** Right: All events were gated on single cells. **B.** Left: unstained cells. **B.** Right: cells only stained with secondary AlexaFluor 488. **C.** Cells positive H3K14ac. **D.** Population hierarchy.

2.2.9 Confocal microscopy

In order to visualise the distribution of histone modifications under OND and recovery, immunofluorescence staining of fixed, adherent cells was applied and analysed using a confocal microscope. Confocal microscopy offers increased resolution and contrast compared to widefield microscopy, through introducing a pinhole at the confocal plane of the lens, to eliminate out-of-focus light.

Cells were grown sub-confluent on gelatine-coated glass cover slips in 6-well plates in 3ml of Claycomb medium and were either exposed to OND, OND and recovery, or left untreated. Cells were then washed twice with PBS, fixed with 1 ml of ice cold methanol for 10 min on ice, and were permeabilized for 10 min in 1ml of PBS containing 0.3 % TritonX-100. After one hour of blocking (PBS, 0.1 % Tween, 5 % BSA), the slides were incubated with anti-histone (all 2 µg/ml, H3 1 µg/ml) or anti-polyamine (5 µg/ml) antibodies overnight at 4 °C. Wells were washed three times for 10 min with 1 ml of PBS containing 0.1 % Tween (PBST) and were incubated with a secondary antibody coupled to a fluorophore (2 µg/ml, AlexaFluor 488, Invitrogen) and 2 µg/ml Hoechst 33342 (Sigma) for 45 min in PBST. After three washes with PBST the slides were embedded upside down in 10 µl of 70 % glycerol on an object slide and sealed Fixo gum (Marabu). Samples were analysed under a Leica SP5 II confocal system (Leica Microsystems GmbH) using a 63 x oil immersion NA1.4 objective lens. The pinhole was kept constant at 1 Airy Unit (AU), laser power and gain were adjusted for each sample set up according to the fluorescence intensity of the untreated cells. 1024 x 1024 images were acquired using a pinhole size of 1.0 Airy units, 60 – 100nm pixel pitch.

2.2.10 Single Molecule Localization Microscopy

Super-resolution fluorescence microscopy provides a resolution beyond the classical Abbe/Raleigh or diffraction limit of approximately 200 – 250nm. This can be achieved with techniques capturing information contained in evanescent waves, like with structured illumination microscopy (SIM) or using super lenses. But also computational techniques can provide super-resolution images, based on the sequential imaging of bursts of photons emitted from individual “blinking” fluorophores, called single molecule localisation microscopy (SMLM).

The serial recording of blinking fluorophores allows the individual detection of two fluorophores, which have almost the same spatial coordinates. Two blinking fluorophores, which emit at different times, can be resolved down to a distance of ~10 nm (Markaki et al., 2010). Blinking is induced by initiating fluorophores to switch between a dark state, which is induced by bleaching of the sample, and the subsequent recovery to the bright, fluorescent state (Żurek-Biesiada et al., 2015). Typically, thousands of frames are acquired, which are computed afterwards into a joint localisation map (Figure 14) Depending on the fluorophore, special buffer systems are necessary to induce blinking.

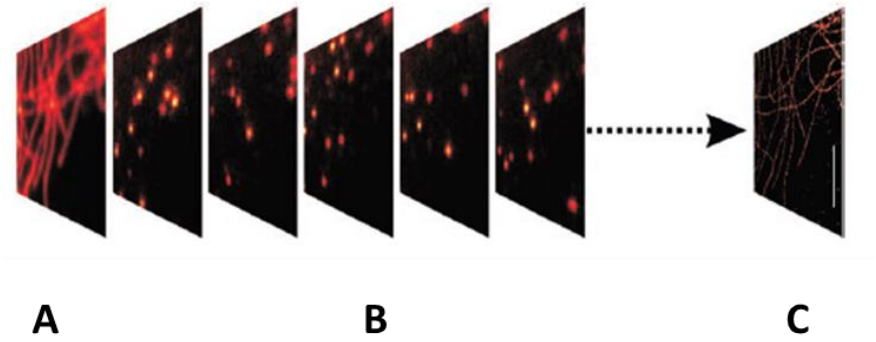

Figure 14. Principle of SMLM.
A. Microscopy image acquired in widefiled mode under low intensity light exposure. **B.** Multiframe acquisition of blinking fluorophores. **C.** Single molecule positions, localisations, contribute to the joint assignment map of the labelled structure. Image adopted from Van de Linde et al., Nature Protocols 2011.

For super resolution microscopy, cells were stained for H3K14ac as indicated in 2.2.9. The DNA was stained for 40 min with 1 µM Vybrant dye cycle Violet (Life Technologies) or 30 min with 0.02 nM YOYO-1. Since YOYO-1 also stains RNA, cells were additionally incubated with 0.5 U/ml RNase A and 20 U/ml RNase T1 (Ambion, USA) for one hour at 37 °C.

After DNA staining, the cells were washed twice with PBS, embedded in 20 µl of imaging buffer (40 µg/ml glucose oxidase, 0.5 mg/ml catalase, 10 % glucose in 80 % glycerol and 20 % PBS) and analysed using a custom built microscope equipped with a single objective lens (Leica Microsystems, 1.4 NA, 63 x oil immersion with a refractive index of 1.518) and a 12 bit, air-cooled CCD camera (PCO, Sensicam QE).

For samples stained with AlexaFluor 647, 50 – 100mM mercaptoethylamine (MEA) was added to the imaging buffer containing 60 % glycerol and 40 % PBS. For two colour imaging of DNA and AlexaFluor 647, the concentration of MEA was reduced to 3mM; a concentration that facilitates blinking of the cyanine dye AlexaFluor 647 without affecting blinking of Vybrant dye cycle Violet. Widefield acquisitions were taken with

homogeneous illumination of the whole field of view, as achieved by 6.7 fold expansion of the laser beam.

SMLM images are acquired upon illumination with a collimated laser beam covering an area of approximately ~25 µm diameter in the imaging plane. Vybrant dye cycle Violet was excited using a 491 nm laser (Calypso 05 series, Cobolt, Sweden) at 70 mW and 30000 frames were acquired with 50 ms exposure time. AlexaFluor 647 was excited with a 647 nm laser (LuxX diode laser, Omicron, Germany) at 60 mW and 25000 frames were acquired with an exposure time of 25 ms.

For YOYO-1, 30000 frames with an exposure time of 50 ms were acquired at 30 mW laser power. In the dual colour experiments, imaging of AlexaFluor 647 (9000 frames with 25 ms exposure time, 647 nm excitation, 60 mW) was performed prior to imaging of DNA stained with Vybrant dye cycle Violet. For imaging of AlexaFluor 488, 23000 frames with camera exposure time of 25 ms were acquired at 70 mW. For Vybrant dye cycle Violet, YOYO-1 and AlexaFluor 488, a bandpass filter of 525/50 nm (Chroma) and for AlexaFluor 647 long pass filter of 655 nm (Chroma) was used (Kirmes, Szczurek et al., 2015).

SMLM data analysis for extraction of single molecule fluorophore positions from raw tiff data stacks was performed using fastSPDM in Matlab (Gruell F, Kirchgessner M, Kaufmann R, Hausmann M, Kebschull U. Accelerating Image Analysis for Localization Microscopy with FPGAs. In: 2011 21st International Conference on Field Programmable Logic and Applications. IEEE; 2011. page 1–5).

The acquisition, computational analysis and compilation of the SMLM pictures was performed by Aleksander Szczurek, Cremer Group IMB, shared first author of Kirmes et al., 2015.

2.2.11 Calculation of chromatin-free regions

To distinguish between “control chromatin” and “OND-chromatin”, chromatin-free regions were defined as DNA dye-free areas and calculated from SMLM or confocal images. In ImageJ (http://imagej.nih.gov/ij/), reconstructed 8 bit images were subjected to histogram stretching in order to cover the entire spectrum of pixel values. A constant threshold was applied to all images and the 8 bit image was converted to a binary format. The area covered by chromatin was calculated by counting the number of pixels in this binary image. The total area of the nucleus was obtained after the chromatin free “holes”

were filled (ImageJ function “fill holes”). Then, the chromatin-free area was calculated by subtracting the area occupied by chromatin from total nuclear area (Figure 15).

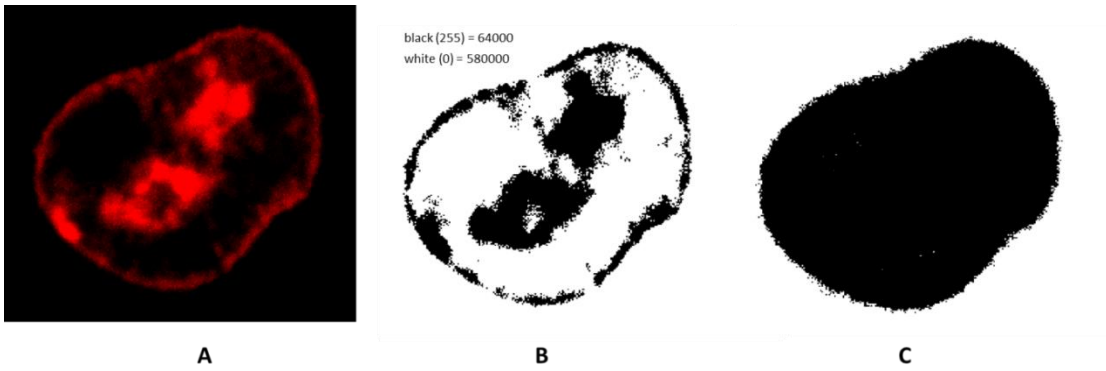

Figure 15. Calculation of chromatin-free regions.
A. Confocal picture of the DNA of an OND phenotype cell. **B.** Binary format of the picture with the number of 0 pixels and 255 pixels. **C.** total area of the nucleus, subtraction of the 255 value (black, chromatin) from the total area reveals the chromatin free area.

2.2.12 Transmission electron microscopy

In transmission electron microscopy (TEM), an electron beam is transmitted through an ultra-thin specimen. The image, generated from the interaction of the electron with the specimen, is magnified and detected by a CCD camera. Due to the small de Broglie wavelength of electrons, TEM overcomes the diffraction limit and provides high resolution images.

Hl-1 cells were seeded in 3.5 cm dishes and grown to a confluent monolayer. The cells were fixed for 30 min with 2 ml of 1 % glutaraldehyde in PBS containing 1 mM Ca^{2+} and 0.5 mM Mg^{2+}. Afterwards, cells were washed three times with PBS and fixed for two hours with 2 ml of 2 % osmium tetroxide solution in 0.2 M sodium cacodylate buffer (ratio 1:1). After three PBS washes, the cells were incubated for 10 min with 2 ml of tannic acid, this step was repeated once. Subsequently, the samples were dehydrated with an ethanol dilution series: incubation with 2 ml of 25 %, followed by 50 %, 70 % (2 x), 90 % (2 x), 100 % (3 x) for 10 min each. After fixation and dehydration, cells were incubated overnight with 2 ml of a 1:1 mix of the poly raisin embedding medium PolyBed (50.92 g PolyBed 812, 24.72 g dodecenylsuccinic anhydride DDSA, 26.64 g nadic methyl anhydride, 1.4 g DMP-30) and 100 % ethanol with open lid. On the next morning, the mixture was removed and replaced with 2 ml of the PolyBed mix and incubated for 12 hours at 37 °C and another 48 hours at 60 °C. The embedded cells were removed from the dishes and 1 – 2 mm^2 ultrathin sections of 60 nm were cut with an Ultra

microtom (Leica) equipped with a diamond knife. The sections were placed on grids and contrasted with uranyl acetat for one hour. Imaging was performed with a TEM (Jeol) with 6000 x magnification.
The sections were cut by Stefan Redl, Ketting group, IMB and the imaging was performed together with Christoph Sieber, Max Planck Institute, Mainz.

2.2.13 DNaseI sensitivity assay

The DNaseI enzyme cleaves accessible DNA rather unspecifically, with a small preference for the minor groove and 5' pyrimidine sequences. The smallest substrate of DNase1 is a trinucleotide. It cleaves single, as well as double strands, and needs calcium and magnesium ions for activity. DNase1 assays can be applied to determine chromatin compactness under different conditions, based on the time the enzyme needs to digest the DNA. Compactness of chromatin is estimated in the access of the large molecular weight probe, DNaseI (30 kDa), to chromatin. The fluorescent signal of the DNA dye DRAQ5 (eBioScience) was used as a read out, assuming that liberation of the dye upon DNA digestion decreases the signal.
Cells were seeded at a density of 1 x 10^4 per well in 8-well-chamber-microscopy slips (IBIDI) and cultured for two days. HL-1 cells were fixed with 300 µl of 4 % PFA per well for 15 min on ice. The cells were permeabilized with 300 µl of permeabilisation buffer for 10 min at room temperature as described under 2.2.9. The DNA was stained with 5 µM of DRAQ5 (eBioscience) in 320 µl PBS for 30 min and subsequently washed twice with PBS. The incubator at the Leica SP5 confocal microscope was pre-heated to 37 °C and the DNaseI buffer was equilibrated inside. The wells of the IBIDI chambers were filled with 150 µl of 1 x DNaseI buffer (New England Biolabs) and placed on the microscope stand. Another 150 µl of DNaseI buffer containing DNaseI were added. The final concentration of DNaseI in per well was 5 U/ml. Images were taken every 4 min until no further change in the fluorescent signal was detectable. The microscope settings were: 7 % 633 nm laser excitation, 100HyD Gain, 643 – 749 nm emission range, 512 x 512 resolution (voxel size 246 x 246 x 481.5 nm), 2 Airy Units pinhole, 600 Hz scanner speed. The pictures were processed in ImageJ, aligning the time lapse pictures to a stack. The decay in fluorescence was analysed with the ImageJ plugin "time series analyser" (http://rsb.info.nih.gov/ij/plugins/time-series.html). The decay in fluorescence intensity was normalized to dye bleaching curves, which were acquired in advance.

2.2.14 Fluorescence Recovery After Photobleaching (FRAP)

In order to answer the question if histones become displaced from the DNA upon OND, FRAP of core histone H2B and the linker histone H1.1 were performed. In FRAP, recovery time of fluorescence is correlated with mobility kinetics of the respective fluorescent protein (Figure 16).

HeLa cells stably transfected with mCherry-H2B (Core Facility IMB) or with GFP-H1.1 (kind gift of Prof. Jurek Dobrucke and Dr. Miroslaw Zarebski) were grown to 50 % confluency on glass cover slips. The samples were sealed airtight upside down on object slides with a cavity filled with 200 µl of ischemic stress buffer or RPMI 1640 without phenol red (Life Technologies) containing 10 % fetal bovine serum (Gibco) using Picodent Twinsil two component glue (Wipperfuerth, Germany).

Live cell acquisitions were taken under a SP5 II confocal system (Leica Microsystems GmbH) using a 63 x oil immersion NA1.4 objective lens and a heated incubation chamber at 37 °C (Table 9).

Table 9. Parameters for the acquisition of FRAP data.

	H2B-mCherry	**H1.1-GFP**
FRAP image acquisition	256 x 256 pixel, effective pixel size 96.5 nm, excitation: 6 % power of 561 nm, emission: 602 – 711 nm	256 x 256 pixel, effective pixel size 96.5 nm, excitation: 13 % power of 488 nm, emission: 500 – 591 nm
bleaching protocol	one 256 x 256 pixel scan in 2 x 2 µm, 80 % 561 nm laser	100 ms point bleach, 80 % 488 nm laser
time/frame	0.328 s	1 s
FRAP read-out in:	2 x 2 µm square ROI	1.5 µm in diameter circle ROI

Eleven individual FRAP measurements were performed for each data set. Each FRAP acquisition was aligned using the "StackReg" ImageJ plugin, to compensate for movement of the bleached area during fluorescence recovery. FRAP data was further analysed within a respective region of interest using ImageJ and corrected on bleaching throughout the experiment by acquisition of bleaching curves for either H1.1-GFP or H2B-mCherry in independent measurements, to accommodate possible differences in bleaching rates (Kirmes, Szczurek et al., 2015). FRAP experiments were performed together with A. Szczurek.

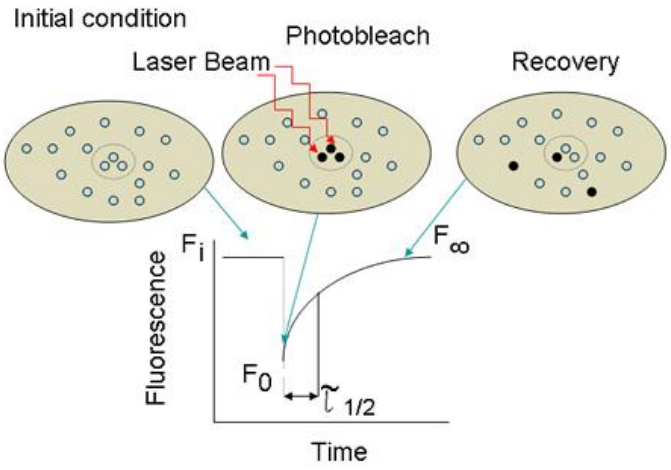

Figure 16. Principle of FRAP.
The protein of interest is stably tagged with a fluorescent protein. An initial photobleaching step bleaches all fluorescent proteins in the area covered by the laser beam. The recovery of the fluorescent signal in this particular area is now observed over time. The faster the signal recovers, the more mobile the tagged protein is. Image modified from Roy et al., 2002.

2.2.15 Chromatin immunoprecipitation followed by sequencing

Chromatin immunoprecipitation (ChIP) is used to identify DNA regions which are bound by the protein of interest. An antibody against a transcription factor, a histone modification or another molecule, which binds DNA, is applied to selectively isolate the bound sequence. In order to determine which genomic regions become deacetylated and re-acetylated in OND and OND and recovery, NGS of H3K14ac ChIP material was performed (ChIPseq) for untreated cells and treated cells.

HL-1 cell were grown confluent in 10 cm dishes, washed twice with PBS and trypsinised. Trypsin was inhibited by the addition of 5 ml of soybean trypsin inhibitor (Sigma). Cells were spun at 300 x g for 5 min at 4 °C and the pellet was resuspended in 10 ml of HNB buffer (15 mM Tris-HCl pH 7.6, 500 mM sucrose, 60 mM KCl, 0.25 mM EDTA, 0.125 mM EGTA, 0.5 % Triton X-100, 1 mM Dithiothreitol (DTT), 0.5 mM Phenylmethylsulfonyl fluoride (PMSF)) to remove the cytoplasm. The resulting nuclei were spun at 500 x g and resuspended in 150 µl of NE buffer (20 mM Tris-HCl, pH 7.6, 70 mM NaCl, 20 mM KCL, 5 mM $MgCl_2$, 3 mM $CaCl_2$) which permeabilises the nuclei and provides the ions needed for enzyme performance. Subsequently, 0.3 µl of Micrococcal Nuclease (Mnase) per 5 x 10^6 cells were added.

Mnase is an enzyme derived from *Staphylococcus aureus* and is a relatively non-specific endo-exonuclease. It digests double-stranded, single-stranded, circular and linear nucleic acids, according to the accessibility of the sequence. After 8 min of incubation the

digestion was stopped by adding 5 mM EDTA and 5 mM EGTA. The digestion time is dependent on the enzyme concentration and the cell density. Our experimental setup revealed a nucleosomal ladder with mono-, and di-nucleosomes, with a fragment size ranging from approximately 147 – 294bp. DNA fragmentation is needed to obtain a satisfying resolution, when sequencing the pull-down DNA.

The nuclei were lysed for 15 min on ice in 800 µl of ChIP-buffer (2 parts SDS-buffer: 100 mM NaCl, 50 mM Tris-Cl, pH 8.1, 5 mM EDTA, pH 8.0, 0.5 % SDS and one part Triton buffer: 100 mM Tris-Cl, pH 8.6, 100 mM NaCl, 5 mM EDTA, pH 8, 0.5 % Triton X-100) containing protease inhibitors (Complete Mini, Roche) and 5 mM sodium butyrate. The samples were spun at 14000 rpm for 10 min at 4 °C to pellet the debris.

A 30 µl test sample of the supernatant was digested with 1 µl of RNAse (RNAse A cocktail, Ambion) and 1 µl of Proteinase K for 30 min at 37 °C and another 30 min at 56 °C. The digested sample was further purified using a spin column (MinElute, Quiagen), measured with Nanodrop, and 800 µg were run on a 1 % agarose gel to check for Mnase digestion.

For the immunoprecipitation 20 µl of magnetic protein G beads (Merck Millipore) were washed with PBS containing 0.1 % Tween and added to 10 µg of the chromatin. Since SDS in the ChIP buffer would impair antibody binding, the buffer was diluted out by adding five volumes of Triton dilution buffer and additional protease inhibitor. Subsequently, the antibodies were added to the different chromatin preparations; 2 µg of normal rabbit IgG control (R&D Systems), and 20 µl of anti-H3K14ac (Cell Signaling) and 2 µg of anti-H3 (abcam). Incubation was performed over-night with rotation at 4 °C.

The bead-immuno-precipitate complexes were washed twice with 1 ml of low salt buffer (0.1 % SDS, 1 %Triton X-100, 2 mM EDTA, 20 mM Tris-HCl pH 8.1, 150 mM NaCl), with 1 ml of lithium-chloride buffer (250 mM LiCl, 1 % IGEPAL, 1 % sodium deoxycholate, 1 mM EDTA, 10 mM Tris, pH 8,1) and with 1 ml of TE-buffer (10mM Tris-HCl pH8.1, 1mM EDTA). During washing, the tubes were rotated at 4 °C and the beads were captured using a magnetic rack (DynaMag2, Life technologies). The beads were then resuspended in 100 µl of freshly prepared elution-buffer (1 % SDS, 100 mM $NaHCO_3$) and the samples were digested and purified as indicated for the test sample.

The DNA concentration was measured using a Qubit fluorometer which is designed to quantify low amounts of DNA. DNA sequencing libraries were prepared with the NEBNext ChIP-Seq Library Prep Master Mix Set for Illumina and sequenced as indicated in 2.2.4.

The raw data was analysed for quality and mapped to the mouse genome version mm9 with Bowtie version 1.0.0. The duplicates were marked and removed with MarkDuplicates from Picard Tool, version 1.92 and broad peaks were called using MACS2 version 2.1.0, with a false discovery rate (FDR) of max. 0.1. MACS2 settings were chosen based on the recommended settings when analyzing nucleosome data: -nomodel shift 37-extsize 73. Numbers are based on the fact that DNA wrapped around a nucleosome is about 147 bp.
For each condition, the pull down (H3K14Ac) and the IgG control were compared to the input samples. For all analyses, replicate input samples were combined. Peak annotation was performed with PeakAnnotator, version 1.4 and ChIPSeeker was applied for the identification of regulatory elements. This work was performed by Dr. Anke Busch, Core Facility Bioinformatics, IMB. Further, tables were sorted for decreasing H3K14ac peaks in OND and genes associated with these peaks were analysed for "biological processes" and "Overrepresented Diseases" connected to heart, muscle, fibrosis and hypoxia/ischemia (GeneRanker, Genomatix).

2.2.16 Labeling of nascent RNA with BrU

To quantify how much RNA is produced under OND conditions and after recovery, newly synthesized RNA was pulse-labeled with bromouridine (BrU), a uridine derivate which becomes incorporated into RNA, if present during synthesis.
For the incorporation, 2 mM BrU (Sigma Aldrich) were added to a 10 cm dish of HL-1 cells and incubated for one hour, either under normal culture conditions, during OND, or for 1 hour of recovery from OND. To estimate background incorporations, one sample without exposure to BrU was analysed. All experimental conditions were performed in triplicates.
Following BrU pulse labeling, RNA was extracted using Trizol as indicated in 2.2.4 and isolated RNA was subsequently digested to nucleosides with nuclease P1 (Roche), U snake venom phosphodiesterase (Worthington), and alkaline phosphatase (Fermentas). RNA nucleosides were subject to liquid chromatography/Mass-spectrometry (LC/MS) analysis. Separation was performed on an Agilent 1290 UHPLC system equipped with ReproSil 100 C18 column (3 µm, 4.6 x 150mm, Jasco GmbH) maintained at 30 °C. Identification and quantification of nucleosides was performed on an Agilent 6490 triple

quadruple mass spectrometer. The mass spectrometry analysis was performed by Dr Michael Musheev, Niehrs Group, IMB.

2.2.17 ATP energy depletion assay

Hypoxia inhibits the respiratory chain in the cell's mitochondria and deoxyglucose inhibits glycolysis. When together, these effects induce loss of energy, in the form of ATP, during OND. To measure ATP depletion, HL-1 cells were grown to confluency in 3.5 cm dishes and subjected to OND and OND with a subsequent recovery time course of 5, 15, 60, and 240 min. After treatment, cells were washed twice with PBS, and ATP was extracted with 300 µl of boiling MilliQ water, as described in Yang et al., 2002.
The ATP concentration in the samples was determined using a bioluminescence assay, utilizing recombinant firefly luciferase and its substrate D-luciferin (ATP Determination Kit, Invitrogen). The luciferase signal was read out on a plate reader (Tecan) and compared to a standard curve. The readout of the assay and the subsequent calculations were performed by Dr Iryna Charapitsa, Reid Group, IMB.

2.2.18 Treatments

In order to prevent histone deacetylation upon OND, cells were pre-treated with 5µM of the HDACI TSA one hour prior to OND. The synthesis of polyamines was inhibited by a 48 hour pre-treatment with 200µM ornithine carboxylase (ODC) inhibitor difluoromethylornithine (DFMO).

3. Results

3.1 Transcriptome analysis of cardiac ischemia-reperfusion and OND

3.1.1 Cardiac IR induces a transcriptional burst

Next generation mRNA sequencing of tissue, taken from mice with acute myocardial infarction and reperfused infarction, revealed alterations in the transcriptional profile after ischemia and IR. The mRNAs expressed in cells of infarcted pieces were compared to the expression profiles of cells comprised in pieces taken from equivalent regions of sham-treated mice.

Ischemia and IR induce differential gene expression in the affected region of the heart. With reperfusion time, more genes become up- than down-regulated. The major response to ischemia and ischemia-reperfusion is gene up-regulation, with a transcriptional burst observed after 2 and 24 hours of restored blood flow (Figure 17).

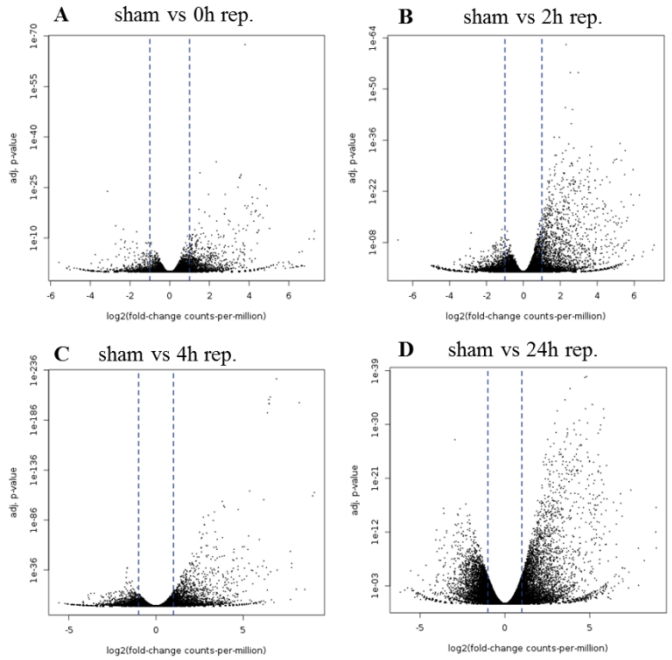

Figure 17. Differential gene expression profiles in the heart.
Volcano plots depicting the p-value on the y-axis versus the log2 fold change on the x-axis. Negative log2 fold changes correlate with gene down-regulation and positive values indicate gene up-regulation. **A.** Ischemia, induces differential gene expression. **B.** After two hours of reperfusion, the number of up-regulated genes increases and subsequently decreases after 4 hours of restored blood flow (**C**). **D.** After 24 hours of reperfusion, differential gene expression increases again. Rep: reperfusion.

Gene lists were analysed for Gene Ontology (GO) annotations, for an overview of biological processes in the heart after ischemia and IR (Table 10, Table 11).

Table 10. Transcriptional changes and GO terms for 0h and 2h of reperfusion.
Terms connected to chromatin organisation are highlighted in red and terms connected to oxygen are highlighted in blue. Tkfs: transcription factors, Biol: biological, proc: process, pos: positive, neg: negative, reg: regulation, ROS: reactive oxygen species.

	0h reperfusion	**2h reperfusion**
genes up	222	699
genes down	38	65
biological processes up regulated	immune system process p=2.15E-47 response to stress p=6.36E-32 pos. regulation of cell death p=1.72E-11 apoptotic process p=1.86E-10 neg. regulation of cell death. p=17E-09 vasculature development p=5.54E-08 regulation of ROS p=6.82E-07 response to oxygen p=2.05E-06 response to calcium ion p=6.77E-06 response to oxidative stress p=4.60E-05	immune system process p=1.28E-65 response to stress p=7.51E-52 response to wounding p=2.80E-36 apoptotic process p=7.78E-33 regulation of metabolism p=2.39E-22 cell differentiation p=7.11E-22 neg. regulation of cell death p=1.47E-21 vasculature development p=7.75E-19 pos. reg. cell death p=6.01E-17 response to oxygen p=1.37E-16 phosphorylation p=7.43E-14 response to ROS p=3.73E-10 cation homeostasis p=4.12E-08 transcription, DNA-templated p=4.00E-08 fibroblast proliferation p=3.04E-05 muscle cell proliferation p=5.24E-05
biological proceses down regulated	reaction on pH elevation p=1.60E-05	locomotion p=4.79E-05 neuron development. p=30E-05

Table 11. Transcriptional changes and GO terms for 4h and 24h of reperfusion.
Terms connected to chromatin organisation are highlighted in red and terms connected to oxygen are highlighted in blue.

	4h reperfusion	**24h reperfusion**
genes up	1281	2399
genes down	520	249
biological processes up regulated	immune system process p=2.46E-79 response to stress p=8.49E-48 response to wounding p=7.14E-40 cell differentiation p=3.13E-38 regulation of cell proliferation p=1.72E-31 positive regulation of metabolism p=7.06E-30 vasculature development p=3.45E-23 neg. regulation of cell death p=1.80E-22 regulation of phosphate metabolism p=3.42E-20 pos. regulation of cell death p=8.66E-18 muscle cell differentiation p=2.78E-10 cation homeostasis p=1.91E-10 vasoconstriction p=2.82E-06 regulation of ROS metabolism p=6.93E-06 pos. reg. of fibroblast proliferation p=5.18E-05 response to oxidative stress p=1.12E-04	immune system process p=7.95E-88 response to stress p=5.68E-55 response to wounding p=3.40E-40 cellular metabolic process p=1.43E-26 actin filament organization p=5.13E-19 blood coagulation 4.29E-19 vasculature development p=4.67E-18 neg. regulation of cell death p=3.44E-17 pos. regulation of cell death p=1.04E-14 calcium ion homeostasis p=2.78E-10 response to oxygen p=5.14E-10 DNA replication p=8.78E-06 response to oxidative stress p=1.58E-04 chromosome localization p=4.23E-04 muscle tissue development p=5.17E-04 fibroblast proliferation p=8.53E-04
biological proceses down regulated	no p-value lower than p=E-03	replication-dependent nucleosome organization p=1.61E-13 chromatin assembly p=6.31E-09 replication-independent nucleosome organization p=9.97E-08 cation homeostasis p=1.19E-07 cardiac muscle contraction p=8.05E-06 DNA packaging p=1.27E-06 actin-mediated contraction p=9.57E-05 DNA conformation change p=6.61E-05

The number of induced genes increases more than ten-fold within 24 hours of reperfusion. IRI can be considered as a sterile inflammation, it triggers the activation of the immune system while infiltrating immune cells induce the transcriptional burst, observed after 24 hours. Cell death is provoked and suppressed at the same time; injured cells are removed and the survival of viable cells is promoted. Vascularization is induced in order to restore the blood supply. Cell proliferation of fibroblasts counterbalances for the loss of contractile myocytes, leading to fibrosis and stiffness of the heart. The induced gene expression profile under ischemia and after IR shows that oxygen deprived cells are exposed to ROS.

Comparison of the four ischemic treatments discovered 92 genes, which become up-regulated in acute ischemia and that remain induced after reperfusion. Ten of these genes were identified as transcription factors, among them the immediate early gene Egr1, Egr2, Fos, Fosb and Junb, which interact in an auto-regulatory pathway induced upon stress (Figure 18).

Interestingly, with regard to further effects presented later in this thesis, the transcription of spermidine/spermine N(1)-acetyltransferase (Sat1), a rate-limiting enzyme in the catabolic pathway of polyamine metabolism, is six-fold increased after 4 hours of reperfusion.

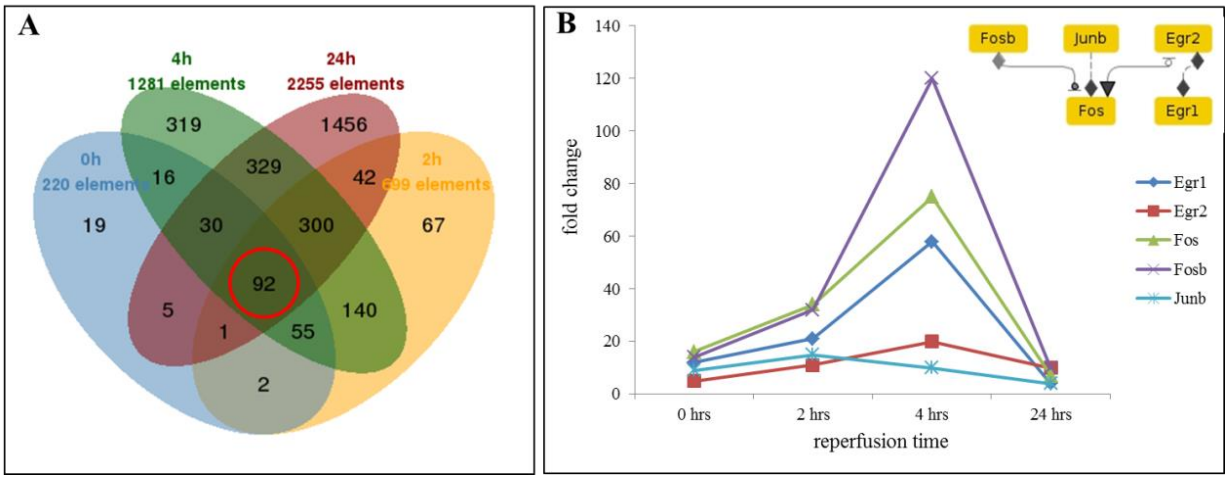

Figure 18 Genes whose expression is consistently induced in the heart upon ischemia.
A. Commonly expressed under the respective conditions. **B.** The expression of the stress induced, pathway-connected transcription factors Egr1, Egr2, Fos, FosB and JunB.

Fewer genes become repressed than induced in ischemia and IR. After 24 hours of reperfusion, histone genes of cluster 1 (Hist1h) and cluster 2 (Hist2h) become down-regulated; their repression is associated with impaired chromatin organisation as presented later in this thesis. Five genes are down-regulated in all four ischemic conditions and none of them was identified as a transcription factor (Figure 19).

A **down-regulated genes**

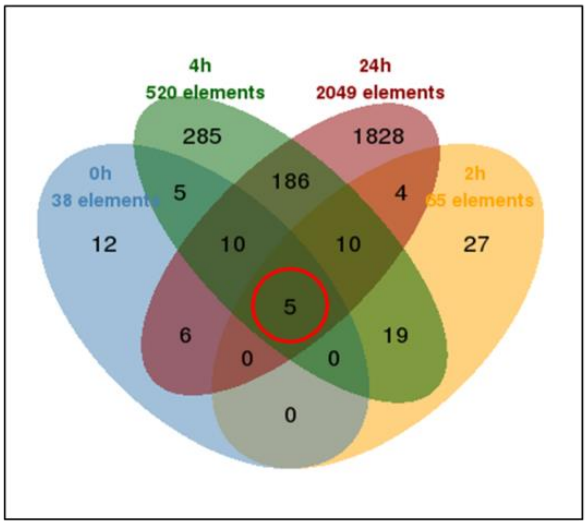

B

Gene	fold change
Hist1h2ba	-2.0
Hist1h2bb	-2.0
Hist1h3a	-2.8
Hist1h3b	-2.5
Hist1h3c	-2.6
Hist1h3d	-2.2
Hist1h3e	-2.1
Hist1h3f	-2.1
Hist1h3g	-2.4
Hist1h3h	-2.5
Hist1h3i	-3.0
Hist1h4a	-2.5
Hist1h4b	-2.6
Hist1h4c	-2.7
Hist1h4d	-2.4
Hist1h4f	-2.4
Hist1h4h	-2.5
Hist1h4j	-2.6
Hist1h4k	-2.5
Hist1h4m	-2.2
Hist1h4n	-2.2
Hist2h2ab	-2.3
Hist2h2ac	-2.2
Hist2h2be	-2.1
Hist2h4	-2.9

Figure 19. Commonly repressed genes in the heart.
A. Commonly down-regulated under different ischemic conditions. Five genes are down-regulated in all four conditions (red circle). **B.** After 24 hours of recovery, 21 genes of histone cluster 1 are repressed (grey) and 4genes of histone cluster 2 (blue).

3.1.2 OND in HL-1 cells induces gene down-regulation

For a better understanding of the transcriptional response of cardiomyocytes to ischemia and IR, next generation mRNA sequencing of the murine cardiomyocyte cell line HL-1 was performed. The OND sample corresponds to 0h reperfusion. Additionally, 1 hour and 4 hours of recovery were analysed. The obtained data reflects the response of one cardiac cell type, without the contribution of infiltrating immune cells.

The major response to OND is gene down-regulation, with the number of up-regulated genes increasing with recovery time. After a recovery of 4 hours, the amount of induced and repressed genes is almost equal (Figure 20).

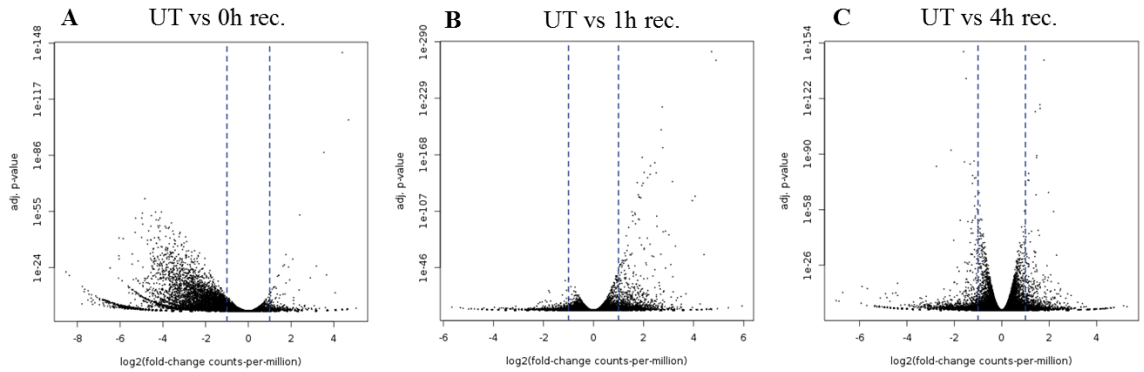

Figure 20. Differential gene expression profiles in HL-1cells.
Volcano plots depicting the p-value on the y-axis versus the log2 fold change on the x-axis. Negative log2 fold changes correlate with gene down-regulation and positive values indicate gene up-regulation. **A.** Under OND, more genes with higher fold changes are down-regulated than up-regulated. **B.** After one hour of recovery, the number of up-regulated genes increases whereas down-regulated genes decrease. **C.** After four hours of recovery, the number of down-regulated genes increases again, almost to the same level as up-regulated genes. Rec: recovery.

The number of up-regulated genes increases six times within 4 hours of recovery. The major response to OND is gene repression: forty times more genes are down-regulated than up-regulated (Table 12, Table 13).

The main biological processes induced upon OND are involved in the regulation of gene expression, RNA synthesis and in compensation for the loss of muscle components. Energy consuming processes like metabolism, cell cycle and DNA repair are shut down. Upon short-term recovery, transcription and metabolism are reinitiated and muscle cell recovery, angiogenesis and the regulation of calcium homeostasis become activated.

The reaction to stress, in form of reintroduced oxygen, triggers an inflammatory response. As observed for tissue pieces, cell death is provoked and suppressed at the same time. Genes induced after four hours of recovery are mainly involved in the cellular response to misfolded or damaged protein and endoplasmic reticulum stress. The non-annotated transcript LOC100504841 is induced under all experimental conditions.

Table 12. Transcriptional changes and GO terms for 0h and 1h of recovery.
GO terms were thresholded for p=values lower than p= 09E-05. Terms connected to chromatin organization are highlighted in red, terms connected to oxygen are highlighted in blue.

	0 hrs recovery/OND	**1 h recovery**
genes up	46	239
Tkfs up	20%	18%
genes down	1912	52
Tkfs down	8%	no
biological processes up regulated	muscle development and differentiation p=3.6E-08 response to external stimulus p=9.7E-06 pos. reg. of gene expression p=7.8E-06 negative regulation of gene expression p=4.2E-05 pos. reg. of RNA biosynthetic process p=5.5E-05 neg. reg. of RNA biosynthetic process p=9.6E-05	transcription, DNA-templated p=4.2E-20 transcription from pol II promoter p=5.3E-20 neg. reg. of metabolic process p=1.4E-20 neg. reg. of RNA metabolism p=4.8E-16 pos. reg. of e metabolic process p=4.7E-15 pos. reg. of gene expression p=9.2E-15 negative reg. of gene expression p=1.4E-14 pos. reg. of RNA metabolism p=2.6E-10 pos. reg. of cell death p=2.7E-10 neg. reg. of cell death p=3.1E-10 skeletal muscle development p=1.9E-09 hematopoiesis p=2.3E-09 response to stress p=2.5E-09 regulation of cell cycle p=1.5E-08 vasculature development p=3.2E-08 cellular response to calcium ion p=1.2E-06 pos. reg. of cell proliferation p=4.3E-06 response to oxygen p=3.4E-05 inflammatory response p=9.7E-05
biological processes down regulated	nucleic acid metabolic process p=8.6E-35 cellular macromolecule metabolic process p=2.4E-31 RNA metabolic process p=4.3E-27 regulation of biosynthetic process p=6.9E-27 RNA biosynthetic process p=9.0E-24 regulation of gene expression p=8.7E-20 cell cycle processes p=5.7E-19 DNA repair p=5.7E-10 chromatin modification p=7.0E-08 chromatin organization p=1.2E-07 pos. reg. of chromosome organization p=2.1E-06 mRNA processing/spicing p=3.0E-06 DNA conformation change p=5.2E-06	no p-value lower than p=E-03

Table 13. Transcriptional changes and GO terms for for 4hrs of recovery.
GO terms were thresholded for p=values lower than p= 09E-05. Terms connected to chromatin organization are highlighted in red.

	4 hrs recovery
genes up	304
Tkfs up	9%
genes down	223
Tkfs down	4%
biological processes up regulated	response to endoplasmic reticulum stress p=9.7E-07 response to unfolded protein p=8.0E-06 response to topologically incorrect protein p=1.8E-05 cellular response to unfolded protein p=2.5E-05 intrinsic apoptotic signaling pathway in response to endoplasmic reticulum stress p=2.9E-05
biological processes up regulated	DNA replication-dependent nucleosome organization p=3.7E-12 protein-DNA complex assembly p=3.5E-10 chromatin assembly p=1.0E-09 chromatin assembly or disassembly p=6.5E-09 DNA packaging p=3.3E-08 DNA conformation change p=3.3E-08 chromatin organization p=5.4E-05 DNA replication-dependent nucleosome organization p=3.7E-12 protein-DNA complex assembly p=3.5E-10 chromatin assembly p=1.0E-09

GO terms associated with repressed genes are mainly connected to chromatin and nucleosome/DNA organisation. After four hours of recovery, histone genes, coding for all variants, become repressed, as observed for cardiac IR after 24 hours (Figure 21). First transcriptional evidence for impaired chromatin organisation can be found under OND conditions, even though histone genes are not down-regulated yet (Table 12). Three commonly repressed non-annotated transcripts were identified in all experimental conditions (Figure 21).

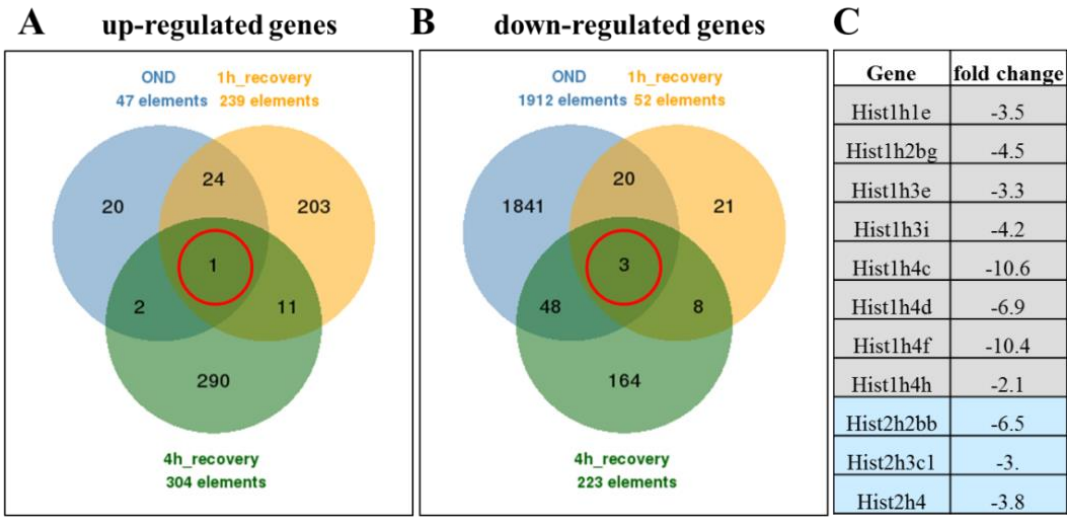

Gene	fold change
Hist1h1e	-3.5
Hist1h2bg	-4.5
Hist1h3e	-3.3
Hist1h3i	-4.2
Hist1h4c	-10.6
Hist1h4d	-6.9
Hist1h4f	-10.4
Hist1h4h	-2.1
Hist2h2bb	-6.5
Hist2h3c1	-3.
Hist2h4	-3.8

Figure 21 Consistently up- and down regulated genes
A. Consistently up-regulated genes. **B.** Consistently down-regulated genes **C.** Repressed histone genes after 4 hours of recovery; cluster 1 (grey) cluster 2 (blue).

3.1.3 Transcription in HL-1 cells is generally impaired under OND

To obtain a quantitative overview of transcriptional activity during OND and after recovery, newly synthesized RNA was labeled with BrU. The amount of incorporated BrU was measured by mass spectrometry and arises from, *de novo* synthesized RNA.
After one hour of OND, less labelled RNA was detected, as compared to one hour of bromouridine incubation without OND. After one hour of recovery with BrU present in the medium, the amount of labelled RNA significantly increased. After 3.5 hours of recovery, BrU labelled RNA levels where lower than after one hour BrU incubation with or without previous OND treatment. This experiment shows that RNA synthesis decreases significantly under OND conditions. Upon recovery, transcription levels increase, compared to cells which did not experience OND. A longer recovery time does not further promote RNA synthesis (Figure 22).

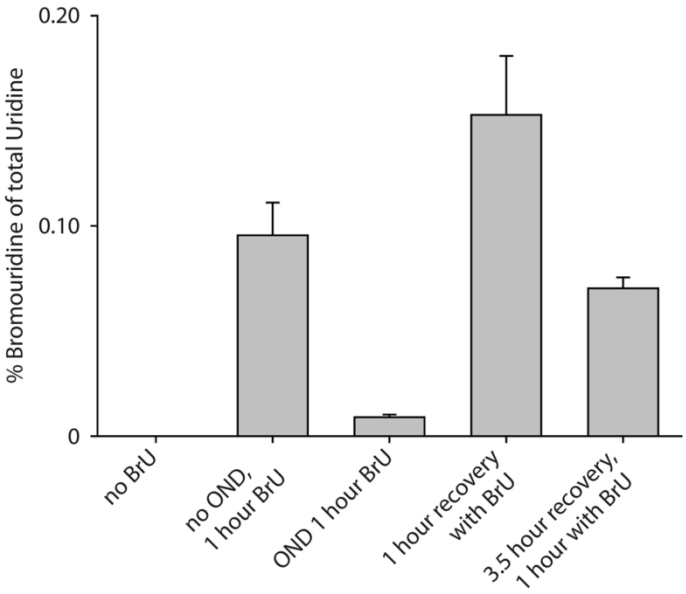

Figure 22. RNA synthesis is impaired by OND.
One hour of BrU incubation without OND was compared to one hour incubation during OND and after OND. Transcription decreases in OND, is highly induced after one of recovery and decreases after 3.5 hours of recovery.

3.1.4 Egr1, Egr2, Fos and FosB are induced upon OND and during ischemia

For the validation of the OND tissue culture model of cardiac ischemia-reperfusion injury, differentially expressed genes from the *in vivo* and the *in vitro* data sets were analysed for commonalities. The genes Egr1, Egr2, Fos and FosB are commonly induced in OND and after one hour of recovery and ischemia followed by two hours of reperfusion. After four hours of recover/reperfusion Egr1, Egr2, Fos, Fosb, JunB and Atf3 are no longer commonly expressed but immune factors, like Nlrp6, and heat shock proteins are highly induced in the mouse heart and, to lower extent, in the tissue culture model (Figure 23).

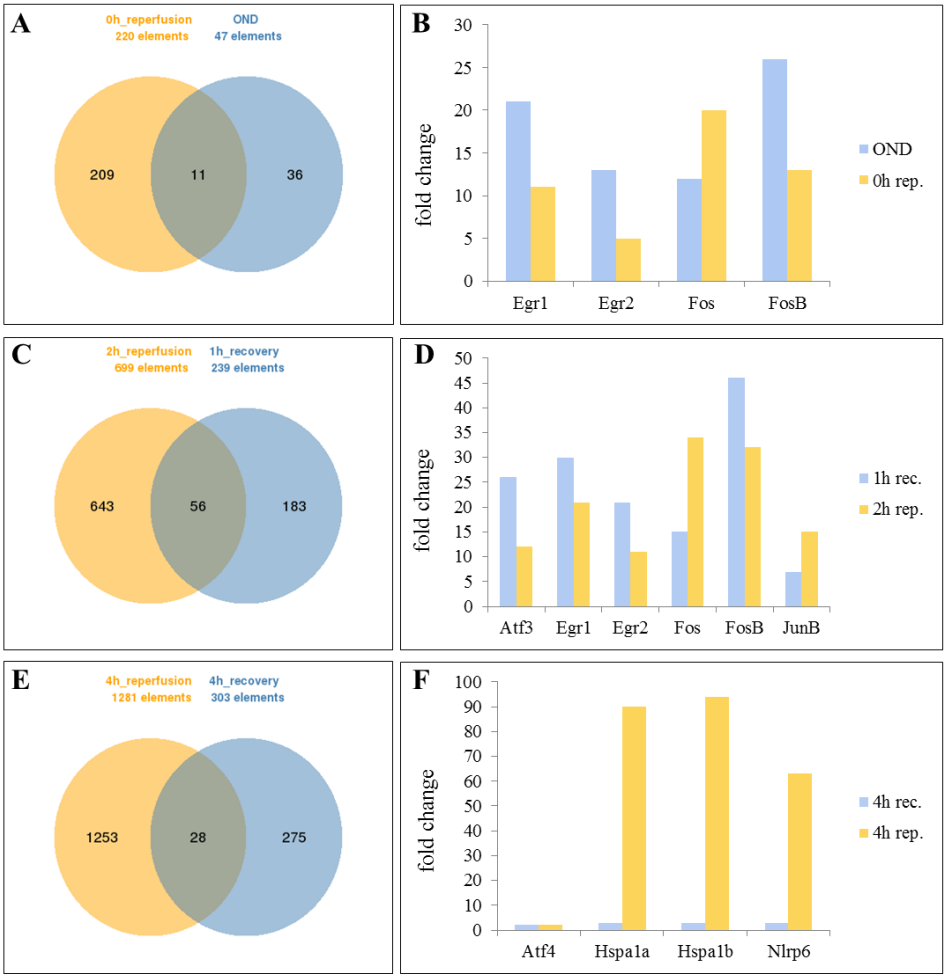

Figure 23. Genes commonly induced in OND/ ischemia and recovery/ reperfusion.
A. Eleven genes are commonly up-regulated in OND and ischemia. B. The genes Egr1, Egr2, Fos and Fosb are induced *in vivo* and *in vitro* ischemia. **C.** Fifty six genes are commonly up-regulated after short-term recovery/reperfusion. **D.** The expression of Egr1, Egr2, Fos and Fosb further increases. The factors Atf3 and JunB become commonly expressed. **E.** Twenty eight genes are commonly up-regulated after 4 hours of recovery/reperfusion. **F.** Atf4, heat shock proteins and immune factors, like Nlrp6 become induced.

Ischemia and OND induce muscle cell differentiation for the compensation of cardiomyocyte death. Both, although to a different extent, trigger a response of the immune system. Calcium homeostasis becomes disturbed in *in vivo* and *in vitro* ischemia. Short-term recovery/reperfusion triggers stress and immune responses, induces transcription, proliferation of muscle cells and fibroblasts, as well as angiogenesis pathways, and oxygen and calcium sensing pathways. After four hours of reperfusion/recovery, cells in the heart, as well as in the culture dish, react to wounding and inflammation, with apoptosis becoming induced (Table 14).

Two non-annotated transcripts are commonly induced in OND/ischemia, A330023F24RIK and E030016H06RIK. No genes were found to be commonly induced after short-term recovery/reperfusion. Four hours of reperfusion/recovery share twelve

down-regulated genes; eight of them are non-annotated transcripts. GO term analysis resulted in p-values lower than the threshold.

Two non-annotated transcripts are commonly induced in OND/ischemia, A330023F24RIK and E030016H06RIK. No genes were found to be commonly induced after short-term recovery/reperfusion. Four hours of reperfusion/recovery share twelve down-regulated genes; eight of them are non-annotated transcripts. GO term analysis resulted in p-values lower than the threshold.

Table 14. GO terms for OND/ischemia and recovery/reperfusion.
The *in vivo* and the *in vitro* model of ischemia and reperfusion have altered biological processes in common. Terms connected to oxygen are highlighted in blue.

OND and 0h rep.	1h rec. and 2h rep.	4h rec. and 4h rep.
pos. reg. of metabolic process p=2.8E-07 muscle cell differentiation p=3.1E-06 hemopoiesis p=4.2E-06 pos. reg. of gene expression p=6.4E-06 immune system development p=7.0E-06 pos. reg. of RNA metabolism p=4.2E-05 response to calcium ion p=7.0E-05	muscle cell differentiation p=7.0E-12 Neg. reg.of apoptotsis p=4.8E-10 pos.reg. of gene expression p=2.8E-10 pos. reg.of RNA metabolism p=3.7E-09 response to stress p=3.7E-08 pos. reg. of RNA synthesis p=1.6E-07 regulation of cell cycle p=2.4E-07 vasculature development p=4.0E-07 pos. reg. of cell proliferation p=4.0E-07 hemopoiesis p=6.1E-07 pos.reg. of cell death p=2.3E-06 neg. reg. of RNA metabolism p=6.6E-06 pos. reg. of apoptotic process p=1.3E-05 neg. reg. of gene expression p=1.5E-05 response to calcium ion p=5.2E-05 inflammatory response p=7.8E-05 response to oxygen p= 8.4E-05 connective tissue development p=9.0E-05	response to wounding p=9.8E-07 inflammatory response p=9.2E-06 pos. reg. of apoptosis p=1.3E-05 pos. reg. of homeostasis p=1.4E-05

3.1.5 Recovery/reperfusion induces impaired chromatin organisation

After 24 hours of reperfusion, twenty five histone genes were found to be repressed in the heart (Figure 19). After four hours of recovery in the OND tissue culture model, the expression of eleven histone genes was found to be decreased (Figure 21). Seven histone genes are commonly down-regulated after four hours of recovery and 24 hours of reperfusion (Figure 24).

Interestingly, transcripts of histone 1 (Hist1h1c) and histone 3 (Hist1h3d) are increased after one hour of recovery in HL-1 cells and return to basal-levels after four hours of recovery. Hist1h2bg is induced after one hour of recovery but becomes down-regulated

after four hours of recovery (Figure 24). The repression of histone genes implicates impaired chromatin organization upon IR/OND-recovery.

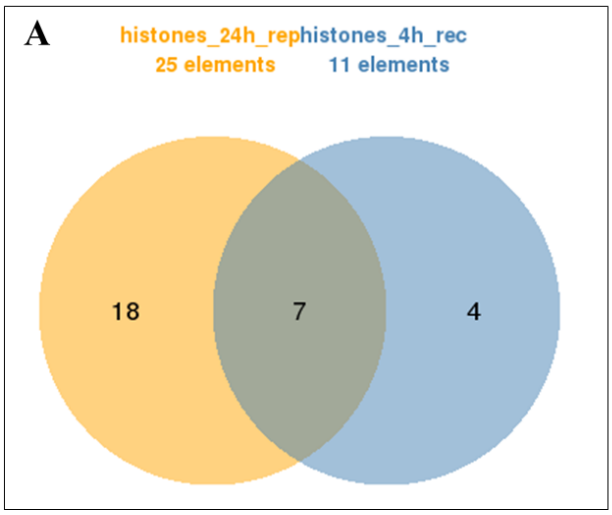

B

Gene	fold change 4h rec.	fold change 4h rep.
Hist1h3e	-3.3	-2.1
Hist1h3i	-4.2	-3
Hist1h4c	-10.6	-2.7
Hist1h4d	-6.9	-2.4
Hist1h4f	-10.4	-2.4
Hist1h4h	-2.1	-2.5
Hist2h4	-3.8	-2.9

C

Gene	fold change 1h rec.	Fold change 4h rec.
Hist1h1c	2.7	0
Hist1h2bg	2	-4.5
Hist1h3d	2	0

Figure 24. Down-regulated histone genes in OND and ischemia.
A. Seven histone genes are commonly down regulated recovery or after reperfusion. **B.** Down-regulated histone genes in grey belong to cluster 1, in blue to cluster 2. **C.** Three histone genes become up-regulated after one hour of recovery.

3.2 Western Blot analysis of histone modifications

3.2.1 Histones become deacetylated in OND

To answer the question if OND induces changes in chromatin organisation, quantification of active and repressive histone modifications was performed by Western Blot. HL-1 cardiomyocytes, mouse cardiac endothelial cells (MCEC) and mouse fibroblasts (3T3) were treated with OND or OND followed by four or 24 hours of recovery. Triplicates of extracted histones were probed for acetylation (ac) and methylation (me) of lysine residues (K) of core histone 3 (H3). The band intensities were normalized to H3 total signal. Acetylation of histones is a hallmark of gene activation, whereas methylation of histones has different impacts on transcription, depending on the modified residue. H3K9me3 and H3K27me3 are repressing modifications, with H3K4me3 correlated with gene activation.

Upon OND, lysine residues in the tail of core histone 3 (pan Ac H3) become deacetylated in all cell lines tested. In HL-1 cells, acetylation levels recover within 4 hours after OND treatment. 3T3 and MCE cells fully recover their acetylation within 24 hours (Figure 25).
OND induces 50 % deacetylation of H3K9 in all cell types tested. After four hours of recovery, acetylation levels are higher than in controls. After 24 hours of recovery, H3K9ac in 3T3 and MCE cells further increases, but levels in HL-1 cells decrease to control values (Figure 26). Starving conditions induce a 90 % loss of acetylation of H3K14. After 4 hours of recovery, acetylation of lysine 14 in 3T3 and MCE cells almost reaches control levels. HL-1 cells recover their K9 acetylation status only up to 60 % and hardly reach control intensities after 24 hours of recovery. Also MCE cells do not recover completely (Figure 27). H3K27 becomes about 90 % deacetylated upon OND in all cell types tested. After 4 hours of recovery, acetylation of lysine 27 in 3T3, HL-1 and MCE cells reaches 70 % of control levels. After 24 hours of recovery, H3K27ac levels decrease to approximately 50 % of control levels in all cell lines tested (Figure 28).
Under OND, acetylation of histone H3 significantly decreases in all cell types tested. The amount of deacetylation is cell-type depending; 3T3 fibroblasts become less deacetylated than cardiomyocytes and endothelial cells. The general loss of histone acetylation, inducing gene repression, is in line with the observation of impaired transcription, as observed by spectroscopy.
Histone acetylation generally increases after restitution of oxygen and nutrients but the recovery dynamics vary among cell types. Recovery kinetics is fast, re-acetylation happens within the first 10 minutes under standard culture conditions.

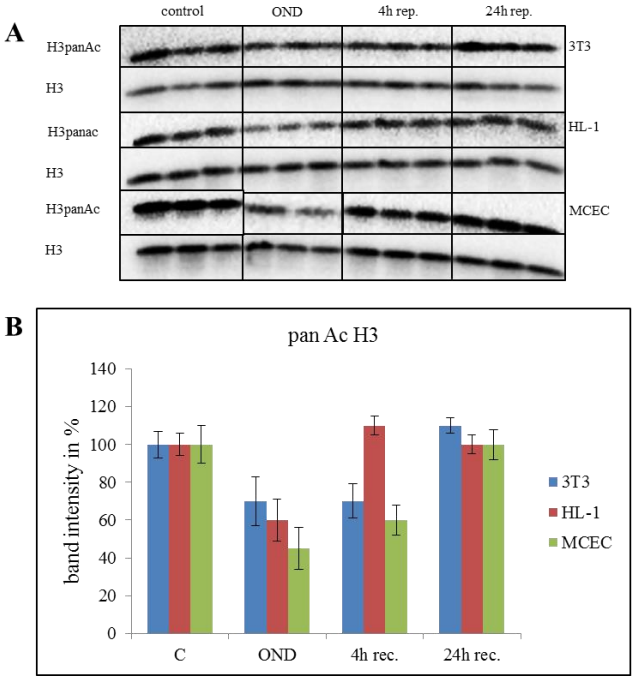

Figure 25. Ac H3 in OND and recovery.
A. Western Blot of pan Ac H3 for control, OND and 4 and 24 hours of recovery. **B.** The acetylation levels of H3 decrease under OND and recover within 24 hours under normal culture conditions. HL-1 cells recover faster in the first 4 hours of the recovery period.

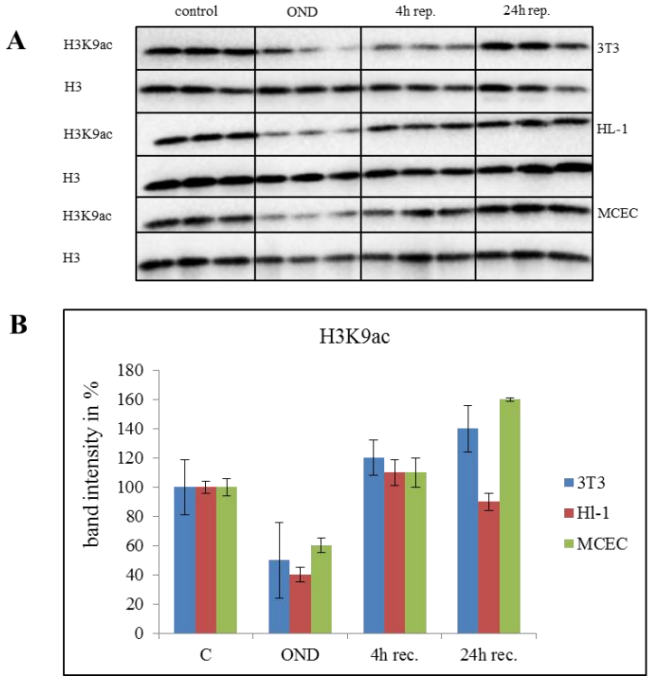

Figure 26. H3K9ac in OND and recovery.
A. Western Blot of H3K9ac for control, OND and 4 and 24 hours of recovery. **B.** The acetylation levels of H3K9 decrease by half during OND and increase higher than control levels upon recovery, except for HL-1 cells.

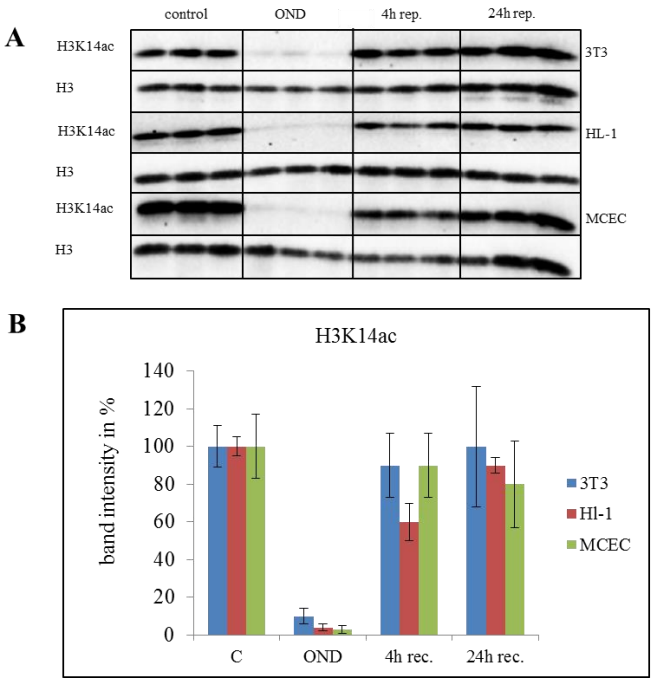

Figure 27. H3K14ac in OND and recovery.
A. Western Blot of for H3K14ac for control, OND and 4 and 24 hours of recovery. **B.** The acetylation levels of H3K14 decrease by 90 % in OND and increase to control levels upon recovery, except for HL-1 cells. After 24 hours, neither HL-1, nor MCE cells reached control intensities.

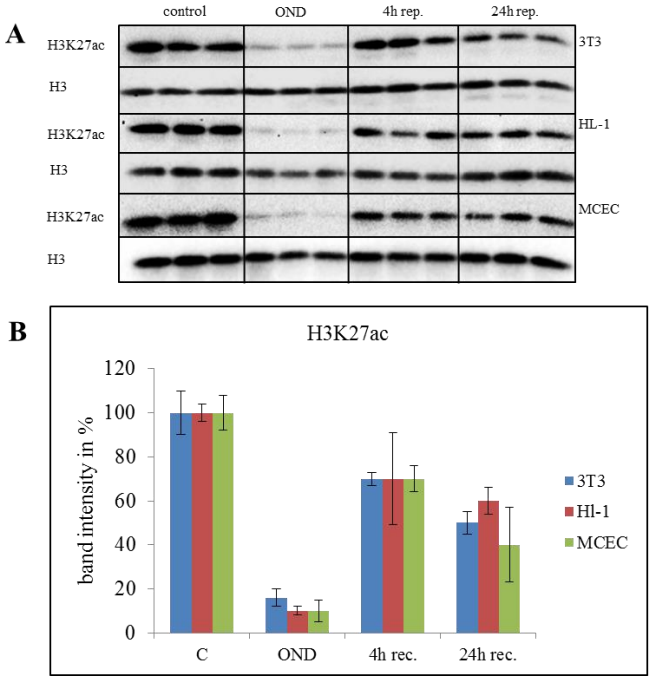

Figure 28. H3K27ac in OND and recovery.
A. Western Blot of H3K27ac for control, OND and 4 and 24 hours of recovery. **B.** The acetylation levels of H3K27 decrease by 80 – 90 % during OND and increase to 70 % control levels upon 4 hours of recovery. After 24 hours, levels of H3K27ac of 3T3, HL-1, MCE only reach 50 % of control intensities.

3.2.2 Histone methylation is constant upon OND

The band intensities of H3K4me3 after OND treatment in 3T3 and MCE cells are as high as control intensities, in HL-1 cells levels slightly decrease. In 3T3 and MCE cells, H3K4me3 signal does not change after four hours of recovery. In HL-1 cells, four hours of recovery induce a decrease of H3K4me3 to 60% of control intensities. After 24 hours of recovery, all cell lines recover to control levels of (Figure 29).

The tri-methylation levels of H3K9 do not change under OND in 3T3 cells, but slightly decrease in HL-1 and MCE cells. After four hours of recovery, H3K9me3 levels in HL-1 and MCE cells increase moderately, whereas 3T3 cells display 150% of the control intensity. After 24 hours of recovery, H3K9me3 is constant in 3T3 cells but decreases to 80% of control values in HL-1 and MCE cells (Figure 30).

Levels of H3K27 do not change significantly under OND in any cell line tested. Upon 4 four hours of recovery, H3K27me3 is slightly increased in 3T3 cells. After 24 hours of recovery, H3K27me3 decreases to 80% of control values in HL-1 and MCE cells (Figure 31).

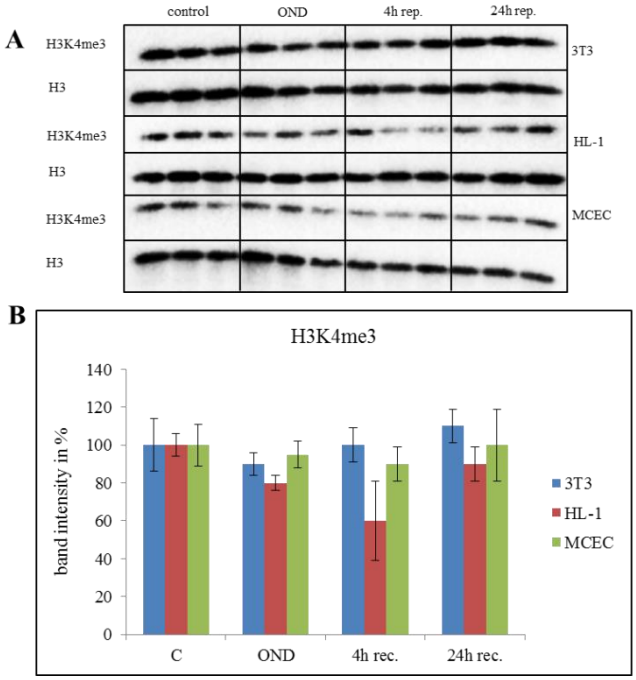

Figure 29. H3K4me3 in OND and recovery.
A. Western Blot of H3K4me3 for control, OND and 4 and 24 hours of recovery. **B**. The tri-methylation levels of H3K4 remain constant during OND in 3T3 and MCE cells and slightly decrease in HL-1 cells. After 4 hours of recovery, levels of H3K4me3 in 3T3 and MCE cells do not changes significantly but decrease to 60 % in HL-1 cells. After 24 hours of recovery, K4 methylation in all cell lines reaches control levels.

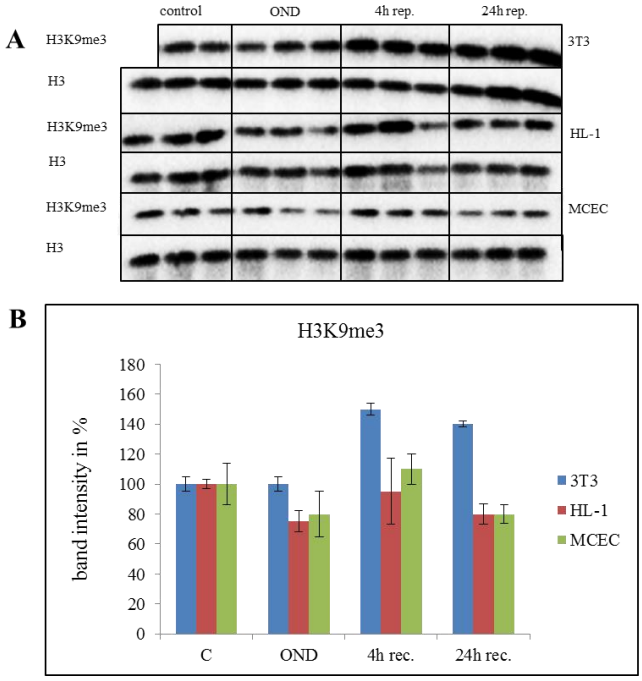

Figure 30. H3K9me3 in OND and recovery.
A. Western Blot of H3K9me3 for control, OND and 4 and 24 hours of recovery. **B.** H3K9me3 decrease by 20 % in OND in HL-1 and MCE cells but remains constant in 3T3 cells. After 4 hours of recovery, H3K9me3 increases in all cell types. After 24 hours of recovery, H3K9me3 in 3T3 remains high but decreases to 80 % in HL-1 and MCE cells.

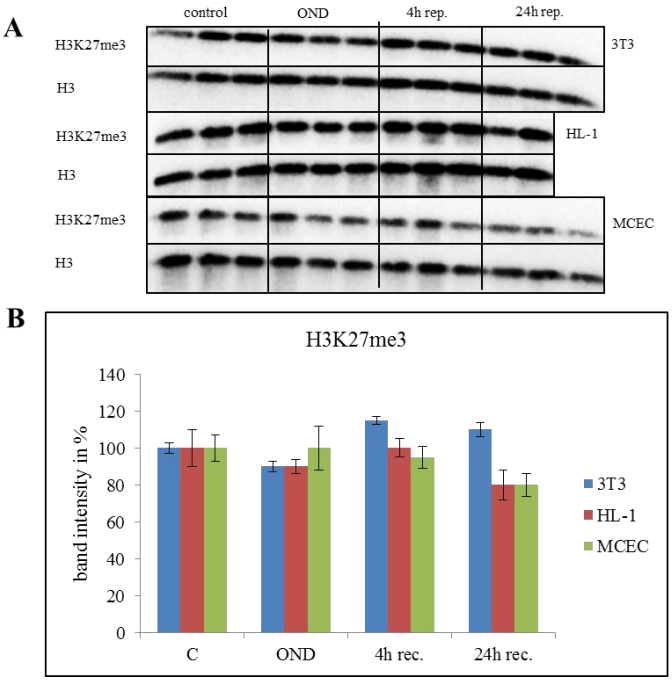

Figure 31. H3K27me3 in OND and recovery.
A. Western Blot showing triplicates of isolated histones probed for H3K27me3 for control, OND and 4 and 24 hours of recovery. **B.** The tri-methylation levels of H3K27 do not changes significantly during OND. After 4 hours of recovery, H3K27me3 staining in HL-1 and MCE cells is at control levels. In 3T3 cells, H3K4me3 is slightly increased. After 24 hours of recovery, K27 methylation decreases to 80 % of control intensity in HL-1 and MCE cells.

3.2.3 Histones become re-acetylated within the first minutes of recovery

In order to evaluate shorter recovery times than four hours, a series of 10 to 60 minutes of recovery was analysed for H3K14ac and its opposing mark H3K14me3 in HL-1 cells. The activating histone mark H3K14ac, decreased by 90 % under OND, recovers within the first 10 minutes of reperfusion. The repressing mark H3K14me3 does not change under OND and does not show alterations during recovery (Figure 32).

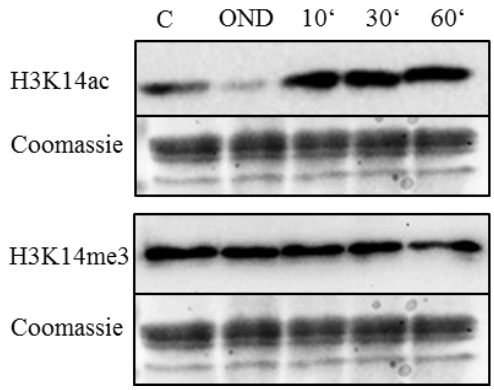

Figure 32. H3K14ac and H3K14me3 recovery time course.
The active histone mark H3K14ac decreases under OND and recovers within 10 minutes of reoxygenation. The repressive mark H3K14me3 does not change under these experimental conditions. Coomassie brilliant blue staining was used as a loading control.

3.2.4 Histone modifications are not altered in ischemia and reperfusion

Western Blot analysis of extracted histones from tissue pieces of IR hearts revealed no detectable differences between the conditions and antibodies tested (Figure 33). Considering the different cell types and the combination of affected and non-affected cells comprised in a piece of cardiac ischemic tissue, the response might be masked.

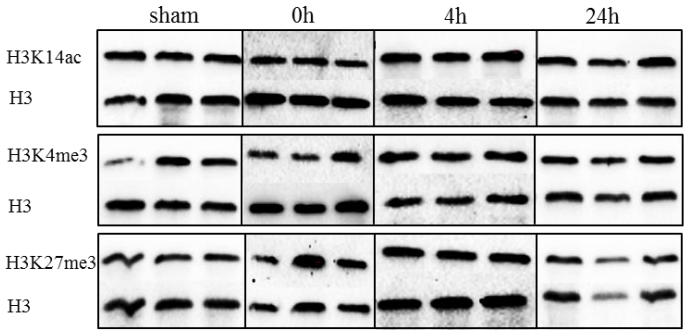

Figure 33. histone marks in IRI.
H3K14ac, H3K4me3 and H3K27me3 levels do not change significantly in ischemia and after 4 and 24 hours of reperfusion.

3.3 Confocal microscopy analysis

3.3.1 The signal of histone H3 and acetylated H3 decreases in OND

After quantification of histone modifications upon OND by Western Blot, their distribution in the nucleus was analysed by confocal microscopy. Activating and repressing histone marks were investigated in HL-1 cardiomyocytes.

In control cells, H3 signal is evenly distributed in the nucleus and in the cytoplasm. Unlike observed on Western Blot, H3 signal in the nucleus decreases upon OND. After 10 minutes of recovery, the signal is higher than in control cells (Figure 34). H3 pan acetylation is distributed along with the diffuse DNA staining and excluded from DNA-dense clusters. Under OND, signal-sparse regions appear in the middle of the nucleus and pan Ac H3 staining is shifted to the nuclear periphery. Upon recovery, the signal is distributed as in control cells, but fluorescence intensity is increased (Figure 35). H3K9ac is distributed like pan Ac H3. Upon OND, the signal intensity decreases. After 10 minutes of recovery, H3K9ac signal displays higher intensities than in control cells (Figure 36). H3K14ac pattern distributed like pan Ac H3, but the signal is more granular. Under OND, the staining signal is mostly located at the nuclear periphery, as observed for pan Ac H3. Signal-sparse regions are visible inside the nucleus. Upon recovery, the H3K14ac pattern looks as in control cells (Figure 37).

H3K27ac is distributed like the previously described acetylation marks. In OND, sparsely stained regions are visible, which disappear after 10 minutes recovery. The signal intensity only increases in some cells, the majority of cells displays staining intensities as controls (Figure 38).

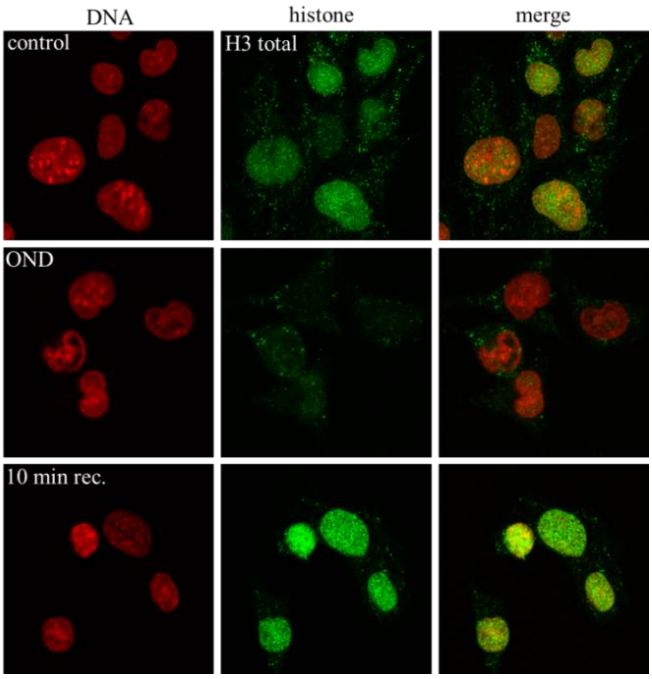

Figure 34. H3 and DNA staining for controls, OND, and recovered cells.
In control cells, H3 signal is distributed evenly in the nucleus und partly in the cytoplasm. Under OND, H3 signal decreases, bright spots in the cytoplasm are still detectable. After 10 minutes of recovery, H3 signal appears brighter than in control cells.

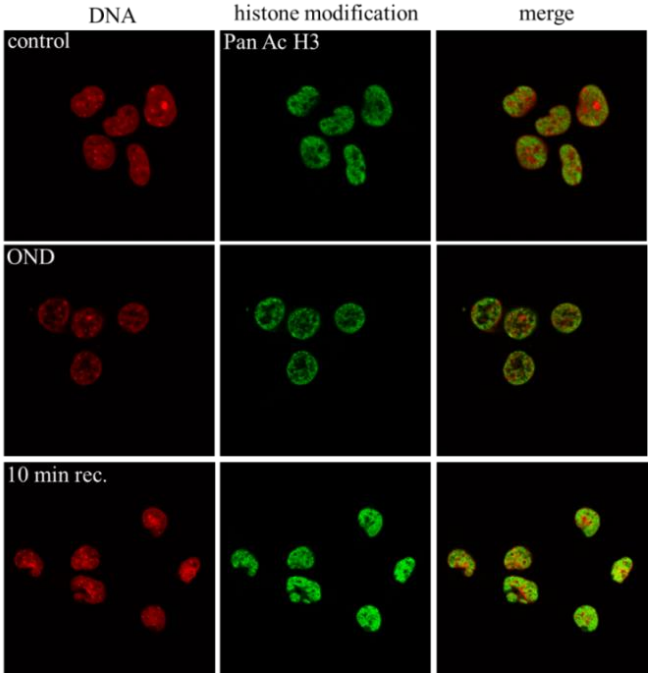

Figure 35. Pan Ac H3 and DNA staining for controls, OND, and recovered cells.
In control cells, the signal is distributed evenly in the nucleus. Under OND, pan Ac H3 is mainly located at the nuclear periphery and the middle of the nucleus is sparse of signal. After 10 minutes of recovery, the acetylation signal is distributed as in control cells but the signal is brighter.

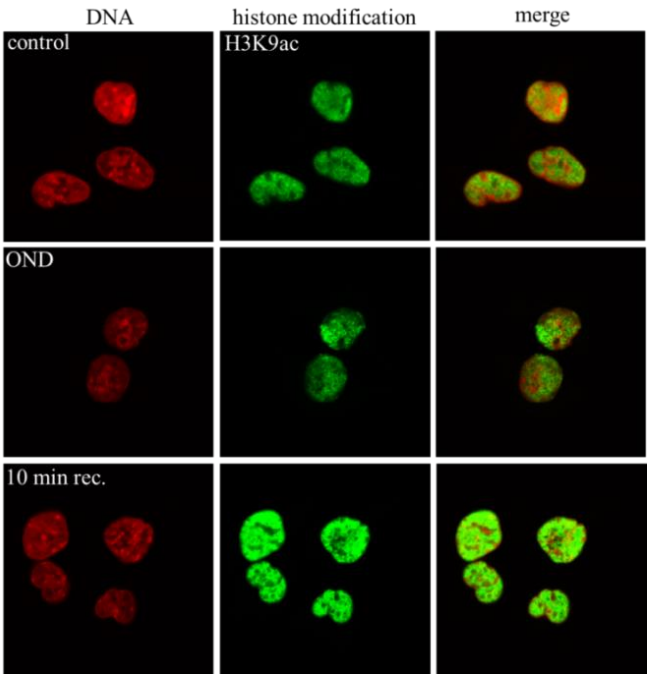

Figure 36. H3K9ac and DNA staining for controls, OND, and recovered cells.
H3K9ac signal is distributed evenly in the nucleus, but excluded from heterochromatin. Under OND, H3K9ac intensity decreases. After 10 minutes of recovery, the acetylation signal is brighter than in control cells.

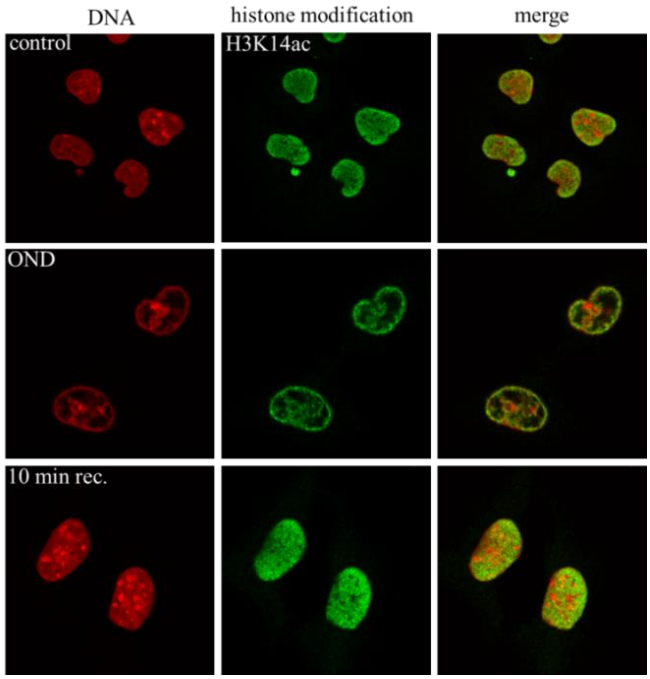

Figure 37. H3K14ac and DNA staining for controls, OND, and recovered cells.
H3K14ac is distributed evenly in the nucleus, but excluded from DNA-dense regions. Under OND, the signal is mainly detected at the nuclear periphery; the middle of the nucleus shows only few staining. After 10 minutes of recovery, the H3K14 acetylation pattern signal looks as in control cells.

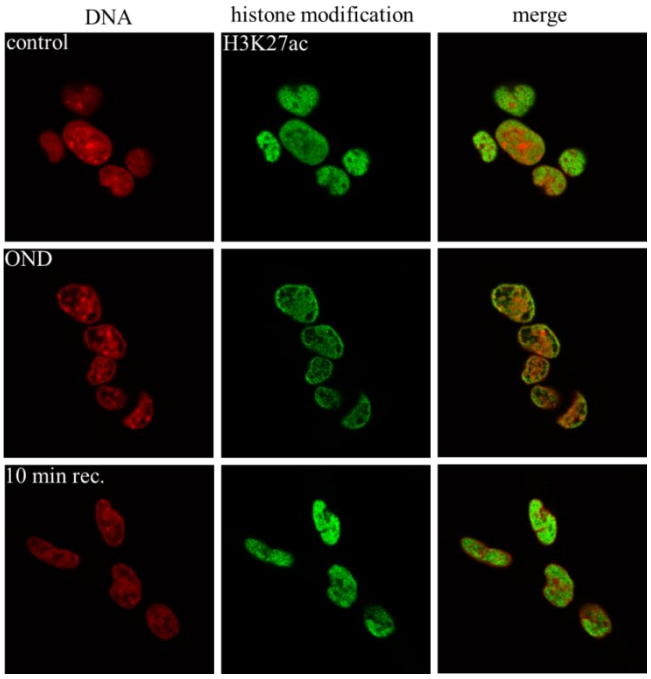

Figure 38. H3K27ac and DNA staining for controls, OND, and recovered cells.
In control cells, the signal is distributed evenly in the nucleus, excluded from chromocenters. Under OND, H3K27ac signal decreases, some sparse regions are visible. After 10 minutes of recovery, the acetylation signal is distributed and as intense as in control cells.

3.3.2 Histone methylation is not altered significantly upon OND

The activating histone modification H3K4me3 is evenly distributed in the nucleus, associated with diffuse DNA and excluded from DNA-dense regions, as expected for an activating mark. Under OND, the distribution of H3K4me3 becomes more granular and some brighter spots are visible. After recovery, the distribution and the signal intensity of H3K4me3 is similar to control cells (Figure 39).

. The repressing histone mark H3K9me3is located at the DNA-dense regions, the chromocenters, and at the nuclear periphery. Under OND, the pattern of H3K9me3 covers a larger area of the nucleus. After 10 minutes of recovery, H3K9me3 signal is not strictly associated with chromocenters anymore, but covers the nucleus (Figure 40).

. The staining of the repressing mark H3K27me3 is covering the whole nucleus. Upon OND, the staining looks more intense and the distribution looks more granular. No further changes are detectable after 10 minutes of recovery (Figure 41).

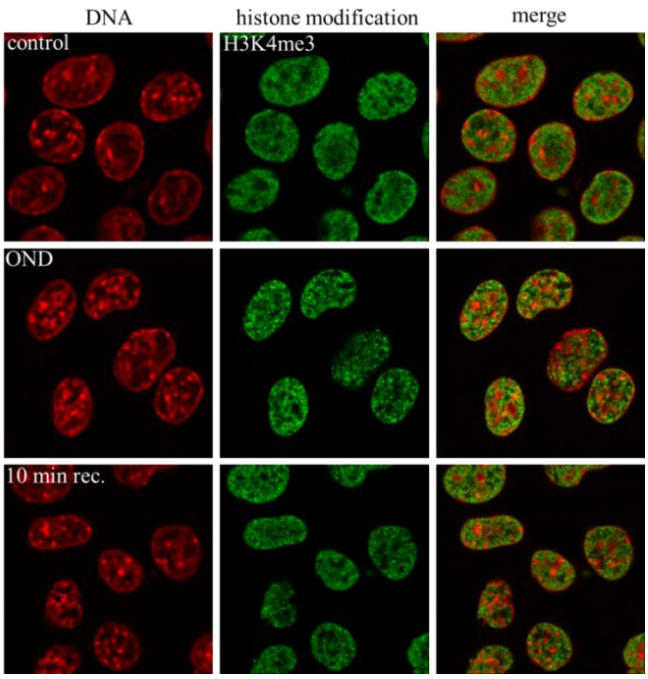

Figure 39. H3K4me3 and DNA staining for controls, OND, and recovered cells.
In control cells, the signal is distributed evenly in the nucleus, excluded from chromocenters. Under OND, H3K4me3 staining looks more granular. After 10 minutes of recovery, H3K4me3 signal distribution and intensity looks as in control cells.

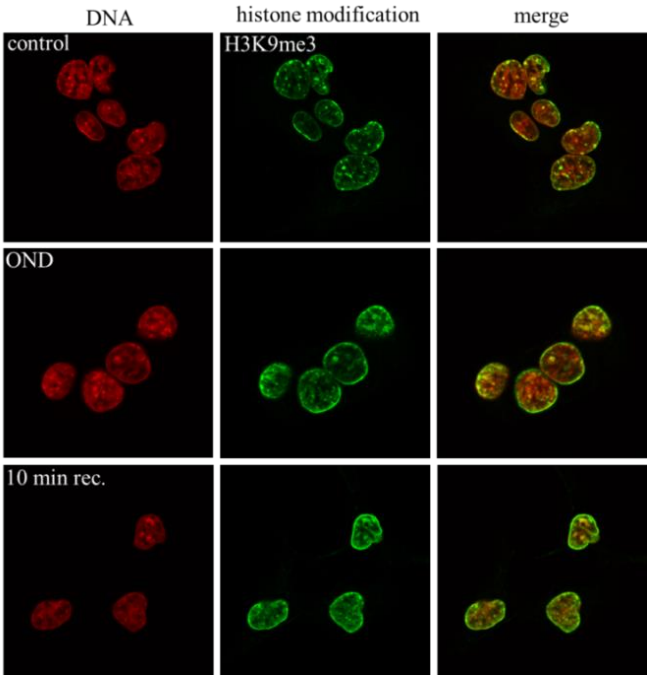

Figure 40. H3K9me3 and DNA staining for controls, OND, and recovered cells.
In control cells, the signal of H3K9me3 is strictly located with the chromocenters and the nuclear periphery. Under OND, the distribution of H3K9me3 becomes broader, being most intense at chromocenters and periphery. After 10 minutes of recovery, the signal is not mainly associated with the chromocenters anymore but covers the nucleus.

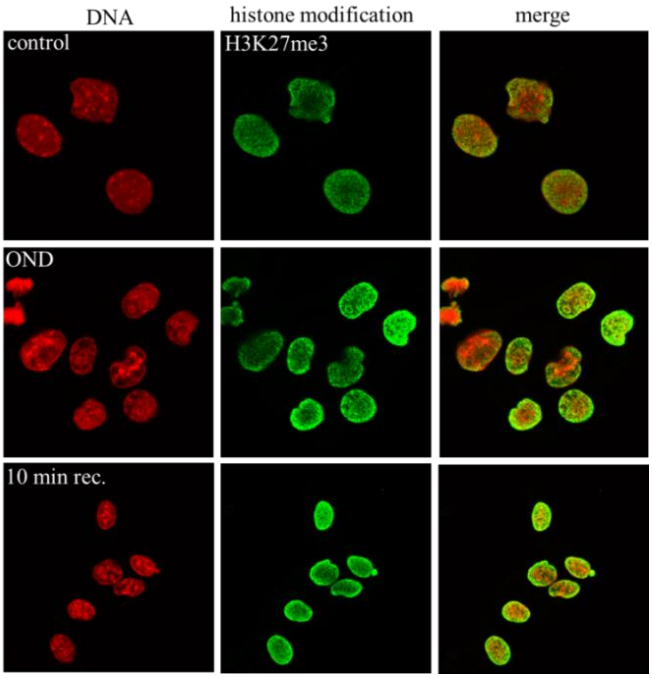

Figure 41. H3K27me3 and DNA staining for controls, OND, and recovered cells.
H3K27me3 is evenly distributed in control nuclei. Upon OND, the signal intensity of H3K27me3 increases is some cells. 10 minutes of recovery do not induce further changes in H3K27me3 intensity and distribution.

3.3.3 H3S28p increases upon OND and recovery

Phosphorylation at serine 10 on the tail of H3 (H3S28P) is required for chromatin condensation during mitosis and is also associated with the transcriptional activation resulting from stimulation by external stimuli like mitogens and stress (Han et al., 2006).
In control cells, the signal of H3S28P is dotted and of low intensity. Under OND, the fluorescent intensity of the dots increases. After 10 minutes of recovery, the nucleus is covered by an intense H3S28P signal (Figure 42).

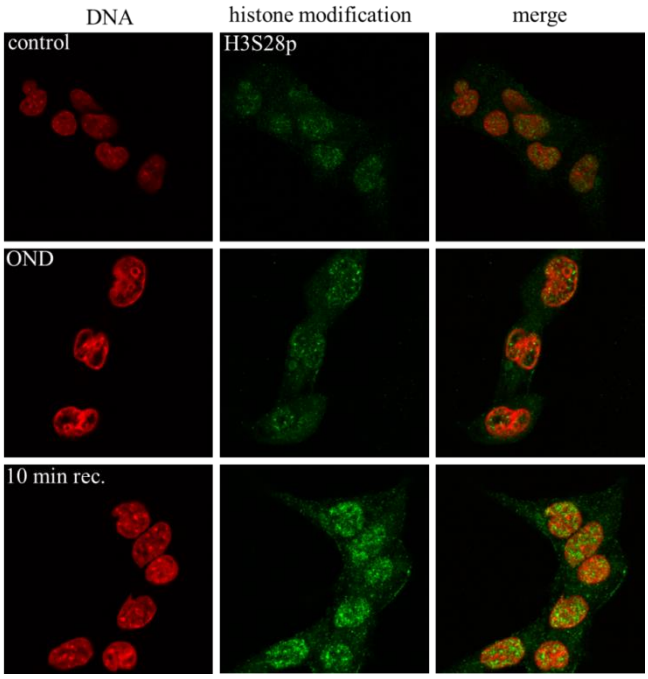

Figure 42. H3S28P and DNA staining for controls, OND, and recovered cells.
In control cells, the signal is low and visible as dots in the nucleus. Under OND, H3S28P staining intensity increases. After 10 minutes of recovery, the nucleus is covered with an intense signal of H3S28P.

Analysis of histone modifications on cardiac tissue sections revealed no definite results, due to irreproducibility (data not shown).

3.3.4 Chromatin compacts under OND conditions

Microscopical analysis of HL-cells revealed changes in DNA conformation upon OND treatment. Under starving conditions, the DNA compacts into atoll-like clusters, leaving sparse, DNA-free regions in the nucleus. Histone modifications, like H3K9ac e.g., are located on the perichromatin, facing the DNA-free areas (Figure 43).

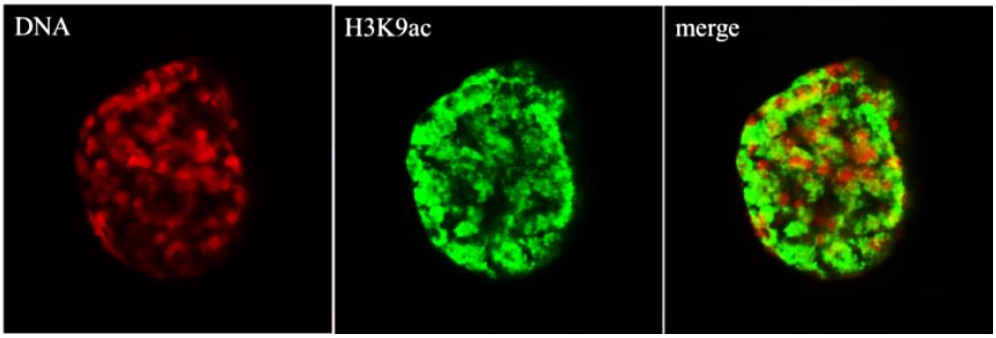

Figure 43. Changes in DNA structure and H3K9ac in OND.
Upon OND treatment, DNA compacts, introducing DNA-sparse regions in the nucleus (red). H3K9ac encases the DNA, most intensely at the nuclear periphery.

3.3.5 The combination of oxygen and nutrient deprivation induces the OND phenotype

In order to test if any of the components of oxygen and nutrition can induce DNA compaction and histone deacetylation in HL-1 cells, treatments were analysed separately. Oxygen deprivation is sufficient to induce DNA compaction, but neither decrease H3K14ac levels, nor alters its distribution. Ischemic buffer, containing deoxyglucose as an inhibitor of glycolysis, cannot induce DNA compaction but moderately decreases H3K14ac levels. Only when in combination, oxygen and nutrient deprivation induces the OND phenotype of compacted DNA and deacetylated histones (Figure 44).

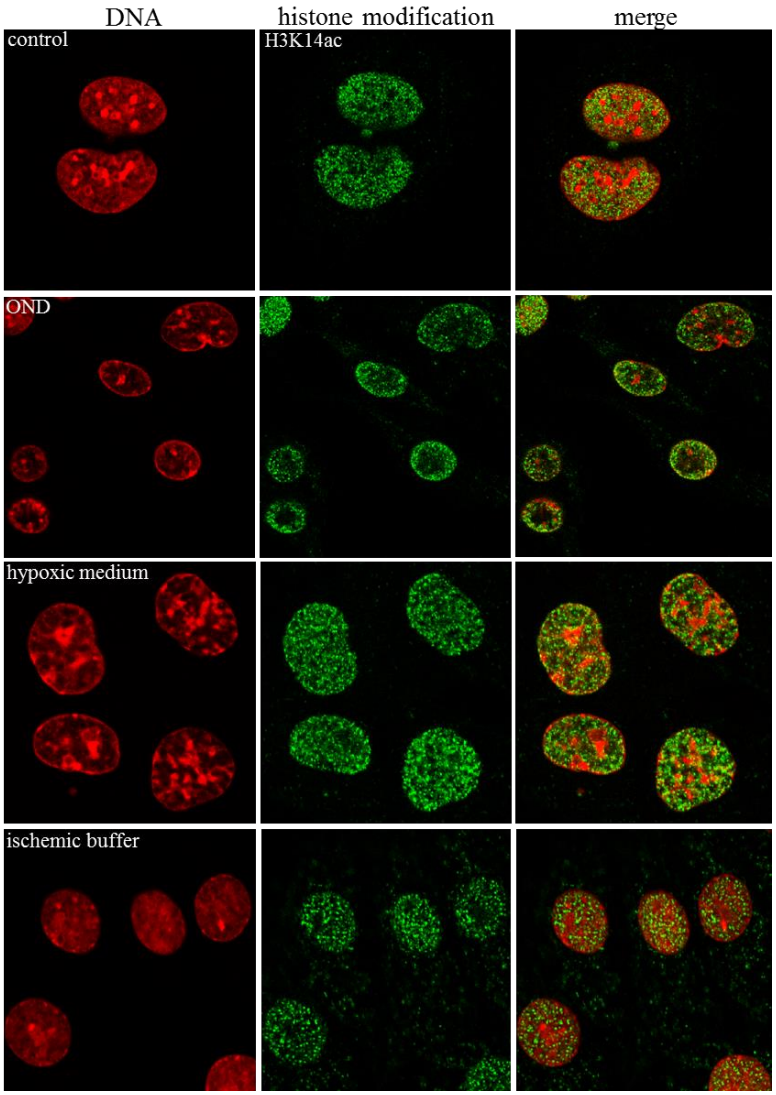

Figure 44. OND. hypoxia, and nutrient deprivation.
OND treatment causes DNA compaction and a decrease of H3K14ac. Hypoxic culture medium induces DNA compaction, but does not impair acetylation. The application of ischemic buffer does not induce chromatin compaction, but induces a moderate decrease in H3K14ac.

3.4 SMLM analysis of DNA structure and histone acetylation

3.4.1 OND induces ring-like structures and DNA-sparse voids

Since detailed analysis of DNA conformational changes upon OND was not possible, considering the low resolution of confocal microscopy, SMLM was applied, using the photo-convertible DNA dye Vibrant DyeCycle Violet, which undergoes reversible photoswitching and can be used to compile a high resolution image of the structure of chromatin.

Untreated HL-1 cells show a typical DNA staining pattern, with rather intense staining occurring inside the nuclear envelope and in discrete foci within the nucleus. There is a general diffuse staining of DNA within the nucleus, with small inter-nuclear compartments of lacunas (*) and interchromatin channels, visible between individual chromatin domains. H3K14ac occurs in a punctate distribution throughout the nucleus, with individual foci predominantly located at the edge of chromatin domains (Figure 45).

An ischemic environment provokes DNA compaction, visible as condensed chromatin present at the sub-nuclear envelope, as double arrangement of densely stained DNA or as hollow intra-nuclear atolls. The inter-chromosomal space expands, consisting of DNA-sparse voids and staining for H3K14ac signal decreases. Diffused DNA staining, as observed in control cells, is also present in OND cells (Figure 45). Neither confocal microscopy, nor wide-field microscopy can provide these details.

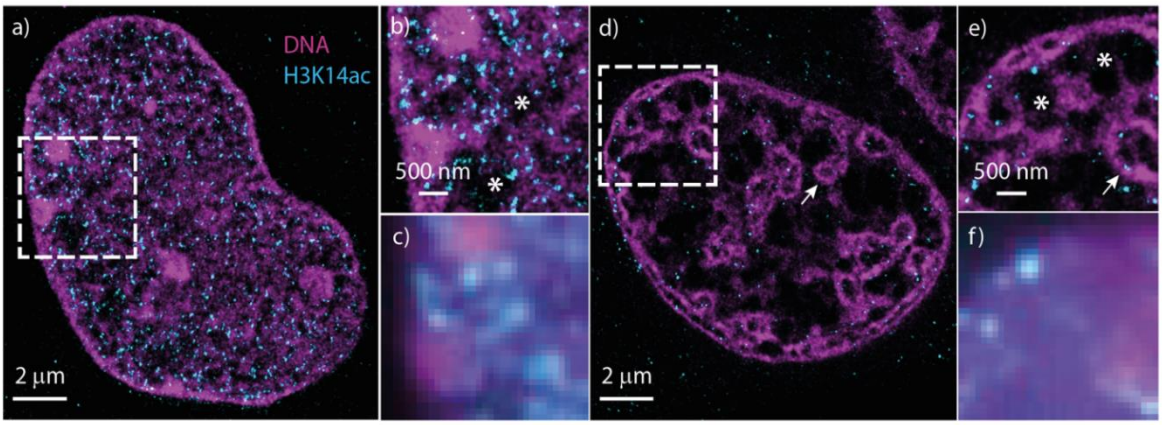

Figure 45. SMLM images of a control and an OND treated cell.
A.The DNA of control cells is evenly distributed in the nucleus, with an intense staining at chromocenters and the nuclear periphery. **B.** Lacunas (*) are small and H3K14ac signal is located on the perichromatin. **C.** Widefiled mode cannot provide these details. **D.** In OND, DNA compacts and forms ring-like structures. **E.** The size of lacunas increases and the signal H3K14ac signal decreases. F. Widefield mode cannot provide these details. B and E are magnifications of the areas indicated in dashed squares.

Two alternative DNA staining methods were tested, in order to confirm the observed DNA structure alterations. DNA was stained with YOYO-1, which also blinks under the experimental conditions, and by the incorporation of 5-ethynyl-2′-deoxyuridine (EdU), combined with Click-it chemistry. Both alternative methods showed the same condensed DNA structures in OND, as observed for staining with Vibrant DyeCycle Violet (data not shown).

3.4.2 The signal of core histone H3 decreases under OND conditions

Confocal microscopy analysis of histone H3 staining indicated a lower fluorescent signal in OND treated HL-1 cells (Figure 34). SMLM analysis also revealed a reduced density of chromatin-associated histone H3 in the nucleus from 3813 ± 250 per μm^2 in controls to 842 ± 503 per μm^2 in OND treated cells. The levels observed in the cytoplasm remain similar at 250 per μm^2 (Figure 46).

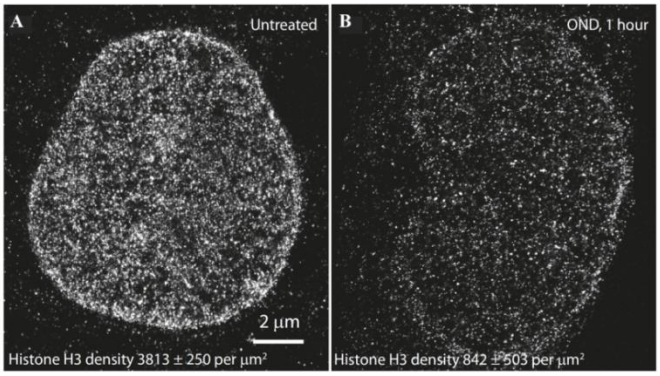

Figure 46. SMLM images of H3 in OND and control cell.
A. H3 signal in untreated cells is densely distributed in the nucleus, 3813 ± 250 counts per µm2. B. In OND treated cells H3 signal counts are reduced to 842 ± 503 per µm2. The amount of signal in the cytoplasm remains the same.

3.4.3 The distribution of Lamin B is not altered upon OND

Because OND induces toroidal DNA structures close to the nuclear periphery, analysis of Lamin B distribution was performed, in order to investigate if invagination of the nuclear membrane occurred under OND. Upon experimental ischemia, the nuclear membrane does not invaginate, nor does Lamin B distribution change (Figure 47).

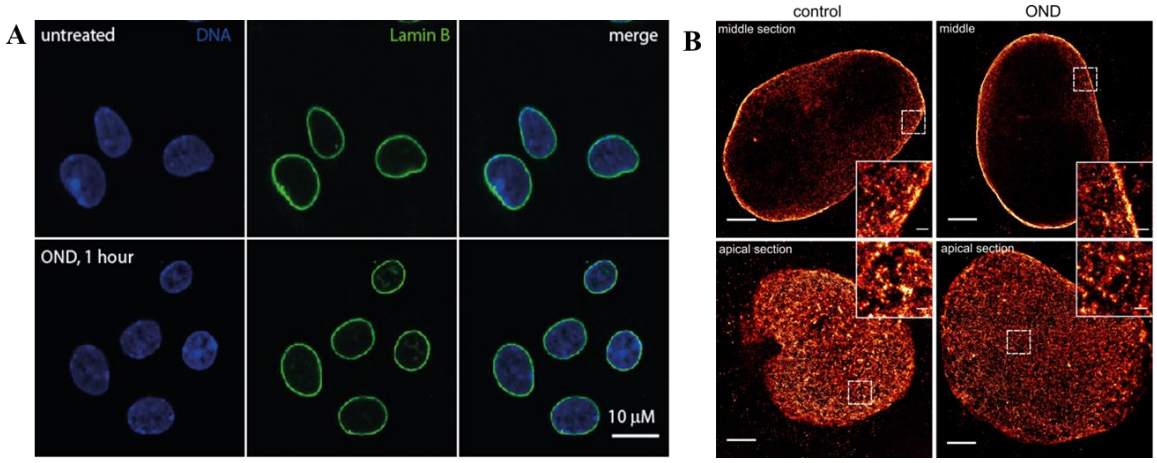

Figure 47. The distribution of Lamin B in control and OND cells.
A. Confocal image of Lamin B staining, as marker for the nuclear lamina. The Pattern of Lamin B does not change upon OND. **B.** SMLM images of Lamin B of middle and apical sections, close-ups show nuclear pore complexes. The distribution of Lamin B does not change upon OND. This experiment was performed by Christina Heiser.

3.4.4 Recovery from OND induces a more open chromatin conformation

SMLM analysis of a 240 minute time series of restitution of normoxia and nutrients showed that DNA compaction is reversible. Within 5 to 15 minutes of recovery, nuclear architecture starts to relax, after 60 minutes the organization looks similar to control nuclei. After 240 minutes of recovery, DNA structure appears more diffused and does not show DNA-dense regions (Figure 48).

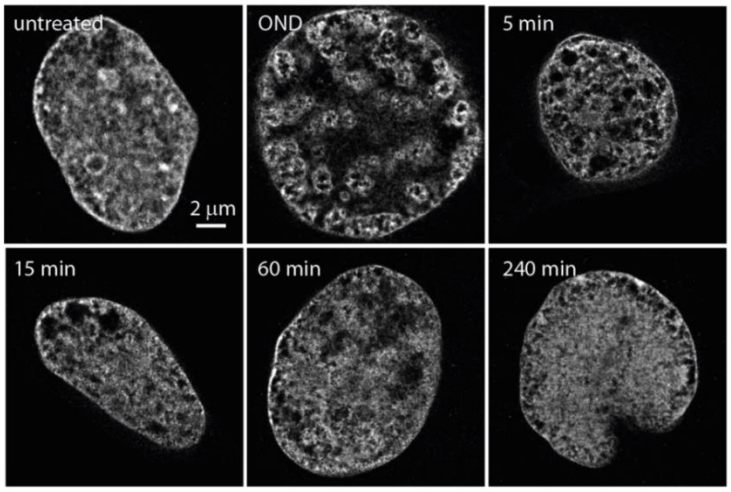

Figure 48. SMLM OND recovery series of HL-1 cells.
OND induces the previously characterized phenotype of ring-like structures and DNA-sparse regions. Within 5 minutes of recovery, DNA starts to de-compact. After 240 minutes of recover, the DNA is fluffy and no chromocenters are detectable.

Calculation from thresholded SMLM pictures of a minimum of nine cells per condition revealed a two fold increase of chromatin-free nuclear area in OND. Already after 5 minutes of recovery, DNA-sparse regions become smaller and fewer. Sixty minutes of oxygen and nutrient supply is sufficient for the majority of cells to restore chromatin architecture. After 240 minutes of recovery, a significant proportion of the cells adopt a more open DNA conformation (Figure 49).

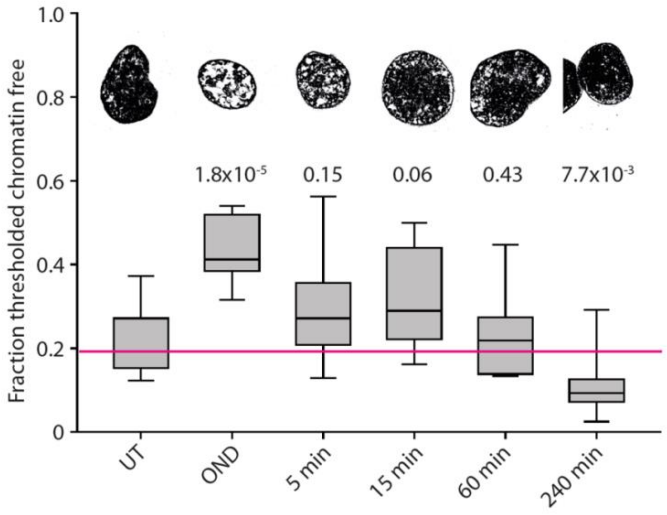

Figure 49. Calculation of chromatin-free areas of OND treated and recovering cells.
A minimum of nine cells was analysed per condition and DNA staining-free regions were calculated using image J. The red line indicates the median of control cells. The numbers above the whiskers are the significances of the changes compared to controls in p-values. Under OND, the chromatin-free area is larger than in controls. After 60 minutes of recovery, values reach control levels. After 240 minutes of recovery, the chromatin-free area is significantly smaller than in control nuclei. UT: untreated. This graph was composed by Aleksander Szczurek, IMB.

Analysis of the DNA conformation in cardiac tissue sections with SMLM failed, due to poorly conserved nuclei structures and high auto fluorescence of the samples (data not shown).

3.4.5 Electron microscopy analysis of the DNA structure under OND

In SMLM, the DNA is stained with a dye and the super-resolution image is reconstructed by computational analysis. To rule out that these procedures introduce biases, TEM was applied, where the DNA is not stained but contrasted and the high resolution is obtained from the small de Broglie wavelength of electrons.

The DNA of untreated cells is diffusely distributed in the nucleus and some DNA-dense regions are visible, as observed by SMLM. OND treated cells display intensively

compacted, clustered DNA close to the nuclear lamina as well as inside the nucleus and the interchromatin space is expanded; as observed by SMLM (Figure 50).

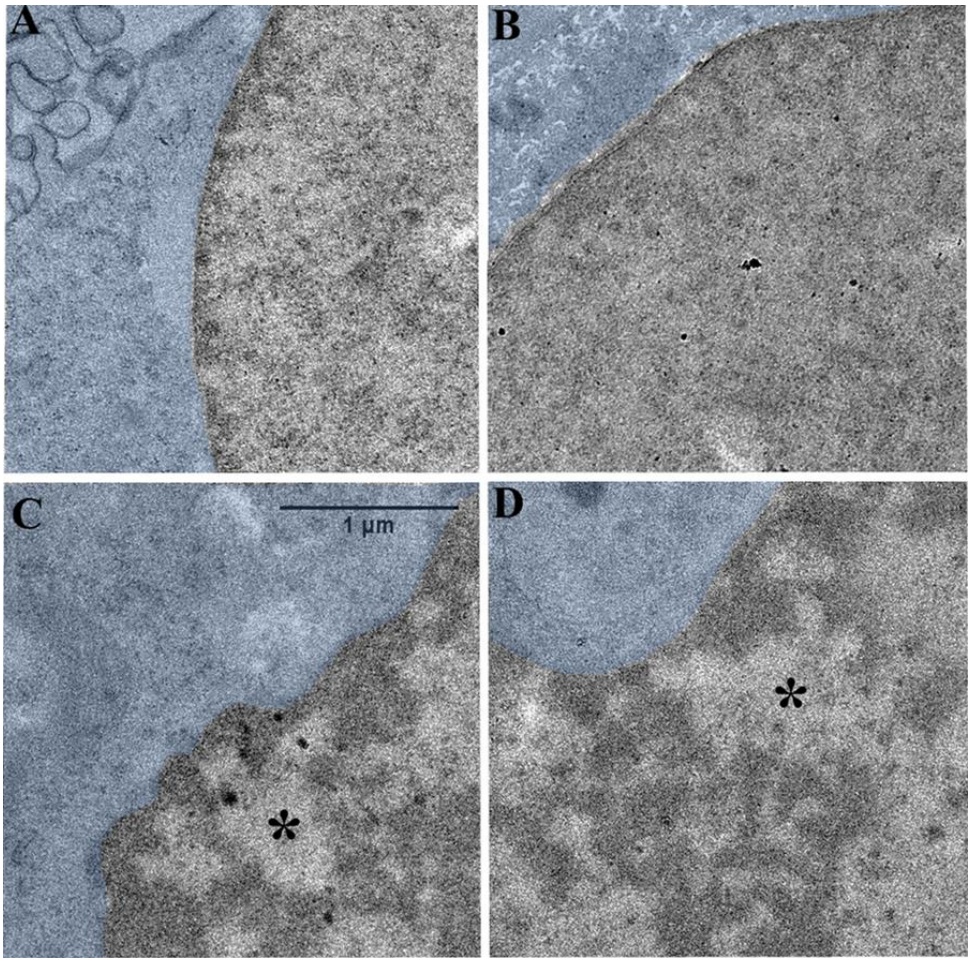

Figure 50. Transmission electron microscopy image.
A. and **B.** Sections of two nuclei of untreated HL-1 cells: The DNA is diffusely distributed in the nucleus.
C. and **D.** Sections of two nuclei of OND treated HL-1 cells: The DNA compacts and DNA-sparse regions expand (*).

3.5 Flow cytometry analysis of histone modifications

3.5.1 Activating histone modifications decrease upon OND

As another confirmation of the changes observed under OND in post-translationally modified histone H3 variants and impaired targeting of core histone H3, flow cytometry analysis of HL-1 cardiomyocytes, subjected to OND and recovery, was performed.

In contrast to Western Blot, chromatin structure and conformation stay intact during immunofluorescence staining and thousands of cells can be analysed, in contrast to microscopical approaches. As observed previously, OND treatment decreases the signal of H3, pan Ac H3, H3K9ac, H3K14ac, H3K27ac and H3K4me3, whereas levels of H3K9me3 and H3K27me3 remain constant (Figure 51).

A slight increase in methylation, seen by confocal microscopy analysis, could not be confirmed. Since microscopy analysis only included approximately ten cells per staining, analysed by eye, whereas the flow cytometer analysed thousands of cells automatically, results obtained by this method are more reliable.

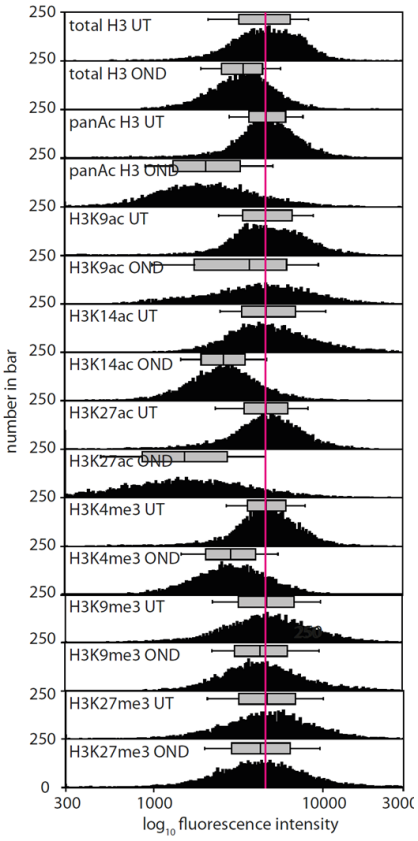

Figure 51. H3, H3 acetylation and methylation signals in untreated and OND treated cells.
Single cell data was binned and plotted against fluorescence intensity. Under OND, fluorescence intensity decreases for H3 total and the activating marks pan Ac H3, H3K9ac, H3K14ac, H3K27ac and H3K4me3. Levels of repressing H3K9me3 and H3K27me3 do not change under OND conditions. UT: untreated.

3.5.2 Acetylation of histones recovers within 15 minutes

To check if the histone re-acetylation is also detectable by flow cytomerty, a 60 minute recovery series for pan Ac H3 was anlysed. The pan Ac H3 antibody detects all acetylated lysine residues in the tail of core histone 3 and is representative for all acetylated residues testet previously. A recovery of 2 to 5 minutes is not suffcient to completely recover the pan acetylation status of HL-1 cells after OND. Within 15 minutes of recovery, the fluorescent signal increases higher than control values and remains as high for the rest of the time course (Figure 52).

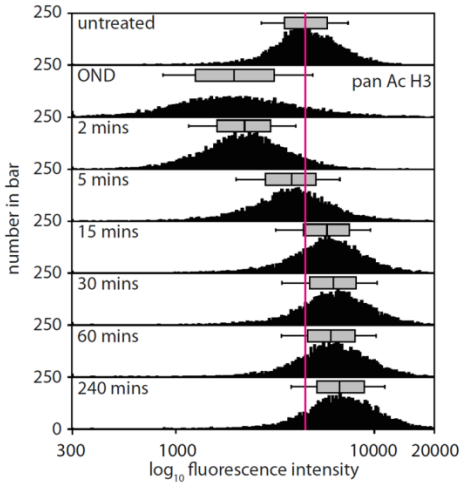

Figure 52. pan Ac H3 signal in untreated, OND treated, and recovering cells.
Single cell data was binned and plotted against fluorescence intensity. Under OND, fluorescence intensity decreases for pan Ac H3. Upon recovery, the fluorescent intensity gradually increases, reaching values higher than for untreated cells.

3.6 Analysis of chromatin compaction under OND conditions

3.6.1 Chromatin digestion time increases upon OND

A DNaseI digestion assay was used as a biochemical approach to confirm that OND treatment induces chromatin compaction. A decay of the fluorescent signal of the interchelating DNA dye DRAQ5 was observed during the digestion progress, which is depended on the accessibility of DNaseI to DNA present within chromatin: open chromatin is more accessible that highly condensed and compacted chromatin.
Untreated cells show a triphasic response to DNaseI treatment. A highly accessible fraction of chromatin, approximately 50 % of the total, becomes digested in the first 15

minutes of the time series. A more compact fraction is digested within the next 40 minutes. A remaining chromatin fraction, approximately 10 % of the total, is predominantly resistant to DNaseI digestion. OND cells show a biphasic response, with a compact fraction dominant for the first 60 minutes of digestion. The remaining fraction of chromatin, around 30 % of the total, is relatively resistant to DNaseI digestion (Figure 53). OND cells do not exhibit a rapidly digested fraction of chromatin, as observed in untreated cells.

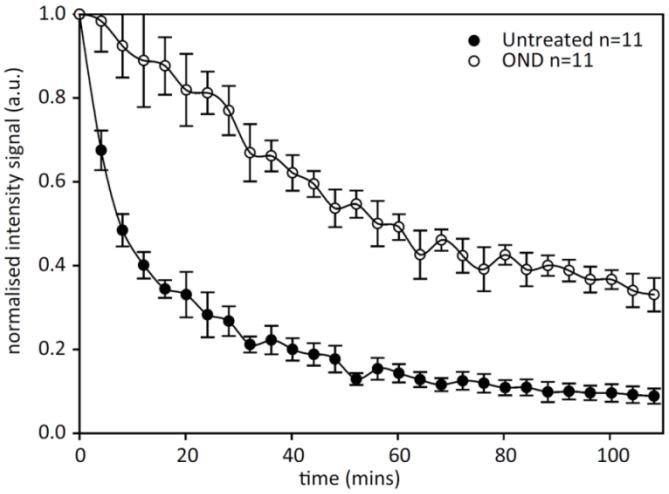

Figure 53. DNA digestion of untreated and OND treated cells.
Chromatin digestion of untreated cells is tri-phasic and faster than of OND treated cells, which show a biphasic digestion .a.u.: arbitrary units.

3.6.2 The mobility of linker histone H1.1 decreases upon OND

Flow cytometry, confocal microscopy, and SMLM indicate that the staining signal for core histone 3 significantly decreases under OND. In order to investigate, if this effect is due to impaired antibody accessibility or because core histones become evicted from chromatin, FRAP measurements were performed on live cells.

HeLa cells, stably transfected with core-histone H2B mCherry, which exhibits significant exchange within chromatin, or linker-histone H1.1 GFP, were subjected to OND and analysed by FRAP. If these histones become displaced from chromatin under OND, the fluorescent signal would recover faster after bleaching, due to increased mobility. Similarly to HL-1 cells, HeLa cells undergo chromatin compaction under OND conditions as well (Figure 54).

Upon OND treatment, the mobility of H2B does not change, indicating that it is not displaced from chromatin upon OND treatment (Figure 55). The mobility of linker

histone H1.1, which maintains higher order chromatin structure and is known to exchange continuously within minutes, is decreased in OND treated cells, arguing against displacement (Figure 56). Further, chromatin compaction upon OND exceeds the compaction of heterochromatin, where H1.1 was still observed to be mobile in control cells (data not shown).

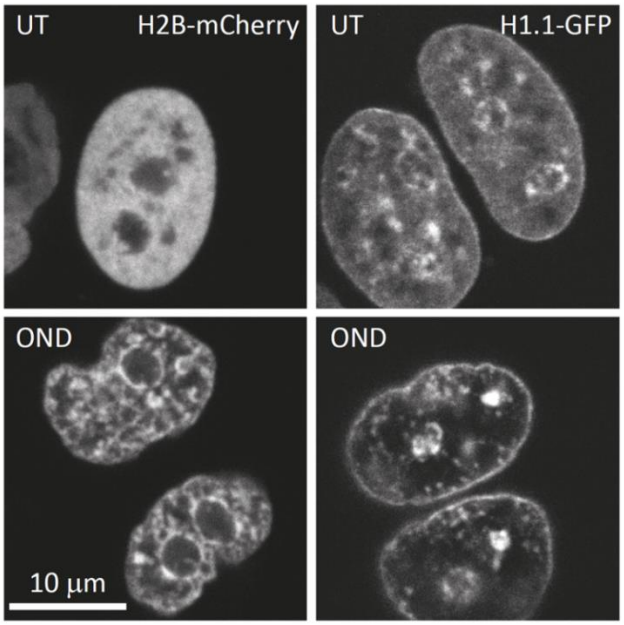

Figure 54. OND induces chromatin compaction in HeLa cells.
In untreated cells, H2B is diffusely distributed in the nucleus and excluded from nucleoli. Under OND, H2B accumulates in dense clusters and rings around the nucleoli. H1.1 signal in untreated cells is granular, with some signal-dense regions. Under OND, signal-sparse voids and signal-dense clusters appear.

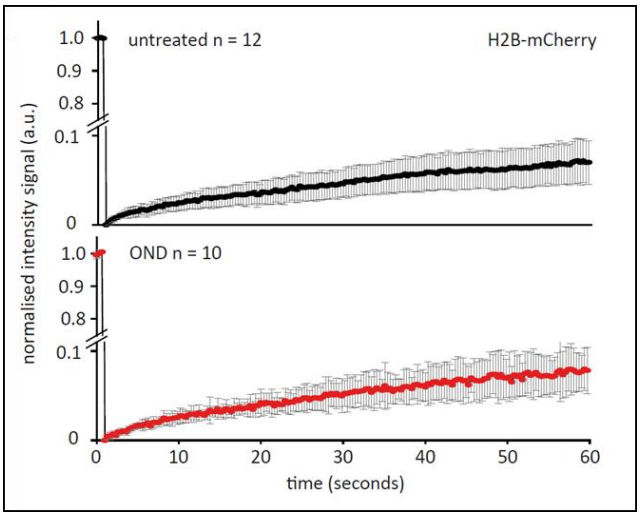

Figure 55. Mobility of core histone H2B does not change under OND conditions.
Normalized intensity of mCherry signal, coupled to histone H2B, is plotted against the time. The recovery time of the fluorescent signal does not change in OND treated cells (red), compared to untreated cells (black).

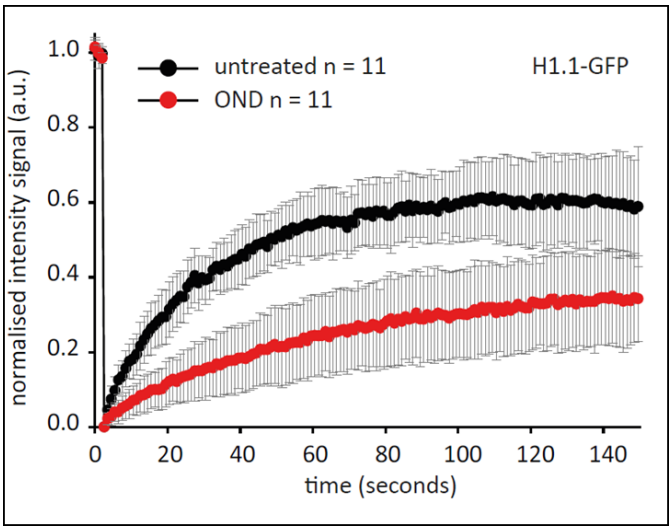

Figure 56. Mobility of linker histone H1.1 decreases under OND conditions.
Normalized intensity of GFP signal, coupled to histone H1.1, is plotted against the time. The recovery time of the fluorescent signal decreases in OND treated cells (red), compared to untreated cells (black).

3.7.1 OND depletes intercellular ATP levels

Oxygen and nutrient deprivation empties cellular energy reservoirs by 90 %, since ATP cannot be sufficiently generated in the respiratory chain under hypoxic conditions and glycolysis is inhibited by deoxyglucose. Upon recovery with nutrients under normoxic conditions, ATP levels gradually increase and rise as high as in untreated cells after 240 minutes, similar to the kinetics of chromatin relaxation (Figure 57).

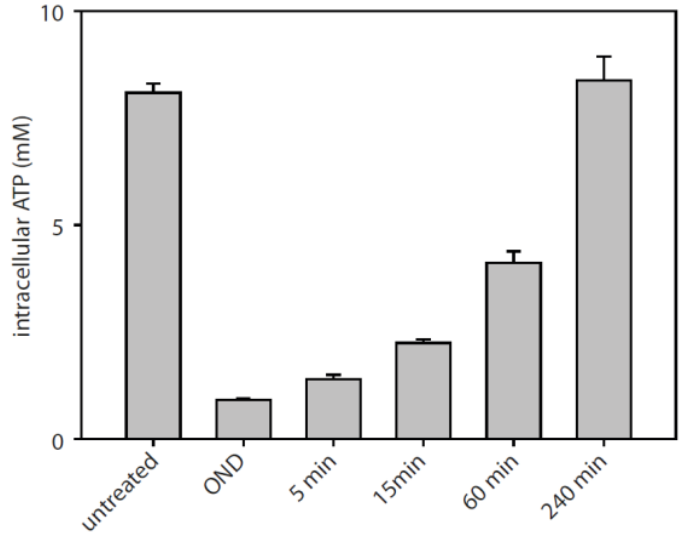

Figure 57. intracellular ATP levels in OND and recovery.
During OND ATP levels become depleted and increase with recovery time. The ATP pool becomes restored within 240 minutes of recovery.

3.7.2 OND induces relocation of the polyamine pool into the nucleus

Polyamines are linear organic cations with two or more amino groups and involved in a variety of cellular pathways. Putrescine is the smallest polyamine (charge of 2^+), followed by spermine (3^+) and spermidine (4^+). The amino acid arginine is converted into ornithine, which is further converted into putrescine by the enzyme ornithine decarboxylase (ODC). Spermidine is synthesized from putrescine and spermine is synthesized from spermidine.

Under normal physiological conditions, cations and positively charged polyamines are predominantly bound to the polyphosphate group of ATP. In control cells, polyamines are mainly localized in the cytoplasm, associated with mitochondria, where ATP concentration is high. Upon OND, when ATP becomes depleted, a high proportion of spermidine and spermine translocates into the nucleus by mass action (Figure 58).

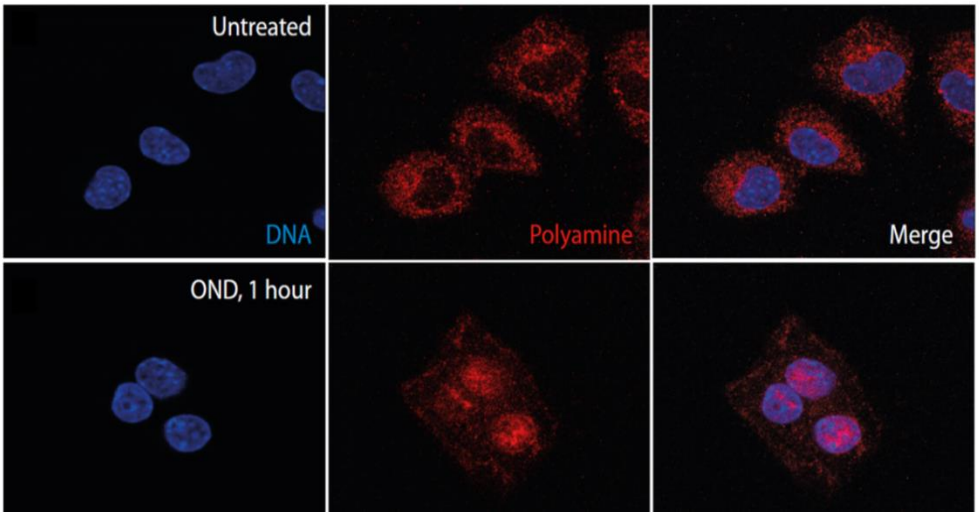

Figure 58. Translocation of polyamines into the nucleus upon OND.
The used antibody recognizes spermine and spermidine. Upon OND, polyamines, previously located in the cytoplasm, translocate into the nucleus. Image compilation by C. Heiser.

3.8 Deacetylated genes are associated with cardiac diseases

As proven by different approaches in this thesis and confirmed by literature, histone deacetylation is a feature of OND and mouse myocardial infarction. It was shown by Granger et al. that the inhibition of histone deacetylation in mice decreases the infarcted area by half (Granger et al., 2008).

In order to determine if histone deacetylation upon OND has an impact on cardiac health, ChIPseq of the histone mark H3K14ac was performed in OND treated and untreated HL-

1 cardiomyocytes. The regions affected by deacetylation were associated with the respective genes (ChipSeeker) and these were further analysed for their impact in cardiac diseases, based on literature reports (Genomatix literature mining, diseases).

In this analysis, H3K14ac was chosen as a representative for acetylated histone H3; H3K14ac highly correlates with H3K9ac and H3K27ac to promote a transcriptionally poised state of associated DNA sequences. H3K14ac is found at promoters, introns, as well as on active enhancers and correlates with gene transcription (Karmodiya et al., 2012).

In conformity with literature, the data analysis revealed that differentially bound peaks of H3K14ac are mainly covering areas, which were identified as promoters and introns, as well as distal intergenic regions; the latter can contain regulatory elements like enhancers (Figure 59).

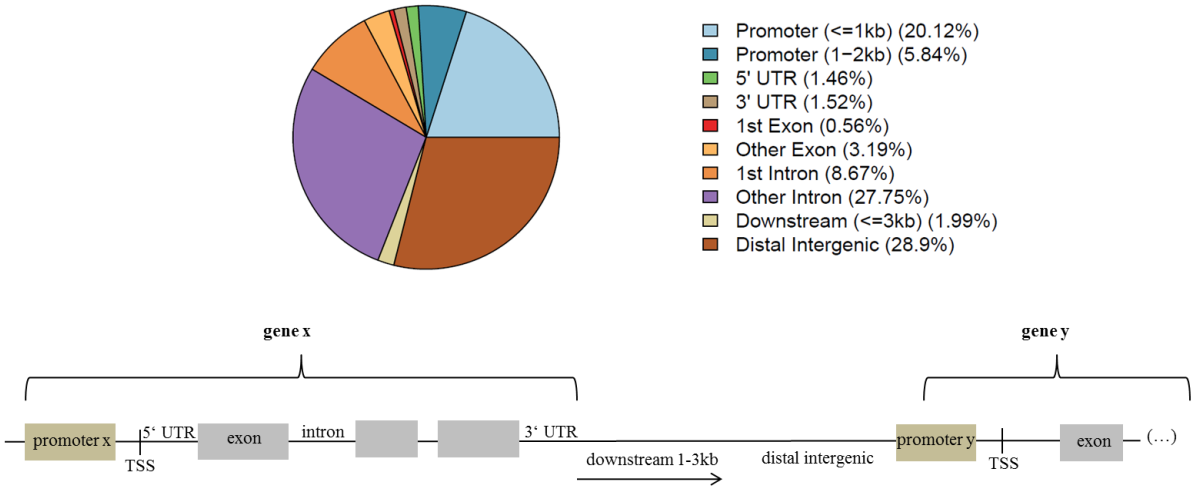

Figure 59. Distribution of differentially bound H3K14ac peaks.
Pie chart showing the distribution of H3K14ac peaks, which are mainly associated with promoters <=1kb, introns and distal intergenic regions. Below: Scheme of the different genomic regions.

Under OND, H3K14 deacetylation mainly takes place at intronic regions. Altered transcription of the genes, which are containing these introns, was reported in fibrosis, cardiac hypertrophy, ischemic cardiomyopathy, hypertensive heart disease and heart failure.

Distal intergenic regions, defined to be more than 3kb away from the actual gene, are the second most deacetylated genomic areas upon OND; these can contain regulatory elements, which have impact on the transcription of neighbor genes. Genes, which were computationally associated with these regions, were found to be involved in (acute)

myocardial ischemia, hypoxia, cardiac hypertrophy, cardiomyopathies, ventricular arrhythmias and sudden cardiac death.

Comparably few promoters and exons are affected by histone deacetylation under OND. Nevertheless, associated genes were found to be differentially expressed in abnormal cardiac conduction and left ventricular dysfunction, respectively.

Although a minor part of decreased H3K14ac peaks was mapped to downstream regions, defined to be 1 – 3kb away from the actual gene, associated genes were found to be altered in cardiomyopathy and cardiovascular morbidity. The least deacetylated regions are 5' and 3' UTRs of genes; no cardiac disease association was found for these genes (Table 15). Remarkably, all cardiac malfunctions reported with the deacetylated genes, are known to be induced by cardiac ischemia and ischemia-reperfusion injury. Ventricular arrhythmias arise from improper electrical activity of the heart. Ischemia induces arrhythmia, due to cell-to-cell electrical uncoupling via gap junctions. Any disturbances in ion homeostasis can induce electrical imbalances; this can be caused by altered gene expression of ion pumps and channels.

Scar formation, or fibrosis, after myocardial infarction is caused by activated, proliferating fibroblasts, which compensate for the loss of dead cardiomyocytes. Furthermore, deposited collagen causes cardiac hypertrophy. Cardiomyopathy is the dysfunction of the heart muscle, which is lacking strength to fulfill its pumping action. This can be caused cardiomyocyte loss, fibrosis, insufficient electrical conduction or the lack of muscle components, due to or altered transcription or mutation.

Table 15. Deacetylated regions, their associated genes and their impact in cardiac diseases.

Deacetylated region	associated genes	Diseases
Promoter	Gja5, Ank3, Cacna1g, Lmna, Dot1l, Tiam3	abnormal cardiac conduction
5‘ or 3‘ UTR	no	no
Exon	Traf2, Scn10a, Prkce	left ventricular dysfunction
Intron	Golm1, Srebf2, Ltbp1, Fstl1, Stk4, Smad3, Wls, Ly6a, Wwtr1, Mrc2, Lpar1, Fbrs, Fabp1, Ski, Mkl1, Smad7, Adamts5, Jak2, Smad2, Cdh11, Srebf1, Prkg1, Smad4, Shroom3, Pgs1, Gja5, Fosl2, Timp2, Fgf7, Prss23, Mir29b-1, Utrn, Wisp1, Adamts7, Bmp6, Adcy5	fibrosis
	Traf3ip2, Nfatc3, Kat2b, Igf2r, Stk4, Dyrk1a, Adra1b, Ly6a, Nfkb1, Raf1, Clcn3, Corin, Slc8a1, Prkce, Scube3, Hdac4, Mkl1, Myoz2, Hlf, Wdr1, Prkag2, Hdac9, Prkg1, Grk5, Ptpn11, Hspb8, Akap13, Adm, Mlip, Mef2a, Esrrg, Ptk2, Prkca, Cacna1h	cardiac hypertrophy
	Oprd1, Rapgef1, Ly6a, Frmd4b, Grk5, Abcb10, Cdh13, Gja5, Ece1	ischemic cardiomyopathy
	Smad3, Corin, Slc8a1, Smad7, Vcl, Timp2, Anxa5	hypertensive heart disease
	Ank2, Fstl1, Rapgef1, Rbm20, Stk4, Corin, Slc8a1, Rnd3, Itpr1, Prkce, Snx13, Orai1, Sumo1, Frmd4b, Anks1, Nrg1, Grk5, Hspb8, Adm, Fadd, Slc7a2, Mylk3, Prkca, Ece1, Hace1, Adcy5	heart failure
Downstream 1-3kb	Tnnc1, Rbm20, Fxn, Rbck1	cardiomyopathy
	Igfbp1, Npr3	cardiovascular morbidity
Distal intergenic (>3kb)	Adrb1, Ppp1r12a, Rheb, Ryr2, Slc6a6, Hif1a	acute myocardial ischemia
	Foxo1, Adrb1, Mir30b, Tead1, Foxo3, Il6st, Gnb2l1, Myocd, Nek6, Gnaq, Ly6a, Camk1, Scube3, Map3k1, Hdac4, Fbln2, Rrad, Rock2, Slc4a3, Casq2, Fhl2, Npr3, Ryr2, Mef2a, Rel, Klf4, Itgb1, Nt5c1b	cardiac hypertrophy
	Adrb1, Tead1, Dusp1, Gnaq, Opa1, Tbx20, Egln3, Lclat1, Cpt2, Lpin1, Cap2, Dag1, Hcn4, Ryr2, Mef2a, Itga7, Plin2, Myof	cardiomyopathies
	Adrb1, Egln3, Slc2a1, Hif1a	hypoxia
	Adrb1, Mir125b-1, Igfbp1, Abcc8, Mir30a, Iqsec1, Trib1, Got2, Rock2, Tek, Rheb, Col5a2, Ryr2, Mef2a, Apob, Vcam1, Hif1a, Egln1	myocardial ischemia
	Adrb1, Kcnh2, Trdmt1, Adrb3, Insig2, Lpin1, Nrg1, Rock2, Sp4, Casq2, Ryr2, Mef2a, Trib2, Apob, Plin2	sudden cardiac death
	Kcnh2, Il6st, Gnaq, Rrad, Sp4, Kcnj5, Hcn4, Casq2, Ryr2	ventricular arrhythmia

Only 7 % of the genes, which show a decrease in H3K14ac under OND, have a decreases expression, as compared to RNAseq data. This is due to the nature of the histone code; combinatorial effects of several modifications determine the final transcriptional potential of the DNA. Nevertheless, genes which become definitely repressed in OND in conjunction with decreased H3K14ac, are reported in cardiac malfunctions like right ventricular hypertrophy (Rock2, Bmpr2, Hif1a, Ghrl, Ppp1r12a) and cardiac death (Apob, Chrm2, Ikzf2).

Even though a global re-acetylation is induced upon returning to normoxia and normoglycemia, about 10 % of the regions remain deacetylated after four hours of recovery. About 8 % of these deacetylated regions are associated with genes, which are repressed after four hours of recovery. Association of these genes with diseases revealed their involvement in hypertrophy (Ece1, Klf15, Wisp1, Slc2a1), fibrosis (Ece1, Klf15) cardiomyopathy and postoperative myocardial infarction (Lpin1).

The given evidence, that histone deacetylation upon OND has impact on the expression of genes, which were found to be altered in cardiac diseases, clearly justifies the application of HDACIs in OND/ischemia and sheds light on their beneficial effects in mouse myocardial infarction.

3.9 Prevention of chromatin compaction by inhibition of HDACs and ODC

In order to reduce chromatin condensation under starving conditions, either the inhibition of histone deacetylation by TSA or the inhibition of the enzyme ornithine decarboxylase (ODC) by difluoromethylornithine (DFMO), or both was investigated using FRAP analysis of H1.1.

Under OND, the mobility of linker histone H1.1 is reduced, due to the compact state chromatin. Treatment with the HDACI TSA either one hour prior to OND or during one hour of OND, increases H1.1 mobility, but does not recover it completely. Pre-treatment or treatment during OND did not reveal different results (Figure 60).

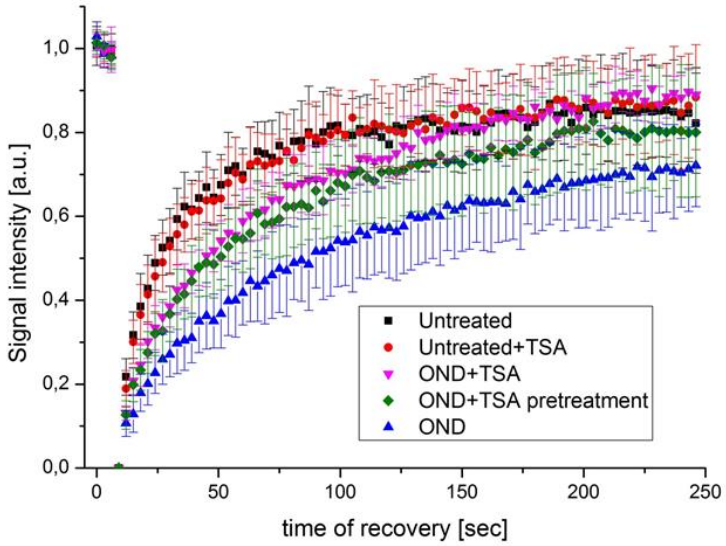

Figure 60. FRAP analysis of H1.1 after TSA treatment.
After TSA treatment, the mobility of linker histone H1.1 increases but does not reach kinetics of control cells. One hour pre-treatment with TSA or treatment during one hour of OND does not reveal any difference.

Treatment with the ODC inhibitor DFMO, either forty eight hours prior to OND or additionally during OND treatment, increases H1.1 mobility, but does not recover it completely. The pre-treatment displays a higher effect on the mobility than the additional treatment during OND (Figure 61).

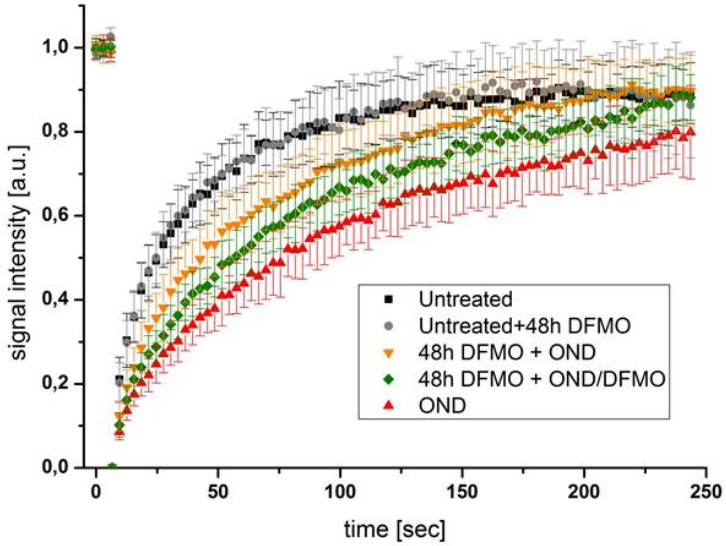

Figure 61. FRAP analysis of H1.1 after DFMO treatment.
After DFMO treatment, the mobility of linker histone H1.1 increases but does not reach kinetics of control cells. Forty eight hours of pre-treatment.

Assuming that chromatin compaction is a detrimental condition induced by OND/ischemia, which must be prevented in order to ameliorate cardiomyocyte performance, usage of HDAC as well as ODC inhibition are promising treatment strategies.

As estimated from histone H1.1 mobility, chromatin compaction under OND is reduced, if either histone deacetylation is inhibited or cells are depleted of polyamines prior to OND. A combinatorial treatment of HDAC and ODC inhibition did not reveal a potentiating effect (data not shown).

4. Discussion

Ischemia is a condition, which contributes to the most devastating human diseases such as ischemic heart disease, stroke and cancer. The heart encounters ischemic episodes in acute coronary syndromes, congenital coronary abnormalities, cardiomyopathies, cyanotic heart disease, and during cardiac surgery. Even though ischemic events cause morbidity and mortality for several million people per year, its consequences for the genomic architecture of cardiomyocytes have not been elucidated yet.

Although it was reported previously that chromatin has the ability to respond to environmental stimuli, this study links, for the first time, alterations in chromatin architecture to ischemic diseases and provides new intervention strategies.

Moderate, transient hypoxia in combination with nutrient deprivation and inhibition of glycolysis induces dramatic, but reversible, compaction of DNA in the murine myocardial cell line HL-1. This DNA compaction is accompanied by a global loss of histone acetylation and transcriptional silencing, triggering subsequent cardiac malfunctions.

The OND tissue culture model is a powerful system for the analysis of ischemia and IRI; transcriptional changes, like the induction of the transcription factors Fos, Jun and Egr1, activation of compensatory mechanisms like angiogenesis and proliferation, as well as the repression of histone genes upon recovery/reperfusion, were observed *in vivo* as well as *in vitro*.

The intense compaction of chromatin into clusters, interspersed between large, chromatin-sparse voids, was first noticed by confocal microscopy, but this technique could not provide the nanoscale resolution to describe these changes in detail. Application of SMLM showed that chromatin clusters are actually dense, ring-like atolls and that the active histone mark H3K14ac is located in the perichromatin, facing the interchromatin compartment. Whether these atolls reflect individual chromosomes, needs further investigation by fluorescent in situ hybridization (FISH) for chromosome painting.

It is worth mentioning that chromatin compaction was pronounced at the nuclear periphery, but investigation of LaminB did not reveal any changes in the structure of the nuclear lamina. Transmission electron microscopy confirmed chromatin compaction, independent of DNA dyes and computational processing, but did not provide additional information.

As shown by FRAP analysis, not only the murine cardiomyocyte cell line HL-1 reacts to OND with chromatin compaction, but also the human cervical carcinoma cell line HeLa intensively condenses its DNA when oxygen and energy supply are low. This observation indicates that chromatin compaction is a cell type independent, general mechanism of how cells respond to OND/ischemia.

Characterization of different chromatin types, by of DNaseI accessibility revealed that untreated cells have three different compaction states of chromatin, resulting in a triphasic digestion curve. OND treated cells display a biphasic digestion curve, with a fraction of compact but digestible chromatin and a fraction, which is resistant to DNaseI digestion. This analysis again illustrates the massive compaction of chromatin upon OND.

The present study shows that energy depletion under OND induces chromatin compaction through the liberation of ATP- and RNA-bound polyamines, which are subsequently attracted by the polyphosphate backbone of the DNA by mass action (Iacomino et al., 2014). This observation is conform with the literature; it is known since 1978 that polyamines can induce DNA condensation (Chattoraj and Gosule, 1978).

The shift of spermine and spermidine from the cytoplasm to the nucleus was shown by confocal microscopy in OND-treated HL-1 cells. Interestingly, we found the enzyme spermidine/spermine N(1)-acetyltransferase Sat1 to be induced six fold during reperfusion in the mouse heart. Sat1 acetylates spermidine and spermine for degradation, this process also produces ROS and toxic aldehydes. Polyamine synthesis is catalyzed by the enzyme ODC, which converts ornithine in putrescine, from which spermidine and spermine are subsequently synthesized by the contribution of S-adenosylmethionine decarboxylase (SAM-DC). Polyamines play an essential role in cell growth, differentiation and apoptosis (Igarashi and Kashiwagi, 2000).

It was shown that polyamine levels are altered in animal models of global ischemia and IR. Ischemia activates a polyamine stress response, characterized by increased ODC and Sat1 activities, leading to the accumulation of putrescine and the decrease of spermidine and spermine. The supplementation of spermine increased cell survival in the heart (Zhao et al., 2007), but also the inhibition of ODC by DFMO reduced the infarct volume in the brain (Temiz et al., 2005). It seems contradictory that the inhibition of polyamine synthesis by DFMO and as well as the supplementation with polyamines has beneficial outcomes in IRI. On one hand, under OND, when polyamines are tightly bound to the backbone of the DNA, pathways involving these molecules become arrested. If exogenously administered polyamines exceed the binding capacity of the DNA, unbound

spermine/spermidine could operate in cellular pathways again. On the other hand, we showed that polyamine depletion by ODC inhibitors or chelating agents can prevent OND-induced chromatin compaction, which we assume to be a key event in IRI. Only comparative animal studies will provide the answer, whether polyamine inhibition or supplementation has more beneficial effects for the long term prognosis after IRI.

Interestingly, the protective effects of IPC were found to be abolished, when mice were treated with DFMO prior to the conditioning stimulus. It was shown that IPC increases myocardial polyamine levels by regulating ODC and Sat1 (Wang et al., 2014), which indicates an involvement of polyamines in the IPC signaling cascade that establishes the resistance towards ischemic insult. This observation raises the question, whether IPC stimuli can persistently modulate chromatin structure and therefore prevent massive condensation under acute, prolonged conditions.

Also divalent cations, like calcium and magnesium, are mediators of chromatin compaction *in vitro* (Visvanathan et al., 2013). As with polyamines, calcium and in particular, magnesium are complexed with ATP and upon its depletion, these ions become liberated. It can be assumed that divalent cations are also able to contribute to chromatin condensation *in vivo*. Therefore, chelating agents could serve as a supplementary therapy in ischemia.

The supplementation of sugar (D-ribose) in the myocardium during the ischemic period is discussed in regard of inhibiting apoptosis (Caretti et al., 2010). According to our results, this treatment strategy could have the additional beneficial effect to prevent chromatin compaction upon ATP depletion.

Furthermore we have shown, by different methodologies, that histone acetylation is globally decreased under OND conditions. Western blot analysis revealed that not only histones of cardiomyocytes, but also histones of fibroblasts and endothelial cells, which are comprised in the heart, become deacetylated. The intensity of deacetylation and also the recovery kinetics vary among cell lines, indicating a cell type depending sensitivity and recovery potential. Although this study failed to demonstrate histone deacetylation in mouse cardiac ischemia, it was shown previously that application of the pan HDACI TSA reduces infarct size in mice by half, which suggests that deacetylation is also taking place in the ischemic mouse heart.

Interestingly, it was reported that hypoxia-treated mouse cardiomyocytes display increased HDAC activity, which provokes deacetylation of histone H3 and H4 (Granger et al., 2008). This finding argues against a passive deacetylation of histones under OND

due to the lack of ATP, which inhibits the synthesis of acetyl-CoA that is necessary for protein acetylation (Wellen et al., 2009). Findings of this study showed that ATP depletion, polyamine synthesis and liberation, as well as activated histone deacetylases are hallmarks of ischemia and can be addressed by drug therapies in infarction (Figure 62).

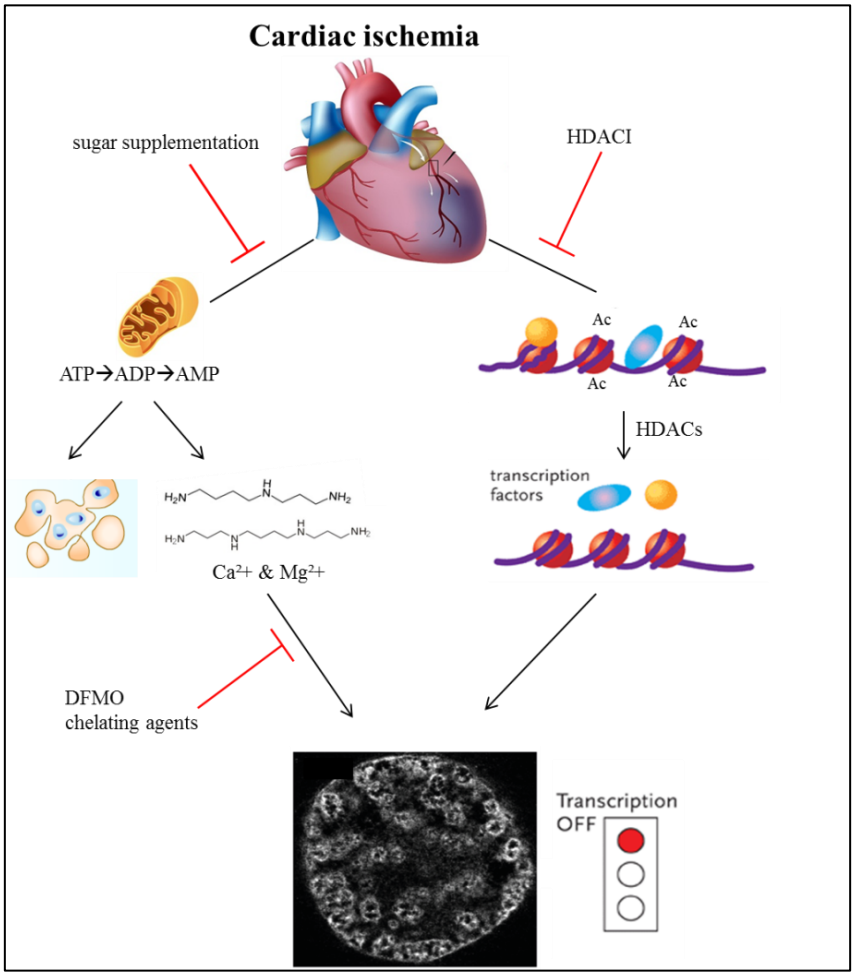

Figure 62. Molecular mechanisms induced in cardiac ischemia.
Cardiac ischemia induces ATP depletion, leading to apoptosis and the liberation of ATP-bound polyamines and divalent cations. By mass action, these are binding to the polyphosphate backbone of the DNA, which induces chromatin condensation. At the same time, ischemia provokes the activation of HDACs, which deacetylate chromatin and therefore induce additional chromatin compaction.

Although increased histone methylation was reported in previous hypoxia studies, in consequence of the oxygen dependency of Jumonji C demethylases, this could not be confirmed in this work. On the contrary, OND induced a reversible decrease in H3K4me3, as observed by western blot and flow cytometry analysis. Levels of H3K9me3 and H3K27me3 remained constant on average. This finding can be explained by the

application of different hypoxia protocols, comparing strong, long term hypoxia of 0.2 % oxygen for 48 hours (Shmakova et al., 2014) versus moderate, transient hypoxia of 1 % oxygen for 1hour (this study).

Besides decreased histone acetylation, also lower signals of H3 total fluorescence were observed under OND using flow cytometry and microscopy. According to the literature, histones can act as damage-associated molecular pattern molecules (DAMPs), when released into the extracellular space upon damage or cell activation. Levels of circulating histones were found to be increased in cancer, inflammation and infection (Allam et al., 2014) and high concentrations of serum nucleosomes were detected in patients with cerebral stroke, especially in patients with large infarction volumes (Geiger et al., 2006). In the present study, the loss of H3 signal in immunofluorescence was caused by the inaccessibility of the antibody to its epitope, due to intensive chromatin compaction. The possibility of histone displacement was ruled out by FRAP analysis of the linker histone H1 and core histone H2B, showing no increased mobility. In contrast to H3, H4 and H2A, core histone H2B exhibits significant exchange within chromatin (Kimura and Cook, 2001) and was therefore investigated in this experiment. Upon OND treatment, H2B mobility did not change, indicating that it does not become displaced from chromatin upon OND treatment. Linker histone H1.1, which maintains higher order chromatin structure, is known to exchange continuously within minutes, even in heterochromatin (Lever et al., 2000). The mobility of H.1.1 was decreased in OND treated cells, excluding H1.1 displacement. In OND, H1.1 is associated with more compact chromatin, even exceeding the kinetics within heterochromatin.

It is worth mentioning that histone marks were reliably detected in OND despite of compaction, as seen by the comparison of western blot and flow cytometry results; specific antibodies recognize the modification, which is exposed even when chromatin is highly condensed.

Not only ischemia, but also the inevitable reperfusion damages the myocardium. Upon restoration of the blood flow, a sterile inflammation is induced: radicals destroy membranes, mitochondria and cause DNA strand breaks. The recruitment of immune cells to the side of injury and their release of cytokines further promote the destruction of the heart muscle.

This study has shown that the compacted chromatin structure is completely reversible within 60 minutes of recovery. Upon regeneration from hypoxia and starvation, chromatin undergoes a phase transition from an ordered, compacted state to a disordered,

more open state, which again introduces changes to the transcriptome. This more open configuration was confirmed by SMLM microscopy and is supported by the repression of histone genes in the tissue culture, as well as in the mouse model. The down-regulation of histone genes implicates an impaired chromatin organization after ischemia/OND.

Furthermore, histone acetylation recovers within the first ten minutes of oxygen and energy restoration, but the reinstated histone code has higher acetylation levels after four hours of recovery, as compared to untreated cells. This more open chromatin state, induced by over-acetylation, repression of core histone genes, and the binding of polyamines to an excess of restocked ATP, promotes an altered transcriptional profile, setting the course for cardiac maladaptation and post-infarct diseases.

ChIPseq of the acetylated histone mark H3K14, correlated with transcriptome analysis of OND-treated and recovered cardiomyocytes, revealed that IRI introduces transcriptional changes at genes, which are known to be differentially expressed in cardiac diseases. These changes are maintained epigenetically, since not all regions become re-acetylated after recovery. These findings could explain the beneficial effect of HDACI in IRI; the inhibition of histone deacetylation has the potential to prevent transformation of the epigenetic landscape during and after cardiac ischemia.

Changes to the epigenome, particularly the histone code, are taking place when pluripotent cells are progressing towards differentiation and their formerly unlimited transcriptional potential becomes buried in heterochromatin. Taken together, this data suggests that a more open, less organized chromatin, as observed upon recovery from OND, is indicative for cellular reprogramming.

The present study cannot answer the question, whether polyamine-induced chromatin compaction upon hypoxia and hypoglycemia is a mechanism by which a protective scaffold is formed on the DNA, preventing radical attacks. It has been reported, that DNA condensation induced by polyamines at sub-millimolar concentrations was ineffective in defending the DNA against γ-radiation, but seemed to slightly promote the damage (Iacomino et al., 2014). Only at amounts exceeding the critical concentration that induces massive DNA compaction, DNA damage was reduced (Douki et al., 2000). Furthermore, it was shown that some DNA lesions like pyrimidone photoproducts and cisplatin-induced intrastrand crosslinks do not occur in heterochromatin (Han et al., 2016).

Chromatin condensation under OND is not exclusively passive: polyamines are attracted by mass action, whereas histone deacetylation seems to be a partly induced process at the cost of cellular energy under already restrictive conditions.

In conclusion, this comprehensive study demonstrates the intimate connection between chromatin architecture and functional genomic output and the ability of chromatin to detect and react to environmental conditions through structural rearrangements. Defining and understanding these effects offers a diverse range of tractable targets for therapeutic intervention in human disease. This study further proposes a new field of application for FDA-approved drugs TSA and DFMO.

5. Outlook

Chromatin compaction is a feature of cells, which are exposed to hypoxia and hypoglycemia. Assuming, that this condition is a devastating consequence of ischemia, intervention strategies should be considered and the state of DNA condensation can be used as a read out for drug effectiveness. Therefore, a high throughput method for the screening of chromatin compaction needs to be established.

Flow cytometry offers the possibility to analyze thousands of cells within minutes for their internal complexity and specific immunostaining. Intercalation of the dye Acridine Orange (AO) in DNA double strands results in green fluorescence (excitation maximum 502 nm, emission maximum 522 nm), whereas dye-base stacking on single strand DNA emits red luminescence (excitation maximum 457 nm, emission maximum 638 nm). This indicates, that the denaturation of DNA can be expressed by the greed to red ratio of AO stained cells. Considering the measurement of chromatin condensation, denaturation correlates with compaction; compacted chromatin is more prone to acid-denaturation than open chromatin (Darzynkiewicz et al., 1985). Preliminary results showed that it is possible to discriminate the AO staining-profiles of OND-treated and untreated cells (data not shown).

Further, it is crucial to analyze if inhibition of chromatin compaction induces additional DNA damage. The base modification 8-hydroxy guanosine is induced by ROS and serves as a marker for oxidative stress. Rising levels of 8-hydroxy guanosine in DFMO or TSA treated cells would be indicative for a protective role of DNA condensation under OND conditions. This potential risk or the cost-benefit of TSA/DFMO treatment in ischemic diseases needs to be evaluated in therapeutic approaches.

Since TSA is an unspecific HDACI, which also inhibits the performance of deacetylases that are not involved in ischemia, an identification of specific HDACs, de-acetylating histones in OND/ischemia, will help to design a more target-oriented therapy with fewer side effects. For this purpose, a sequential knock-down of all HDACs by short-hairpin-RNAs followed by subsequent screening for decreased histone deacetylation upon OND by flow cytometry, can be performed. The potential candidates could be chemically inhibited at the onset of ischemia and during reperfusion.

It is essential to finally prove that chromatin condensation is taking place in the ischemic mouse heart. New techniques, as tissue clearing prior to imaging, could reduce the auto

fluorescence of heart muscle tissue and provide better image quality. Also, isolated nuclei from mouse infarcts can be DNA-stained either with VV and analyzed by SMLM, or with AO and analyzed by flow cytometry for chromatin compaction.

The present study only describes short-time changes in chromatin architecture upon OND and recovery. It is important to analyze if the chromatin landscape remains altered on a long-term range of several passages within cell lines, or even within several month in the IR-mouse model.

Taken together, these findings will add important knowledge to the complex field of IRI and its subsequent disastrous consequences for the heart. This new insight into the connection between chromatin architecture and ischemic diseases will pave the way for new treatment strategies.

6. References

Albiez, H., Cremer, M., Tiberi, C., Vecchio, L., Schermelleh, L., Dittrich, S., Küpper, K., Joffe, B., Thormeyer, T., von Hase, J., et al. (2006). Chromatin domains and the interchromatin compartment form structurally defined and functionally interacting nuclear networks. Chromosom. Res. *14*, 707–733.

Allam, R., Kumar, S.V.R., Darisipudi, M.N., and Anders, H.J. (2014). Extracellular histones in tissue injury and inflammation. J. Mol. Med. *92*, 465–472.

Andreyev, a Y., Kushnareva, Y.E., and Starkov, a a (2005). Mitochondrial metabolism of reactive oxygen species. Biochemistry. (Mosc). *70*, 200–214.

Baines, C. (2009). The mitochondrial permeability transition pore and ischemia-reperfusion injury. Basic Res. Cardiol. *104*, 181–188.

Bartel, D.P. (2009). MicroRNAs: Target Recognition and Regulatory Functions. Cell *136*, 215–233.

Bersohn, M.M., Morey, a K., and Weiss, R.S. (1997). Sarcolemmal calcium transporters in myocardial ischemia. J. Mol. Cell. Cardiol. *29*, 2525–2532.

Bousselmi, R., Lebbi, M.A., and Ferjani, M. (2014). Myocardial ischemic conditioning: Physiological aspects and clinical applications in cardiac surgery. J. Saudi Hear. Assoc. *26*, 94–100.

Cai, Z., Luo, W., Zhan, H., and Semenza, G.L. (2013). Hypoxia-inducible factor 1 is required for remote ischemic preconditioning of the heart. Pnas *110*, 17462–17467.

Carden, D.L., and Granger, D.N. (2000). Pathophysiology of ischaemia-reperfusion injury. J. Pathol. *190*, 255–266.

Caretti, A., Bianciardi, P., Sala, G., Terruzzi, C., Lucchina, F., and Samaja, M. (2010). Supplementation of creatine and ribose prevents apoptosis in ischemic cardiomyocytes. Cell. Physiol. Biochem. *26*, 831–838.

Carreau, A., Hafny-Rahbi, B. El, Matejuk, A., Grillon, C., and Kieda, C. (2011). Why is the partial oxygen pressure of human tissues a crucial parameter? Small molecules and hypoxia. J. Cell. Mol. Med. *15*, 1239–1253.

Chattoraj DK, Gosule LC, S.A. (1978). DNA condensation with polyamines. II. Electron microscopic studies. J Mol Biol *1221*, 327–337.

Claycomb, W.C., Lanson, N. a, Stallworth, B.S., Egeland, D.B., Delcarpio, J.B., Bahinski, a, and Izzo, N.J. (1998). HL-1 cells: a cardiac muscle cell line that contracts and retains phenotypic characteristics of the adult cardiomyocyte. Proc. Natl. Acad. Sci. U. S. A. *95*, 2979–2984.

Cremer, T., and Cremer, C. (2001). Chromosome territories, nuclear architecture and gene regulation in mammalian cells. Nat. Rev. Genet. *2*, 292–301.

Cremer, T., and Cremer, M. (2010). Chromosome territories. Cold Spring Harb. Perspect. Biol. *2*, a003889.

Cremer, T., Cremer, M., Hübner, B., Strickfaden, H., Smeets, D., Popken, J., Sterr, M., Markaki, Y., Rippe, K., and Cremer, C. (2015). The 4D nucleome: Evidence for a dynamic nuclear landscape based on co-aligned active and inactive nuclear compartments. FEBS Lett.

Dahl, C., Grønbæk, K., and Guldberg, P. (2011). Advances in DNA methylation: 5-hydroxymethylcytosine revisited. Clin. Chim. Acta *412*, 831–836.

Darzynkiewicz, Z., Traganos, F., Kapuscinski, J., and Melamed, M.R. (1985). Denaturation and condensation of DNA in situ induced by acridine orange in relation to chromatin changes during growth and differentiation of Friend erythroleukemia cells. Cytometry *6*, 195–207.

Davie, a P. (1996). Early thrombolytic treatment in acute myocardial infarction. Lancet *348*, 1312–1313.

Depre, C., and Vatner, S.F. (2007). Cardioprotection in stunned and hibernating myocardium. Heart Fail. Rev. *12*, 307–317.

Dhalla, N.S. (2000). Status of myocardial antioxidants in ischemia – reperfusion injury. *47*, 446–456.

Dickson, E.W., Lorbar, M., Porcaro, W. a, Fenton, R. a, Reinhardt, C.P., Gysembergh, a, and Przyklenk, K. (1999). Rabbit heart can be "preconditioned" via transfer of coronary effluent. Am. J. Physiol. *277*, H2451–H2457.

Dmitriev, R.I., and Papkovsky, D.B. (2015). In vitro ischemia decreases histone H4K16 acetylation in neural cells. FEBS Lett. *589*, 138–144.

Douki, Bretonniere, C. (2000). Protection against radiation-induced degradation of DNA bases by polyamines. *153*, 29–35.

Flaus, A., and Owen-Hughes, T. (2003). Mechanisms for Nucleosome Mobilization. Biopolymers *68*, 563–578.

Geiger, S., Holdenrieder, S., Stieber, P., Hamann, G.F., Bruening, R., Ma, J., Nagel, D., and Seidel, D. (2006). Nucleosomes in serum of patients with early cerebral stroke. Cerebrovasc. Dis. *21*, 32–37.

Gidday, J.M. (2015). Extending Injury- and Disease-Resistant CNS Phenotypes by Repetitive Epigenetic Conditioning. Front. Neurol. *6*, 1–7.

Gomes, A.Q., Nolasco, S., and Soares, H. (2013). Non-Coding RNAs : Multi-Tasking Molecules in the Cell. 16010–16039.

Gomez, L., Li, B., Mewton, N., Sanchez, I., Piot, C., Elbaz, M., and Ovize, M. (2009). Inhibition of mitochondrial permeability transition pore opening: Translation to patients. Cardiovasc. Res. *83*, 226–233.

Gore, C.J., Clark, S. a., and Saunders, P.U. (2007). Nonhematological mechanisms of improved sea-level performance after hypoxic exposure. Med. Sci. Sports Exerc. *39*, 1600–1609.

Görisch, S.M., Wachsmuth, M., Tóth, K.F., Lichter, P., and Rippe, K. (2005). Histone acetylation increases chromatin accessibility. J. Cell Sci. *118*, 5825–5834.

Granger, D.N. (1988). Role of xanthine oxidase and granulocytes in ischemia-reperfusion injury. Am. J. Physiol. *255*, H1269–H1275.

Granger, A., Abdullah, I., Huebner, F., Stout, A., Wang, T., Huebner, T., Epstein, J. a, and Gruber, P.J. (2008). Histone deacetylase inhibition reduces myocardial ischemia-reperfusion injury in mice. FASEB J. *22*, 3549–3560.

Gregory, R.I., Yan, K.-P., Amuthan, G., Chendrimada, T., Doratotaj, B., Cooch, N., and Shiekhattar, R. (2004). The Microprocessor complex mediates the genesis of microRNAs. Nature *432*, 235–240.

Hammond, E.M., and Giaccia, A.J. (2004). The role of ATM and ATR in the cellular response to hypoxia and re-oxygenation. DNA Repair (Amst). *3*, 1117–1122.

Han, C., Srivastava, A.K., Cui, T., Wang, Q.-E., and Wani, A. a. (2016). Differential DNA lesion formation and repair in heterochromatin and euchromatin. Carcinogenesis *37*, 129–138.

Han, J., Cox, D.G., Colditz, G. a, and Hunter, D.J. (2006). The p53 codon 72 polymorphism, sunburns, and risk of skin cancer in US Caucasian women. Mol. Carcinog. *45*, 694–700.

Hattori, M., Yokoyama, Y., Hattori, T., Motegi, S., Amano, H., Hatada, I., and Ishikawa, O. (2015). Global DNA hypomethylation and hypoxia-induced expression of the ten eleven translocation (TET) family, TET1, in scleroderma fibroblasts. Exp. Dermatol. n/a – n/a.

Hausenloy, D., and Yellon, D. (2013). Myocardial ischemia-reperfusion injury: a neglected therapeutic target. J Clin Invest *123*, 92–100.

Iacomino, G., Picariello, G., Stillitano, I., and D'Agostino, L. (2014). Nuclear aggregates of polyamines in a radiation-induced DNA damage model. Int. J. Biochem. Cell Biol. *47*, 11–19.

Igarashi, K., and Kashiwagi, K. (2000). Polyamines: Mysterious Modulators of Cellular Functions. Biochem. Biophys. Res. Commun. *271*, 559–564.

Islam, K.N., and Mendelson, C.R. (2006). Permissive effects of oxygen on cyclic AMP and interleukin-1 stimulation of surfactant protein A gene expression are mediated by epigenetic mechanisms. Mol. Cell. Biol. *26*, 2901–2912.

Johnson, A.B., and Barton, M.C. (2007). Hypoxia-induced and stress-specific changes in chromatin structure and function. Mutat. Res. - Fundam. Mol. Mech. Mutagen. *618*, 149–162.

Johnson, A.B., Denko, N., and Barton, M.C. (2008). Global Repression of Transcription. Mutat Res *640*, 174–179.

Jurgensen, J., Rosenberger, C., Wiesener, M., Warnecke, C., Horstrup, J., Grafe, M., Philipp, S., Griethe, W., Maxwell, P., Frei, U., et al. (2004). Persistent induction of HIF-1 alpha and -2 alpha in cardiomyocytes and stromal cells of ischemic myocardium. *23*, 1–23.

Karmodiya, K., Krebs, A.R., Oulad-Abdelghani, M., Kimura, H., and Tora, L. (2012). H3K9 and H3K14 acetylation co-occur at many gene regulatory elements, while H3K14ac marks a subset of inactive inducible promoters in mouse embryonic stem cells. BMC Genomics *13*, 424.

Kasper, L.H., Boussouar, F., Boyd, K., Xu, W., Biesen, M., Rehg, J., Baudino, T. a, Cleveland, J.L., and Brindle, P.K. (2005). Two transactivation mechanisms cooperate for the bulk of HIF-1-responsive gene expression. EMBO J. *24*, 3846–3858.

Kirmes, I., Szczurek, A., Prakash, K., Charapitsa, I., Heiser, C., Musheev, M., Schock, F., Fornalczyk, K., Ma, D., Birk, U., et al. (2015). A transient ischemic environment induces reversible compaction of chromatin. Genome Biol *16*, 246.

Kouzarides, T. (2007). Chromatin Modifications and Their Function. Cell *128*, 693–705.

Kriaucionis, S., and Heintz, N. (2009). The nuclear DNA base 5-hydroxymethylcytosine is present in Purkinje neurons and the brain. Science *324*, 929–930.

Kuo, M.H., and Allis, C.D. (1998). Roles of histone acetyltransferases and deacetylases in gene regulation. BioEssays *20*, 615–626.

Lee, Y., Ahn, C., Han, J., Choi, H., Kim, J., Yim, J., Lee, J., Provost, P., Rådmark, O., Kim, S., et al. (2003). The nuclear RNase III Drosha initiates microRNA processing. Nature *425*, 415–419.

Li E, Beard C, J.R. (1993). Role for DNA methylation in genomic imprinting. Nature 362–365.

Liu, L., Cash, T.P., Jones, R.G., Keith, B., Thompson, C.B., and Simon, M.C. (2006). Hypoxia-induced energy stress regulates mRNA translation and cell growth. Mol. Cell *21*, 521–531.

Löfstedt T, Fredlund E, H.-M.L. (2007). Hypoxia inducible factor-2alpha in cancer. Cell Cycle *6*, 919–926.

Luo, W., Li, B., Chen, R., Huang, R., and Lin, G. (2008). Effect of ischemic postconditioning in adult valve replacement. Eur. J. Cardio-Thoracic Surg. *33*, 203–208.

Markaki, Y., Gunkel, M., Schermelleh, L., Beichmanis, S., Neumann, J., Heidemann, M., Leonhardt, H., Eick, D., Cremer, C., and Cremer, T. (2010). Functional nuclear organization of transcription and DNA replication: A topographical marriage between chromatin domains and the interchromatin compartment. Cold Spring Harb. Symp. Quant. Biol. *75*, 475–492.

Marks, P. a, and Dokmanovic, M. (2005). Histone deacetylase inhibitors: discovery and development as anticancer agents. Expert Opin. Investig. Drugs *14*, 1497–1511.

Melvin, A., and Rocha, S. (2012). Chromatin as an oxygen sensor and active player in the hypoxia response. Cell. Signal. *24*, 35–43.

Metivier, R., Penot, G., Hübner, M.R., Reid, G., Brand, H., Kos, M., and Gannon, F. (2003). Estrogen Receptor- ⌴ Directs Ordered , Cyclical , and Combinatorial Recruitment of Cofactors on a Natural Target Promoter. *115*, 751–763.

Murry, C.E., Jennings, R.B., and Reimer, K. a (1986). Preconditioning with ischemia: a delay of lethal cell injury in ischemic myocardium. Circulation *74*, 1124–1136.

Nallamshetty, S., Chan, S.Y., and Loscalzo, J. (2013). Hypoxia: A master regulator of microRNA biogenesis and activity. Free Radic. Biol. Med. *64*, 20–30.

Nan, X., Ng, H.H., Johnson, C. a, Laherty, C.D., Turner, B.M., Eisenman, R.N., and Bird, a (1998). Transcriptional repression by the methyl-CpG-binding protein MeCP2 involves a histone deacetylase complex. Nature *393*, 386–389.

Ng, H.H., Feng, Q., Wang, H., Erdjument-Bromage, H., Tempst, P., Zhang, Y., and Struhl, K. (2002). Lysine methylation within the globular domain of histone H3 by Dot1 is important for telomeric silencing and Sir protein association. Genes Dev. *16*, 1518–1527.

Panning, B., and Jaenisch, R. (1996). DNA hypomethylation can activate Xist expression and silence X-linked genes. Genes Dev. *10*, 1991–2002.

Pedersen, M.T., and Helin, K. (2010). Histone demethylases in development and disease. Trends Cell Biol. *20*, 662–671.

Pepine, C.J., and Deedwania, P.C. (1998). How do we best treat patients with ischemic heart disease? Circulation *98*, 1985–1986.

Perez-Perri, J.I., Acevedo, J.M., and Wappner, P. (2011). Epigenetics: New questions on the response to hypoxia. Int. J. Mol. Sci. *12*, 4705–4721.

Peric-Hupkes, D., and van Steensel, B. (2010). Role of the nuclear lamina in genome organization and gene expression. Cold Spring Harb. Symp. Quant. Biol. *75*, 517–524.

Piper, H.M., and Ovize, M. (1998). A fresh look at reperfusion injury. Cardiovasc. Res. *38*, 291–300.

Popken, J., Brero, A., Koehler, D., Schmid, V.J., Strauss, A., Wuensch, A., Guengoer, T., Graf, A., Krebs, S., Blum, H., et al. (2014). Reprogramming of fibroblast nuclei in cloned bovine embryos involves major structural remodeling with both striking similarities and differences to nuclear phenotypes of in vitro fertilized embryos. Nucleus *5*, 555–589.

Przyklenk, K., Bauer, B., Ovize, M., Kloner, R. a, and Whittaker, P. (1993). Regional ischemic "preconditioning" protects remote virgin myocardium from subsequent sustained coronary occlusion. Circulation *87*, 893–899.

Qin Li, M.C. (2009). c-Myc Mediates a Hypoxia-Induced Decrease in Acetylated Histone H4. Biochimie *10*, 1307–1310.

Ramachandran, S., Ient, J., Göttgens, E., Krieg, A.J., and Hammond, E.M. (2015). Epigenetic Therapy for Solid Tumors: Highlighting the Impact of Tumor Hypoxia. 935–956.

Luger, K, Richmond, R.K., Sargent, D.F., Richmond, T.J., and Ma, A.W. (1997). Crystal structure of the nucleosome ˚ resolution core particle at 2 . 8 A. *7*, 251–260.

Rocha, S. (2007). Gene regulation under low oxygen: holding your breath for transcription. Trends Biochem. Sci. *32*, 389–397.

Rouquette, J., Genoud, C., Vazquez-Nin, G.H., Kraus, B., Cremer, T., and Fakan, S. (2009). Revealing the high-resolution three-dimensional network of chromatin and interchromatin space: A novel electron-microscopic approach to reconstructing nuclear architecture. Chromosom. Res. *17*, 801–810.

Semenza, G.L. (2009). REVIEWS Regulation of Oxygen Homeostasis by.

Shahrzad S, Bertrand K, Minhas K, C.B. (2007). Induction of DNA hypomethylation by tumor hypoxia. Epigenetics *2*, 119–125.

Shmakova, A., Batie, M., Druker, J., and Rocha, S. (2014). Chromatin and oxygen sensing in the context of JmjC histone demethylases. Biochem. J. *462*, 385–395.

Steg, P.G., James, S.K., Atar, D., Badano, L.P., Lundqvist, C.B., Borger, M. a., Di Mario, C., Dickstein, K., Ducrocq, G., Fernandez-Aviles, F., et al. (2012). ESC Guidelines for the management of acute myocardial infarction in patients presenting with ST-segment elevation: The Task Force on the management of ST-segment elevation acute myocardial infarction of the European Society of Cardiology (ESC). Eur. Heart J. *33*, 2569–2619.

Temiz, C., Dogan, A., Baskaya, M.K., and Dempsey, R.J. (2005). Effect of difluoromethylornithine on reperfusion injury after temporary middle cerebral artery occlusion. J. Clin. Neurosci. *12*, 449–452.

Udali, S., Guarini, P., Moruzzi, S., Choi, S.W., and Friso, S. (2013). Cardiovascular epigenetics: From DNA methylation to microRNAs. Mol. Aspects Med. *34*, 883–901.

Verges, S., Chacaroun, S., Godin-Ribuot, D., and Baillieul, S. (2015). Hypoxic Conditioning as a New Therapeutic Modality. Front. Pediatr. *3*, 1–14.

Vinten-Johansen, J. (2004). Involvement of neutrophils in the pathogenesis of lethal myocardial reperfusion injury. Cardiovasc. Res. *61*, 481–497.

Visvanathan, A., Ahmed, K., Even-Faitelson, L., Lleres, D., Bazett-Jones, D.P., and Lamond, A.I. (2013). Modulation of Higher Order Chromatin Conformation in Mammalian Cell Nuclei Can Be Mediated by Polyamines and Divalent Cations. PLoS One *8*, e67689.

Vivar, R., Humeres, C., Varela, M., Ayala, P., Guzmán, N., Olmedo, I., Catalán, M., Boza, P., Muñoz, C., and Díaz Araya, G. (2012). Cardiac fibroblast death by ischemia/reperfusion is partially inhibited by IGF-1 through both PI3K/Akt and MEK-ERK pathways. Exp. Mol. Pathol. *93*, 1–7.

Walsh CP, Chaillet JR, B.T. (1998). Transcription of IAP endogenous retroviruses is constrained by cytosine methylation. Nat. Genet. *20*, 116–117.

Wang, W., Zhang, H., Xue, G., Zhang, L., Zhang, W., Wang, L., Lu, F., Li, H., Bai, S., Lin, Y., et al. (2014). Exercise training preserves ischemic preconditioning in aged rat hearts by restoring the myocardial polyamine pool. Oxid. Med. Cell. Longev. *2014*.

Weber, K.T. (1989). Cardiac interstitium in health and disease: the fibrillar collagen network. J. Am. Coll. Cardiol. *13*, 1637–1652.

Webster, A.L.H., Yan, M.S.C., and Marsden, P. a. (2013). Epigenetics and Cardiovascular Disease. Can. J. Cardiol. *29*, 46–57.

Wellen, K.E., Hatzivassiliou, G., Sachdeva, U.M., Bui, T. V, Justin, R., and Thompson, C.B. (2009). NIH Public Access. *324*, 1076–1080.

Wong LC, Sharpe DJ, W.S. (1991). High-mobility group and other nonhistone substrates for nuclear histone N-acetyltransferase. Biochem Genet. 461–475.

Xia, X., Lemieux, M.E., Li, W., Carroll, J.S., Brown, M., Liu, X.S., and Kung, A.L. (2009). Integrative analysis of HIF binding and transactivation reveals its role in maintaining histone methylation homeostasis. Proc. Natl. Acad. Sci. U. S. A. *106*, 4260–4265.

Xin, M., Olson, E.N., and Bassel-duby, R. (2013). Mending broken hearts: cardiac development as a basis for adult heart regeneration and repair. Nat. Rev. Mol. Cell Biol. *14*, 529–541.

Yang, J., Ledaki, I., Turley, H., Gatter, K.C., Montero, J.C.M., Li, J.L., and Harris, A.L. (2009). Role of hypoxia-inducible factors in epigenetic regulation via histone demethylases. Ann. N. Y. Acad. Sci. *1177*, 185–197.

Yang, N.-C., Ho, W.-M., Chen, Y.-H., and Hu, M.-L. (2002). A Convenient One-Step Extraction of Cellular ATP Using Boiling Water for the Luciferin–Luciferase Assay of ATP. Anal. Biochem. *306*, 323–327.

Zeynalov, Shah, Li, and D. (2009). Heme Oxygenase 1 Is Associated with Ischemic Preconditioning- Induced Protection Against Brain Ischemia. Changes *35*, 264–269.

Zhao, J., Sun, B.K., Erwin, J.A., Song, J., and Jeannie, T. (2009). NIH Public Access. *322*, 750–756.

Zhao, Y.J., Xu, C.Q., Zhang, W.H., Zhang, L., Bian, S.L., Huang, Q., Sun, H.L., Li, Q.F., Zhang, Y.Q., Tian, Y., et al. (2007). Role of polyamines in myocardial ischemia/reperfusion injury and their interactions with nitric oxide. Eur. J. Pharmacol. *562*, 236–246.

Zhao, Z.Q., Nakamura, M., Wang, N.P., Velez, D. a, Hewan-Lowe, K.O., Guyton, R. a, and Vinten-Johansen, J. (2000). Dynamic progression of contractile and endothelial dysfunction and infarct extension in the late phase of reperfusion. J. Surg. Res. *94*, 133–144.

Zucker-Franklin, D. (1990). Atlas der Blutzellen. Funktion und Pathologie.

Żurek-Biesiada, D., Szczurek, A.T., Prakash, K., Mohana, G.K., Lee, H.-K., Roignant, J.-Y., Birk, U., Dobrucki, J.W., and Cremer, C. (2015). Localization microscopy of DNA in situ using Vybrant® DyeCycle™ Violet fluorescent probe: A new approach to study nuclear nanostructure at single molecule resolution. Exp. Cell Res.

Zweier, J.L., and Talukder, M. a H. (2006). The role of oxidants and free radicals in reperfusion injury. Cardiovasc. Res. *70*, 181–190.

7. Appendix

7.1 List of figures

Figure 1. Cross-section of the mammalian heart. 4
Figure 2. The 10 leading causes of death in the world. 5
Figure 3. Myocardial infarction. 6
Figure 4. Molecular key events of acute myocardial IRI. 9
Figure 5. Chromatin organisation. 14
Figure 6. Post-translational modifications of histone tails. 15
Figure 7. DNA methylation. 18
Figure 8. miRNA biogenesis and posttranscriptional gene silencing. 19
Figure 9. Chromatin compartments. 21
Figure 10. Surgery for the induction of myocardial infarction. 29
Figure 11. Hypoxia chamber. 31
Figure 12. Sequencing by synthesis. 33
Figure 13. Gating strategy. 36
Figure 14. Principle of SMLM. 38
Figure 15. Calculation of chromatin-free regions. 40
Figure 16. Principle of FRAP. 43
Figure 17. Differential gene expression profiles in the heart. 47
Figure 18 Genes whose expression is consistently induced in the heart upon ischemia. 50
Figure 19. Commonly repressed genes in the heart 51
Figure 20. Differential gene expression profiles in HL-1cells. 52
Figure 21 Consistently up- and down regulated genes 55
Figure 22. RNA synthesis is impaired by OND. 56
Figure 23. Genes commonly induced in OND/ ischemia and recovery/ reperfusion. 57
Figure 24. Down-regulated histone genes in OND and ischemia. 59
Figure 25. Ac H3 in OND and recovery. 61
Figure 26. H3K9ac in OND and recovery. 61
Figure 27. H3K14ac in OND and recovery. 62
Figure 28. H3K27ac in OND and recovery. 62
Figure 29. H3K4me3 in OND and recovery. 63
Figure 30. H3K9me3 in OND and recovery. 64
Figure 31. H3K27me3 in OND and recovery. 64
Figure 32. H3K14ac and H3K14me3 recovery time course. 65
Figure 33. histone marks in IRI. 65
Figure 34. H3 and DNA staining for controls, OND, and recovered cells. 67
Figure 35. Pan Ac H3 and DNA staining for controls, OND, and recovered cells. 67
Figure 36. H3K9ac and DNA staining for controls, OND, and recovered cells. 68
Figure 37. H3K14ac and DNA staining for controls, OND, and recovered cells. 68
Figure 38. H3K27ac and DNA staining for controls, OND, and recovered cells. 69
Figure 39. H3K4me3 and DNA staining for controls, OND, and recovered cells. 70
Figure 40. H3K9me3 and DNA staining for controls, OND, and recovered cells. 70
Figure 41. H3K27me3 and DNA staining for controls, OND, and recovered cells. 71
Figure 42. H3S28P and DNA staining for controls, OND, and recovered cells. 72
Figure 43. Changes in DNA structure and H3K9ac in OND. 72
Figure 44. OND. hypoxia, and nutrient deprivation. 73
Figure 45. SMLM images of a control and an OND treated cell. 74
Figure 46. SMLM images of H3 in OND and control cell. 75
Figure 47. The distribution of Lamin B in control and OND cells. 76

Figure 48. SMLM OND recovery series of HL-1 cells. 76
Figure 49. Calculation of chromatin-free areas of OND treated and recovering cells. 77
Figure 50. Transmission electron microscopy image. 78
Figure 51. H3, H3 acetylation and methylation signals in untreated and OND treated cells. 79
Figure 52. pan Ac H3 signal in untreated, OND treated, and recovering cells. 80
Figure 53. DNA digestion of untreated and OND treated cells. 81
Figure 54. OND induces chromatin compaction in HeLa cells. 82
Figure 55. Mobility of core histone H2B does not change under OND conditions. 82
Figure 56. Mobility of linker histone H1.1 decreases under OND conditions. 83
Figure 57. intracellular ATP levels in OND and recovery. 83
Figure 58. Translocation of polyamines into the nucleus upon OND. 84
Figure 59. Distribution of differentially bound H3K14ac peaks. 85
Figure 60. FRAP analysis of H1.1 after TSA treatment. 89
Figure 61. FRAP analysis of H1.1 after DFMO treatment. 89
Figure 62. Molecular mechanisms induced in cardiac ischemia. 94

7.2 List of tables

Table 1. Partial oxygen pressures of air and different tissues in the human body. 11
Table 2. Reagents. 25
Table 3. Antibodies. 26
Table 4. Enzymes. 27
Table 5. Kits. 27
Table 6. DNA dyes 27
Table 7. Instruments. 27
Table 8. Software 27
Table 9. Parameters for the acquisition of FRAP data. 42
Table 10. Transcriptional changes and GO terms for 0h and 2h of reperfusion. 48
Table 11. Transcriptional changes and GO terms for 4h and 24h of reperfusion. 49
Table 12. Transcriptional changes and GO terms for 0h and 1h of recovery. 53
Table 13. Transcriptional changes and GO terms for for 4hrs of recovery. 54
Table 14. GO terms for OND/ischemia and recovery/reperfusion. 58
Table 15. Deacetylated regions, their associated genes and their impact in cardiac diseases. 87

7.3 Abbreviation index

Ac	Acetylation
Acetyl CoA	Acetyl coenzyme-A
AO	Acridine Orange
ADP	Adenosine diphosphate
ARNT	Aryl hydrocarbon receptor nuclear translocator
Atf	Activating transcription factor
ATP	Adenosine triphosphate
a.u.	Arbitrary units
AVN	Atrioventricular Node
BrU	Bromouridine
bp	base pair
BSA	Bovine serum albumin
°C	degree Celsius
C57/BL6	C57 black six mouse strain
CBP	Creb binding protein
CDC	Chromatin domain clusters
cDNA	complementary DNA
cm	Centimetre
CHD	Coronary heart disease
ChIP	Chromatin immunoprecipitation
CpG	Cytosine and guanosine islands
CREB	cAMP response element-binding protein.
DAMP	Damage associated molecular pattern
CT	Chromosome territories
DAMPS	Damage associated molecular patterns
DFMO	Difluoromethylornithase
DFX	Deferoxamine
DMEM	Dulbecco's Modified Eagle's Medium
DMOG	Dimethyloxaloylglycine
DNA	Deoxyribonucleic acid
DNMT	DNA methyltransferase
dNTP	deoxy nucleosid triphosphate
DTT	Dithiothreitol
ECG	Electrocardiogram
EDTA	Ethylenediaminetetraacetic
EdU	5-ethynyl-2′-deoxyuridine
Egr1	Early Growth Response
EGTA	Ethylene glycol tetraacetic acid
EPO	Erythropoietin
FACS	Fluorescence associated cell sorting
FAD	Flavin-Adenin-Dinukleotid
FBS	Fetal bovine serum
FDA	Food and drug administration
FISH	fluorescent in situ hybridization
FIH	Factor inhibiting HIF-1
Fos	FBJ Murine Osteosarcoma Viral Oncogene Homolog

FRAP	Fluorescence after photobleaching
FSC-A	Forward scatter area
g	Gram
Gadd45γ	Growth arrest and DNA damage 45γ
GFP	Green fluorescent protein
GO	Gene ontology
H1	Histone H1
H2A	Histone H2A
H2B	Histone H2B
H3	Histone H3
H4	Histone H4
HAT	Histone acetyltransferase
HCl	Hydrochloric acid
HDAC	Histone deacetylase
HDACI	Histone deacetylase inhibitor
HEPES	2-(4-(2-hydroxyethyl)-1-piperazinyl)-ethan sulfonic acid
HIF-1	Hypoxia-inducible-factor-1
Hist	Histone
HMT	Histone methyl transferase
HP	Heterochromatin-protein 1
HRE	Hypoxia response elements
Hsp	Heat shock protein
IC	Interchromatin compartment
IMB	Institute of molecular biology
IPC	Ischemic pre-conditioning
IR	Ischemia-reperfusion
IRI	Ischemia reperfusion injury
JHDM	JmjC domain containing histone demethylases
JmjC	Jumonji C
K	Lysine
k	kilo
MI	Myocardial infarction
LAD	left anterior descending artery
lncRNA	long non-coding RNA
LSD	Lysine demethylases
µ	Micro
M	Molar
max	Maximum
MBD	Methyl-CpG-binding domain
MCEC	Mouse cardiac endothelial cells
Me	Methylation
mCherry	monomeric Cherry
miRNA	Micro RNA
m	Milli
Mnase	Micrococcal nucelase
MPTP	Mitochondrial Permeability Transition Pore
mRNA	messenger RNA
N	Normal
NAD^+	Nicotinamide adenine dinucleotide
NADPH	Nicotinamide adenine dinucleotide phosphate

ncRNA	non-coding RNA
NE	Nuclear extraction
Neg	negative
NOS	Nitric oxide synthase
ODC	Ornithine decarboxylase
ODD	Oxygen dependent degradation domain
OND	Oxygen and nutrient deprivation
P	Phosphorylation
PAGE	Aolyacrylamide gel electrophoresis
PBS	Phosphate Buffered Saline
PcG	Polycomb group
PCI	Percutaneous coronary intervention
PCR	Polymerase chain reaction
PFA	Paraformaldehyde
PHD	Prolyl hydroxylase
piRNA	PIWI-interacting RNA
PMSF	Phenylmethylsulfonylfluorid
Pol II	DNA polymerase II
Pos	positive
PR	Perichromatin
PRC2	Polycomb Repressive Complex 2
PTM	Posttranslational histone modifications
PVDF	Polyvinylidenfluorid
Rec	Recovery
Rep	Reperfusion
RIN	RNA integrity number
RISC	RNA induced silencing complex
RNA	Ribonucleic acid
ROI	Region of interest
ROI	Remote organ injury
ROS	Reactive oxygen species
rpm	Rounds per minute
S	Serine
SAM-DC	S-adenosylmethionine decarboxylase
SAN	Sinoatrial Node
SAHA	Superanilohydroxamic acid
SB	Sodium butyrate
SBA	Sequencing by synthesis
SDS	Sodium dodecyl sulfate
SIM	Structured illumination microscopy
siRNA	small interfering RNA
SMLM	Single molecule localisation microscopy
SSC-A	Side scatter area
Rec	Recovery
Redox	Reduction-oxidation
Rep	Reperfusion
RIK	Riken
RIPC	Remote ischemic preconditioning
RISC	RNA-induced silencing complex
RNS	Reactive nitrogen species

RNOS	Reactive nitrogen oxide species
SAM	S-adenosyl methionine
SNF	Sucrose Non-Fermentable
SRC-1	steroid receptor co factor-1
SWI	Switch
TBS	Tris buffered saline
TEB	Triton extraction Buffer
TEM	Transmission electron microscopy
TET	Ten-Eleven Translocation
TEMED	Tetramethylethylendiamine
TSA	Trichostatin A
UT	Untreated
UTR	Untranslated region
VEGF	Vascular endothelial growth factor
VHL	Hippel-Landau protein
WHO	World Health Organization
Xist	X-inactive specific transcript
5-hmc	5-hydroxymethylcytosine